


Cite this: *RSC Adv.*, 2021, 11, 23725

# Recent advances in metal-free heteroatom-doped carbon heterogenous catalysts

Yalda Rangraz and Majid M. Heravi \*

The development of cost-effective, efficient, and novel catalytic systems is always an important topic for heterogeneous catalysis from academia and industrial points of view. Heteroatom-doped carbon materials have gained more and more attention as effective heterogeneous catalysts to replace metal-based catalysts, because of their excellent physicochemical properties, outstanding structure characteristics, environmental compatibility, low cost, inexhaustible resources, and low energy consumption. Doping of heteroatoms can tailor the properties of carbons for different utilizations of interest. In comparison to pure carbon catalysts, these catalysts demonstrate superior catalytic activity in many organic reactions. This review highlights the most recent progress in synthetic strategies to fabricate metal-free heteroatom-doped carbon catalysts including single and multiple heteroatom-doped carbons and the catalytic applications of these fascinating materials in various organic transformations such as oxidation, hydrogenation, hydrochlorination, dehydrogenation, etc.

Received 3rd May 2021  
Accepted 22nd June 2021

DOI: 10.1039/d1ra03446d

rsc.li/rsc-advances

## 1. Introduction and scope of the review

Heterogeneous catalytic systems not soluble in reaction mixtures have the benefits of better handling properties and easy separation, from an industrial point of view.<sup>1,2</sup>

With the rapidly growing demand for effective organic reactions, developing novel heterogeneous catalysts is highly needed according to the concept of “Green Sustainable Chemistry”. It has been estimated that almost all large-scale production of organic and inorganic chemicals (commercially produced chemical products), energy conversion, pollution mitigation processes, environmental protection, and crude oil refinery utilize heterogeneous catalysts<sup>3–6</sup> and it is no exaggeration to say that heterogeneous catalysts play a key role in creating a more sustainable and cleaner world.<sup>7</sup>

Metals, especially transition metals, have been extensively applied as homogeneous and heterogeneous catalysts in a series of important organic transformations in the forms of nanoparticles (NPs), clusters, coordination metal complexes, or free ions.<sup>8–12</sup>

Notwithstanding their high efficiency, these catalysts have negative environmental impacts and suffer from the high price, susceptibility to gas poisoning, poor durability, and low selectivity.<sup>13–15</sup> Thus, metal-free catalysts are essential for environmental remediation as well as large-scale commercial applications.<sup>16</sup> The replacement of metal heterogeneous catalysts with metal-free catalysts can remarkably address the environmental pollution issues arising from the leaching of

metal nanoparticles during usage in the petroleum and pharmaceutical industries.<sup>17</sup>

In this regard, inexpensive, readily available, environmentally friendly, and stable carbon-based materials (including ordered mesoporous carbon (OMCs), carbon nanotubes (CNTs), graphene oxide (GO), activated carbon (ACs), etc.) have drawn increasing attention in the field of heterogeneous catalysis (Fig. 1).<sup>18–29</sup>

However, pristine carbon materials are inert because uniform charge distribution which is the common property of all carbon materials blocks the electron transfer and decreases the interaction between the carbon materials and the reactants.<sup>30–32</sup>

Introducing heteroatoms like nitrogen, phosphorus, boron, and sulfur into sp<sup>2</sup>-hybridized carbon frameworks can cause the charge delocalization and change of the electronic structure into metal-like, which helps to obtain significant catalytic performance in a similar way of metal-based catalyst or can be applied as a superior alternative to the metal catalyst in industrial processes.<sup>33–40</sup>

In addition, plentiful defects generated by the differences in coordination ability, bond length, and atomic radius of carbon atoms and heteroatoms can serve as active sites, which are beneficial for *in situ* charge transfer to the reactants, thus activating the substrates to promote catalytic reactions.<sup>41–48</sup>

In 1926, Rideal and Wright for the first time reported that the presence of N atoms in carbon framework has a promotional effect on the catalytic performance of charcoal in the oxidation of oxalic acid.<sup>49</sup> Even though results were promising, heteroatom-doped carbon catalysts did not attract as much attention as they would attract nowadays.

Recently, these materials have emerged as one of the hot topics in the field of metal-free catalysis for the synthesis of organic compounds. In the past few years, several reviews have

Department of Chemistry, School of Physics and Chemistry, Alzahra University, Vanak, Tehran, Iran. E-mail: m.heravi@alzahra.ac.ir; mmh1331@yahoo.com



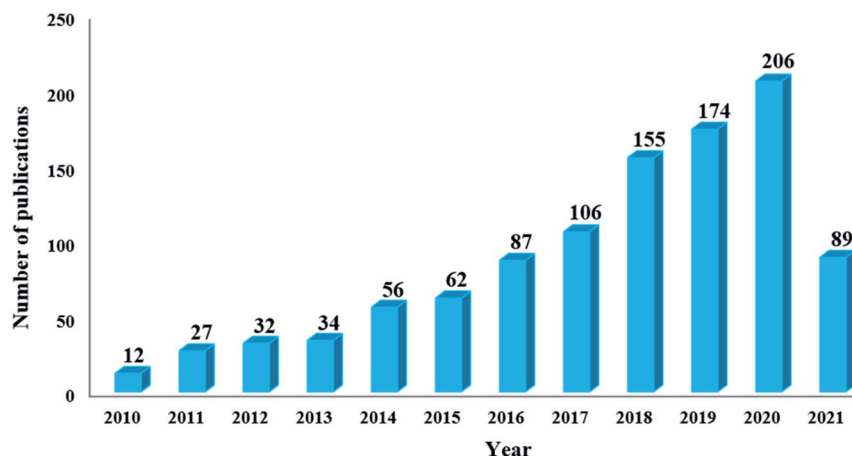


Fig. 1 Number of publications obtained from a Scopus search using "carbon-based materials and heterogeneous catalysis" as keywords.

been published toward the applications of carbon-based materials especially N-doped carbons in heterogeneous catalysis.<sup>7,8,23,50–52</sup> However, a comprehensive review that covers the application of various metal-free heteroatom-doped carbon catalysts (including single-element B-, N-, S-, and P-doped, dual-elements doped, and triple-elements doped carbon catalysts) in the field of organic transformations is highly desirable.

We are interested in novel heterogeneous catalysis, trying to design, prepare, and use them in our contemplated reactions in our laboratory, which delightfully have been mostly successful.<sup>53–68</sup>

Following, the same interest we have collected and reviewed the most recent activities on the applications of different organic transformations being performed effectively under heterogeneous catalysis.<sup>69–75</sup>

In this review, we will mainly focus on the latest developments (2015 onwards) of heteroatom-doped carbon materials (single-element B-, N-, S-, and P-doped, dual-elements doped, and triple-elements doped carbons) as promising metal-free heterogeneous catalysts, including the catalysts preparation methods with an emphasis on their application in various organic transformations (oxidation, hydrogenation, hydrochlorination, dehydrogenation, coupling, *etc.*).

## 1.1 Heteroatom-doped carbon materials

Heteroatom-doped carbon materials, especially graphene, carbon nanotubes, and new generations of heteroatom-doped porous carbons with various structures and morphologies are widely examined as metal-free catalysts.

**1.1.1 Heteroatom-doped graphene.** Graphene, a monolayer of carbon atoms arranged in a honeycomb lattice (six-membered rings), with a uniform  $sp^2$ -hybridized configuration, has emerged as a new nanocarbon during the previous two decades.<sup>22</sup> Different strategies have been developed to synthesize high-quality graphene, like chemical vapor deposition (CVD), epitaxial growth, and micromechanical exfoliation.<sup>26</sup> Superb electronic, physicochemical, optical, mechanical, and thermal properties make it a highly interesting candidate for

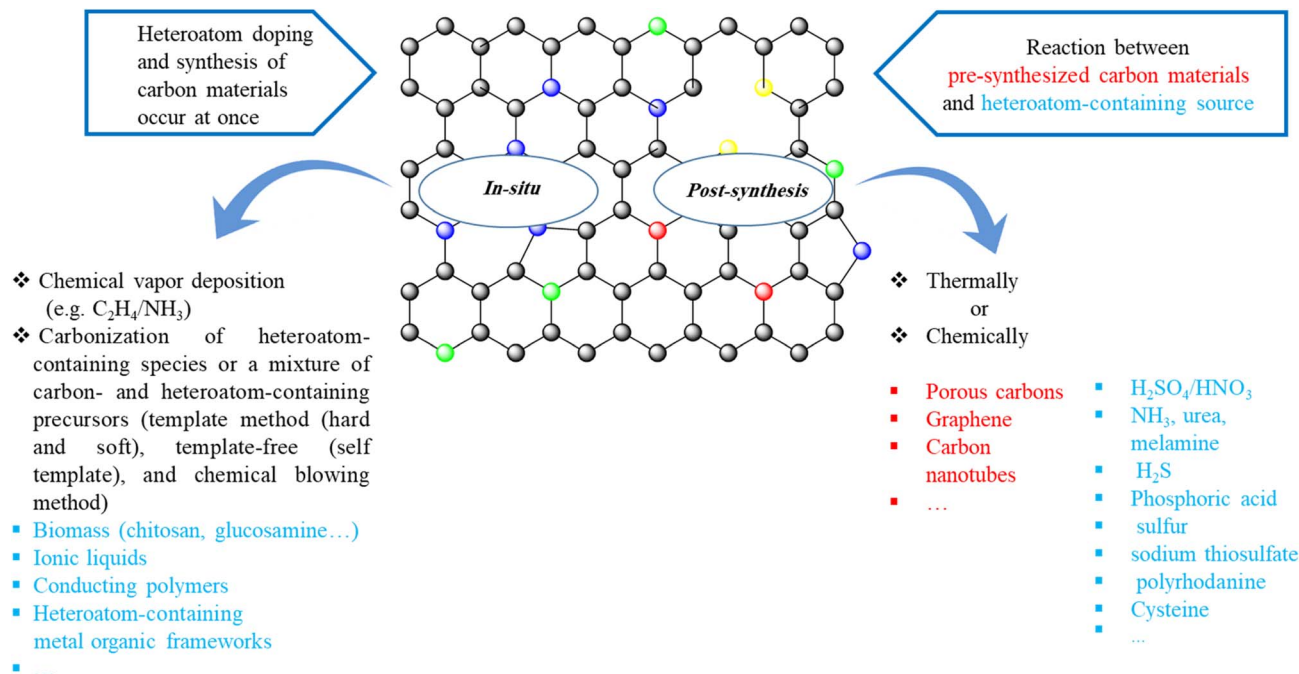
extensive applications in various fields including supercapacitors,<sup>76</sup> biosensors,<sup>77</sup> lithium-ion batteries,<sup>78</sup> and solar cells.<sup>79</sup> Also, investigations have displayed that graphene can be utilized as a metal-free catalyst in a variety of reactions such as oxidative dehydrogenation (ODH) of alkanes, oxygen-reduction reaction (ORR), environmental remediation, and chemical synthesis, opening up a novel material for sustainable and green catalysis.<sup>80–83</sup> However, the zero band gap, poor processability, and difficulties in obtaining high throughput fabrication of pure graphene considerably restrict catalytic activity as well as its broader usages.<sup>84–86</sup> Doping different heteroatoms (B, N, O, P and S) into the graphene lattice modifies its electrochemical and electronic properties through varying the electronic density within the graphene plane, breaks its inertness, creates new active sites and thus significantly enhances catalytic efficiency.<sup>22,82,87–92</sup>

**1.1.2 Heteroatom-doped CNTs.** The discovery of carbon nanotubes (CNTs), two-dimensional graphene sheets rolled up into nanoscale tubes, by Iijima in 1991 led to a new revolution in carbon chemistry.<sup>93</sup> CNTs subdivided into single- (SWCNTs) and multi-wall carbon nanotubes (MWCNTs) have received a great deal of attention owing to their excellent properties, such as high electrical and thermal conductivity, large surface area, and high tensile strength,<sup>38,94–97</sup> indicating versatile applications in several areas including electrical energy storage<sup>98</sup> and solar energy applications<sup>99</sup> (in the areas of nanoscience and nanotechnology). However, the catalytic utilizations of CNTs in organic reactions are limited to be as support for metal NPs or oxides<sup>100,101</sup> by their inert character because of their relatively seamless graphitic structure.<sup>102</sup>

The incorporation of heteroatoms into the backbone of carbon nanotubes or pores into the walls changes their physicochemical and electronic properties, resulting in an increased ability to catalyze some chemical transformations.<sup>103</sup>

**1.1.3 Heteroatom-doped porous carbon.** Porous carbons, a huge family of non-oxide porous materials,<sup>104</sup> demonstrate broad applications in water purification,<sup>105</sup> fuel cells,<sup>106</sup> gas separation,<sup>107</sup> chromatography columns,<sup>108</sup> catalyst supports,<sup>109</sup> and batteries.<sup>110</sup> The widespread use of these materials is





Scheme 1 Summary of methods to synthesize heteroatom-doped carbon materials.

related to their unique characteristics, including the low density, good thermal and mechanical stability, high corrosion resistance, surface hydrophobicity, easy handling (easy availability), and low cost of manufacture.<sup>104,111–113</sup>

More importantly, the rich pore structure of porous carbon materials distinguishes them from traditional carbons in their tunable channels and pore size, and large specific surface area.<sup>114,115</sup>

Based on their pore sizes, porous carbon materials can be classified into three groups: micropores < 2 nm, 2 nm < mesopores < 50 nm, and macropores > 50 nm, according to the recommendation of the International Union of Pure and Applied Chemistry (IUPAC).<sup>116,117</sup>

For a long time, activated carbons synthesized by chemical or physical activation and pyrolysis of starting materials like wood, coal, and fruit shells, have been the most frequently

applied form of porous carbons.<sup>7,118,119</sup> However, because of uncertain structures of different precursors, the pore size and surface chemistry have been uncontrollable. In recent years, the designed synthesis of porous carbons through self-assembly of precursors controlled hydrothermal treatment, and carbonization has gained remarkable attention owing to the exact control and simple modification of the final materials.<sup>120</sup>

In 1999, Ryoo and co-workers<sup>121</sup> reported the first example to fabricate highly ordered carbon molecular sieves by utilizing sucrose and MCM-48 as carbon source and template and opened a route to apply porous carbons in many fields.

Porous carbon can also be doped with heteroatoms, similar to graphene, and CNTs. The introduction of foreign atoms is an effective way of modifying the surface properties of porous carbons, at the same time providing materials with appealing features for many more tasks.<sup>122</sup>

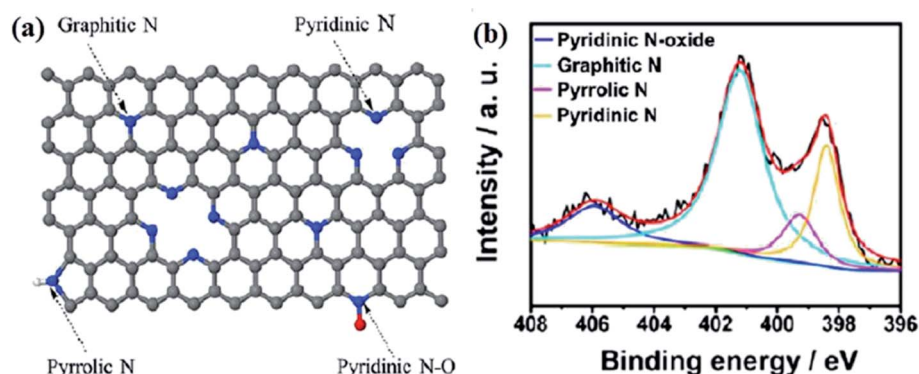
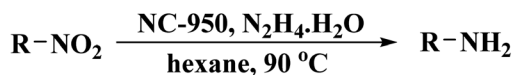


Fig. 2 (a) Bonding configurations of nitrogen atoms in carbon networks. Reprinted with permission from ref. 125. Copyright 2017 American Chemical Society and (b) XPS spectra of N atoms in different configurations. Reprinted with permission from ref. 152. Copyright 2014 American Chemical Society.



R = 4-OMeC<sub>6</sub>H<sub>4</sub>, Ph, 4-MeC<sub>6</sub>H<sub>4</sub>, 2-MeC<sub>6</sub>H<sub>4</sub>, 3-MeC<sub>6</sub>H<sub>4</sub>, 4-CH<sub>2</sub>=CHC<sub>6</sub>H<sub>4</sub>, 4-ClC<sub>6</sub>H<sub>4</sub>, 4-FC<sub>6</sub>H<sub>4</sub>, 4-CNC<sub>6</sub>H<sub>4</sub>, hexyl

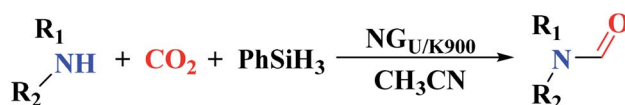
Scheme 2 Reduction of nitro compounds using NC-950.

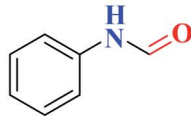
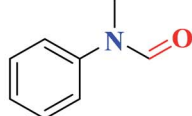
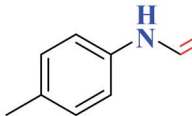
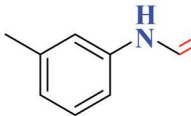
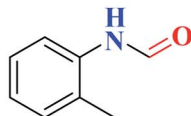
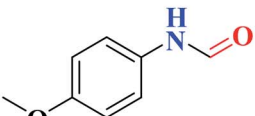
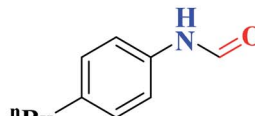
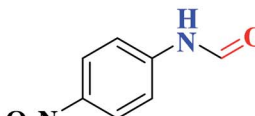
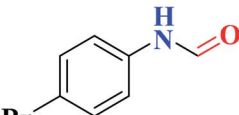
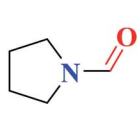
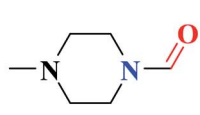
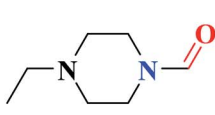
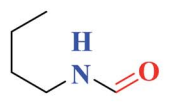
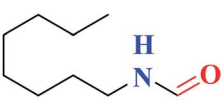
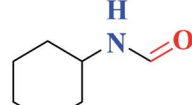
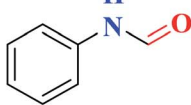
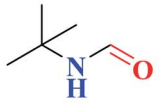
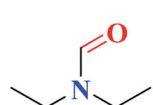
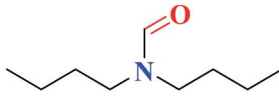
## 1.2 Synthetic strategies for heteroatom-doped carbon materials

Two strategies are frequently applied to prepare heteroatom-doped carbons:<sup>123–126</sup> (1) post-synthetic modification of pre-synthesized carbon materials with heteroatom-containing agents (such as NH<sub>3</sub>, urea, melamine, H<sub>2</sub>S, phosphoric acid,

sulfur, sodium thiosulfate, polyrhodanine, cysteine, *etc.*) chemically or thermally, (2) *in situ* doping (summarized in Scheme 1). In the *in situ* doping method, both the synthesis of carbon materials and the doping of heteroatom happen at the same time. One of the most utilized *in situ* doping methods to prepare heteroatom-doped carbons including CNTs, graphene, or microporous carbon materials is the chemical vapor

Table 1 N-Formylation of different amines via PhSiH<sub>3</sub> and CO<sub>2</sub> catalyzed by NG<sub>U/K-900</sub>



|   |   |  |   |
|---|---|--|---|
|    |    |    |    |
| 100 °C, 6 h, 92%  | 100 °C, 6 h, 97%  | 100 °C, 12 h, 97%  | 100 °C, 12 h, 98%   |
|  |  |  |  |
| 100 °C, 12 h, 87%   | 100 °C, 6 h, 96%  | 100 °C, 6 h, 69%   | 100 °C, 6 h   |
|  |  |  |  |
| 100 °C, 6 h   | r.t., 6 h   | r.t., 12 h, 98%  | r.t., 24 h, 97%   |
|  |  |  |  |
| r.t., 24 h, 98%   | r.t., 24 h, 98%   | r.t., 6 h, 97%   | r.t., 24 h, 97%<br>100 °C, 6 h, 98%   |
|  |  |  |   |
| r.t., 24 h, 64%<br>100 °C, 24 h, 96%  | r.t., 24 h, 90%   | r.t., 24 h, 52%<br>100 °C, 24 h, 99%   |   |





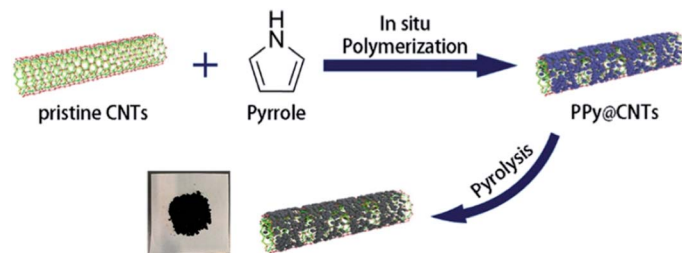
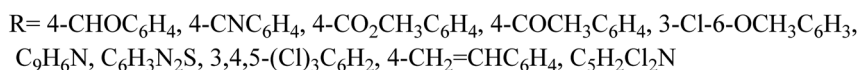
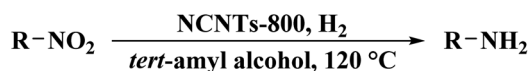


Fig. 3 Synthesis of N-doped CNTs. Reprinted with permission from ref. 189. Copyright 2020 American Chemical Society.



Scheme 3 Reduction of different nitroarenes over NCNTs-800.

deposition (CVD) due to it is appropriate to obtain well-distributed heteroatoms into the carbon framework. Also, direct carbonization of heteroatom-containing species or a mixture of carbon- and heteroatom-containing precursors that has been widely applied to attain heteroatom-doped porous carbons can be classified into three groups: hard-template method, soft-template method, and template-free (self-template) method.

The hard-template synthesis strategy includes multiple stages: (a) preparation of rigid template (e.g., SBA-15 mesoporous silica), (b) infiltration of template pores with precursors containing carbon (and heteroatom), (c) carbonization of the precursors and (d) removal of the template.

The hard-template method has important advantages and leads to the synthesis of heteroatom-doped mesoporous carbons with different morphologies and high specific surface areas, but this method is time-consuming, complicated, and inappropriate for mass production.<sup>127–129</sup>

In addition, the chemicals that are utilized to remove the templates, are hazardous and corrosive (such as basic (NaOH) or acidic (HF) solutions).<sup>111</sup>

Soft-templating is an attractive alternative method that provides many benefits in terms of time, processing, and large-scale production.<sup>130</sup> This method commonly involves the organic–organic co-assembly between organic precursors and amphiphilic molecules like block copolymers and surfactants, and carbonization treatment. The thermally unstable templates are removed during carbonization and generate abundant mesopores in resulting heteroatom-doped carbon structures.<sup>131</sup> Notwithstanding the above-mentioned advantages, the soft template method also shows limitations. Most of the soft templates (block copolymers and surfactants) are relatively high-cost, and their recovery is difficult.<sup>127</sup>

Thus, the development of new template-free methods is highly desired. These methods generally include the direct transformation of molecular precursors into heteroatom-doped porous carbon materials without adding any external template.

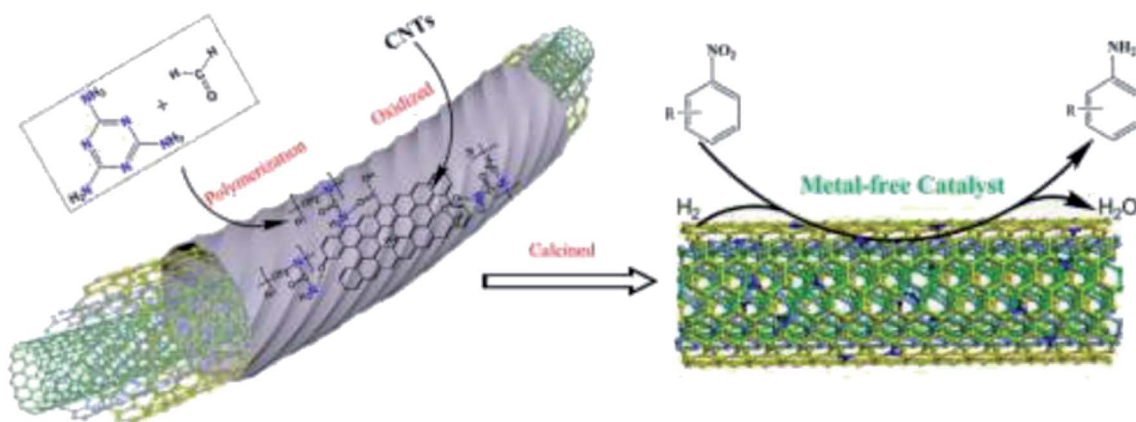


Fig. 4 Preparation of N-CNTs and catalytic application in nitrobenzene hydrogenation. Reprinted with permission from ref. 190. Copyright 2020 Elsevier.



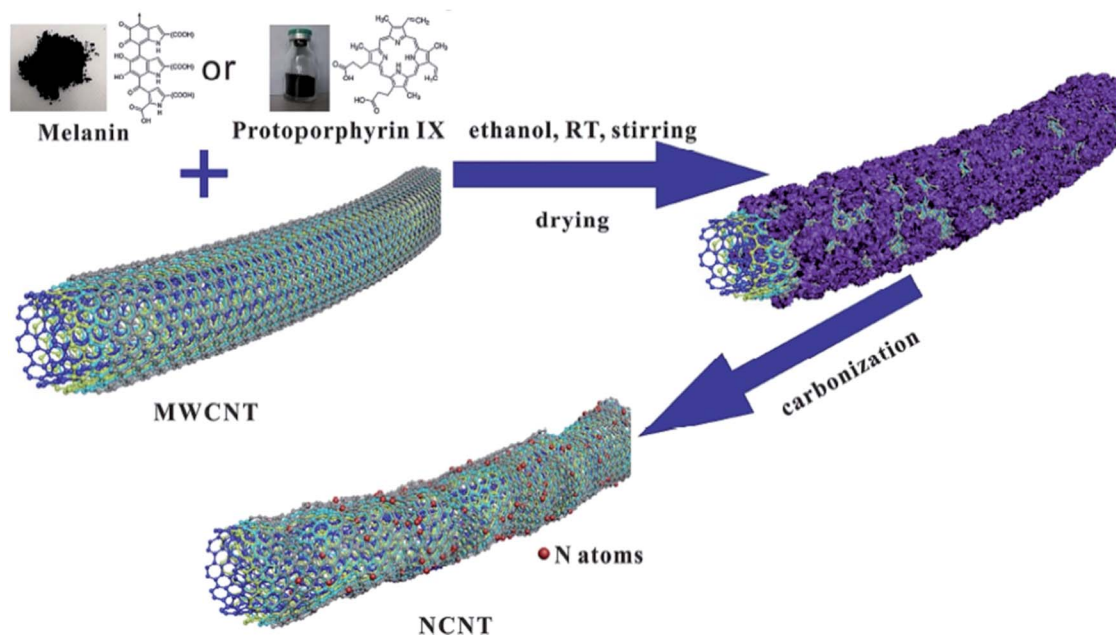


Fig. 5 Preparation of NCNTs. Reprinted with permission from ref. 16. Copyright 2019 Elsevier.

In comparison with template methods, template-free synthesis protocols are facile and benign, although the morphology cannot be controlled as elaborately as that of template-synthesized porous carbon and it is difficult to obtain highly porous carbons.<sup>132</sup>

There exist many heteroatom-containing sources such as biomass, ionic liquids (ILs), polymers, metal-organic framework (MOF), and so on. Besides, among various heteroatom-containing sources,  $\text{NH}_3$ ,<sup>36,133–135</sup> elemental sulfur/thiophene,<sup>136,137</sup> triphenylphosphine,<sup>138,139</sup> and diborane,<sup>140,141</sup> are the most common candidates for N-, S-, P- and B-doping carbon materials, respectively.

Recently, the chemical blowing strategy, which yields micropores during the carbonization process through gas evolution by decomposing ammonium chloride ( $\text{NH}_4\text{Cl}$ ) into  $\text{HCl}$  and  $\text{NH}_3$ , was introduced as a new method to generate highly microporous heteroatom-doped carbons. The possible combination of this approach with thermally decomposable templates, like calcium carbonate ( $\text{CaCO}_3$ ) or magnesium acetate ( $\text{Mg}(\text{OAc})_2$ ), could increase the chemical blowing effect and further introduce auxiliary mesopores.<sup>142</sup>

The dissociation temperature of heteroatom-containing species is one of the most important factors in selecting them as a precursor for *in situ* doping. It is desired that the dissociation temperature of these compounds be close to the growth

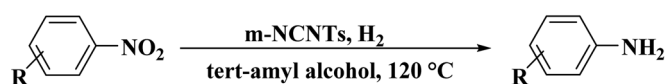
temperature of the carbon.<sup>143</sup> The pyrolysis temperature strongly influences the generation of C–C and C–heteroatom bonds. Generally, a high temperature is favorable for C–C bonds. It is accepted that the post-treatment procedure leads to heteroatom doping only on the surface of carbon materials whereas the direct carbonation method results in the uniform introduction of the heteroatom into the entire carbon framework.<sup>18,144</sup>

Therefore, the selection of the method will significantly influence the conductivity, acidic or basic properties, oxidation stability, and ultimately the performance of the material in a given utilization.<sup>145</sup>

## 2. Recent progress on heteroatom-doped carbon materials as heterogeneous catalysts

### 2.1 Single heteroatom-doped carbons

**2.1.1 N-doped.** Among diverse heteroatoms, N has been the most widely examined for the preparation of heteroatom-doped carbons (as a dopant for C) probably due to the following reasons:<sup>18,48,146,147</sup> (1) the atomic radius of nitrogen is similar to that of carbon with only one more electron in its valence shell, hence the doping of nitrogen into carbon framework can



R = 5-Cl-2-OMe, 4-CHO, 3-Cl-4-I, 4-NC, 4-CONH<sub>2</sub>, [1,2,5]thiadiazole, C<sub>9</sub>H<sub>6</sub>N, 4-COCH<sub>3</sub>, 3,4,5-(Cl)<sub>3</sub>, 2-F-5-COCH<sub>3</sub>, 4-CO<sub>2</sub>CH<sub>3</sub>, 4-Cl, 4-OH, 4-CH=CH<sub>2</sub>

Scheme 4 Chemoselective reduction of different nitroarenes with m-NCNTs.



prevent remarkable lattice mismatch, (2) nitrogen can incorporate into the carbon framework in various locations, therefore leading to multiple possible configurations, (3) N-doped carbon materials have a low health risk and are available and abundant.

Commonly, there are four types of doped nitrogen atoms in a carbon matrix,<sup>148,149</sup> including graphitic N, pyridinic N, pyrrolic N, and pyridinic N-oxide (Fig. 2a) that can be identified using X-ray photoelectron spectroscopy (XPS). The N1s peaks at B.E. of 398.3–399.8, 400.1–400.5, 401.0–401.4, and 404.0–405.6 eV are related to nitrogen atoms in the species of pyridinic, pyrrolic, graphitic, and different N-oxide species, respectively, (Fig. 2b).<sup>150–152</sup>

Graphitic nitrogens, which are also known as quaternary nitrogens, replace carbon atoms situated in the graphitic planes and bond to three C atoms. These N species use four electrons to generate bonds of  $\sigma$  and  $\pi$ , and a remaining electron to occupy the higher-energy  $\pi^*$  state, resulting in the electron-donor property of graphitic nitrogen.<sup>153,154</sup>

Pyridinic nitrogen refers to nitrogen atoms located at the defects or graphitic edges. For the pyridinic N, 2 electrons are applied to generate  $\sigma$ -bonds with C atoms, the other 2 electrons to generate a lone pair, and the fifth electron is in the N  $\pi$ -state.<sup>146,155</sup>

Pyrrolic nitrogens are incorporated into five-member heterocyclic rings and bond to two carbon atoms. These species are thermally unstable, therefore their concentration in carbon materials is low after high-temperature pyrolysis.<sup>156,157</sup>

Pyridinic N-oxides refer to nitrogen atoms bonded to one oxygen atom and two carbon atoms.<sup>158,159</sup> According to experimental and theoretical investigations, N species of graphitic, pyridinic, and pyrrolic reveal efficient interactions with reactants, and hence, they are responsible for N-doped carbon catalysts.<sup>125,160–163</sup>

For example, it has been determined as the active site for the cathodic oxygen reduction reaction in acidic conditions.<sup>164,165</sup>

In another case, the graphitic nitrogen was found to be essential for the reduction of nitroaromatics<sup>16</sup> and oxidation of benzylic alcohols.<sup>166</sup> Also, it has been displayed that the pyrrolic nitrogen promoted the adsorption of the reactants in the acetylene hydrochlorination reaction.<sup>167</sup>

Normally, the presence of nitrogen atoms in the carbon skeleton affords basic property, which boosts the interaction between carbon surface and acidic molecules.<sup>168–172</sup>

More importantly, N doping can greatly influence the charge distribution and spin density of carbon atoms because of the different electronegativity of carbon (2.55) and nitrogen (3.04), leading to the formation of defects in the carbon framework. This in turn can alter the electronic structure of carbon compounds.<sup>123,148,173,174</sup>

**2.1.2 Other heteroatoms-doped carbon materials.** While N-doped carbon materials have experienced many advances over the past decades and provided fascinating concepts, other heteroatoms such as sulfur, phosphorous, and boron have also received worldwide attention in recent years.

**2.1.3 S-doped.** S-doped carbon materials were used in a broad range of potential applications, such as sorption,<sup>175</sup> heterogeneous catalysis,<sup>175</sup> rechargeable batteries,<sup>176</sup> electrochemical capacitors,<sup>177</sup> storage,<sup>178</sup> and energy conversion.<sup>179</sup> The atomic radius of sulfur (S) (105 pm) is much larger compared to C (77 pm), but its electronegativity (2.58) is close to that of C (2.55). Therefore, in comparison with N, P, or B doping, the change of charge distribution is much less for S doping. As result, the improvement of S-doped carbon materials performance is usually ascribed to the modifications in spin density.<sup>180,181</sup>

**2.1.4 P-doped.** Phosphorus (P), an element of the V group of the periodic table, possesses the same number of valence electrons as N and indicates almost analogous chemical and electronic features.

But it has a bigger atomic radius and lower electronegativity (2.19) than nitrogen and carbon atoms. Thus, P doping can produce defect sites and effectively modify the chemical reactivity and electronic properties of carbon materials (pristine carbons). These surface modifications result in an improvement in the performance of catalysts.<sup>18,156,182</sup>

**2.1.5 B-doped.** Boron (B) is the left neighbor of carbon in the periodic table with basically incomparable and unique properties, which make it a suitable selection for the incorporation into carbon compounds. B substitution in the graphitic framework not only improves the thermal stability of the carbon structures but also alters the (optical) electrical and electronic peculiarities, originating from the high electron-withdrawing ability of boron (electronegativity: 2.04).<sup>18,183–185</sup>

## 2.2 Dual- and tri-heteroatom doped carbons

Co-doping by two or three heteroatoms with different electronegativities can display a unique electron distribution and further enhances the catalytic activity of the carbon materials. This intrinsic feature of carbocatalyst can be related to the synergistic effect of incorporated elements.<sup>186</sup>

## 2.3 Catalytic applications

In recent years, the utilization of metal-free heteroatom-doped carbon catalysts in chemical reactions has shown rapid growth. The main purpose of this review is to highlight the current researches in the field of organic transformations catalyzed by heteroatom-doped carbons reported in the literature.

Different applications of these catalysts in the organic reactions are summarized in this section.

**2.3.1 Reduction reactions.** Zhang and co-workers<sup>187</sup> prepared nitrogen-doped carbons (NC-T) through the thermal treatment of the chitosan and melamine as the crude materials. The application of these catalysts was investigated in the reduction of nitro compounds. With increasing pyrolysis temperature, the activity of NC-T increased due to the enhanced ratio of N species of graphitic, which are active sites for reaction.

NC-950 was found to be highly effective for the selective hydrogenation of nitro compounds in hexane at 90 °C using hydrazine hydrate ( $\text{N}_2\text{H}_4 \cdot \text{H}_2\text{O}$ ) as the reductant, affording

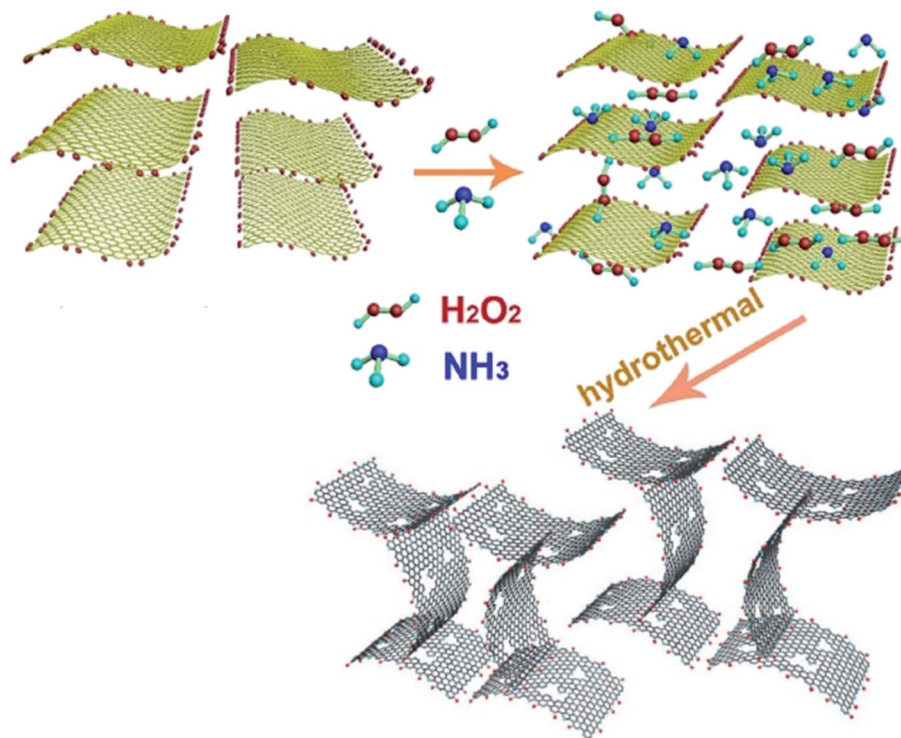
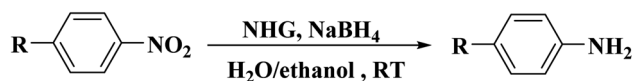


Fig. 6 Preparation of NHG. Reprinted with permission from ref. 191. Copyright 2019 Elsevier.



R = H, 4-CH<sub>3</sub>, 4-Cl, 4-CO<sub>2</sub>H, 4-Br, 4-NC

Scheme 5 Hydrogenation of nitrobenzenes over NHG.

respective amines in yields ranging from 87.5 to 100% (Scheme 2). The catalytic activity of NC-950 was compatible or even superior to those of the reported metal catalysts.

The use of nitrogen-doped graphene nanosheets, NG, as metal-free catalysts in the *N*-formylation of amines was described by Chen *et al.*<sup>188</sup> NG catalysts were synthesized through direct calcination and activation of a mixture of urea,

graphene nanosheets, and potassium carbonate, followed by leaching with HCl solution and washing with deionized H<sub>2</sub>O to eliminate residual K. A broad range of amines (aliphatic, aromatic and heterocyclic amines) were effectively transformed into the desired products in the attendance of NG<sub>U/K-900</sub> (calcination at 900 °C) and CO<sub>2</sub>/PhSiH<sub>3</sub> under mild conditions (Table 1). Also, the catalyst displayed outstanding reusability during 12 cycles with almost unchanged catalytic efficiency.

Very recently, another strategy for the preparation of a series of N-doped carbon nanotubes (NCNTs) was reported by Li *et al.*<sup>189</sup> (Fig. 3). The resulting materials were synthesized using the pyrolysis of *in situ* polymerized pyrrole on the surface of CNTs under a N<sub>2</sub> flow at different temperatures.

To improve the catalytic performance, the outside diameter of CNTs, carbonization temperature, and the concentration of



Fig. 7 Preparation of N-GQDs and N-RGO mesh. Reprinted with permission from ref. 194. Copyright 2018 John Wiley and Sons.





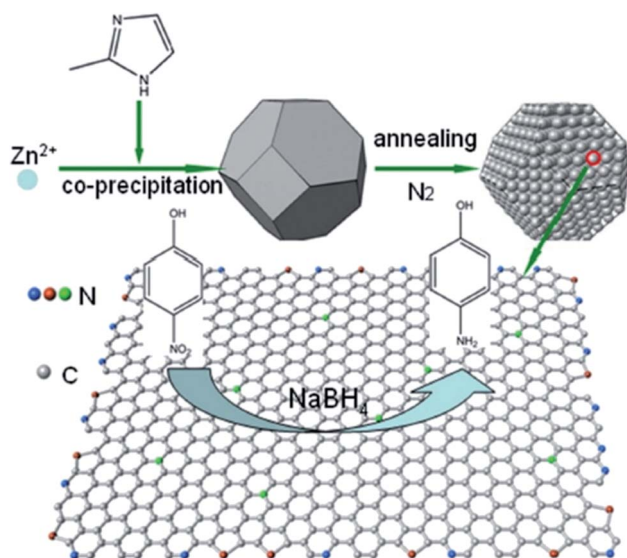
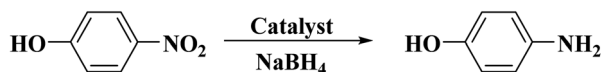


Fig. 8 Preparation of N-C for the reduction of 4-nitrophenol. Reprinted with permission from ref. 195. Copyright 2018 John Wiley and Sons.



Scheme 6 Hydrogenation of *p*-nitrophenol using SG.

pyrrole were examined. The characterization data exhibited that the optimal NCNTs-800 had a unique structure with similar contents of graphitic and pyrrolic N.

The catalytic efficiency of NCNTs-800 was assessed for the selective reduction of various nitroaromatics, affording excellent selectivity even in the attendance of a fragile iodo group (Scheme 3). In addition, the catalyst was used in seven successive runs with a negligible decrease in activity.

In 2019, Hao and co-workers<sup>190</sup> introduced a series of N-doped carbon nanotubes (CNTs) with diverse nitrogen amounts and species and defects as metal-free catalysts for the hydrogenation of nitrobenzene (Fig. 4). These catalysts were obtained *via* an *in situ* preparation and post nitridation treatment. The potential active centers of N-doped CNTs were examined in terms of DFT calculations of H adsorption on CNTs and N species as well as catalytic activity in the reduction of nitrobenzene. N-doped carbon nanotubes synthesized by post nitridation showed good performance, achieving about 60% conversion of nitrobenzene and around 90% selectivity for aniline. Also, the catalyst afforded stable product yield during six runs. Pyrrolic N species in the N-doped CNTs were found to

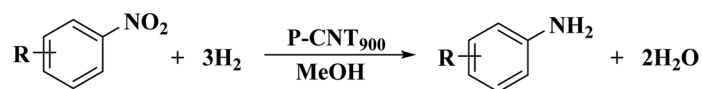
be active sites for hydrogen activation using chemisorption and dissociation of molecules of hydrogen during the reaction.

Other metal-free N-CNTs were prepared with a pyrolysis process using protoporphyrin IX or melanin as the dopant by Li *et al.*<sup>16</sup> (Fig. 5). Multiwalled carbon nanotubes with diverse diameters were used as the catalyst, and their efficiency was compared with carbon black and graphene. The amount of graphitic N was efficiently controlled by changing the heating rate during the carbonization process. The characterization data showed that the N heteroatoms remarkably destroyed the carbon skeleton of CNTs, resulting in a reduction in the crystallinity. The synthesized N-CNTs were assessed for the reduction of 4-nitrophenol to 4-aminophenol under 120 °C and 2 MPa H<sub>2</sub> and N-CNTs with outer diameters of ≤20 nm fabricated using melanin at 800 °C indicated remarkable enhanced catalytic performance. The applicability and chemoselectivity of the optimal catalyst were further explored for a wide variety of substituted nitroarenes including electron-withdrawing and electron-donating groups and products were afforded in high yield and selectivity (Scheme 4). The authors found a good correlation between the graphitic N amount of N-CNTs and catalytic performance. Moreover, recycling tests displayed that the catalyst was highly stable without the loss of its catalytic activity after six times.

Xi and co-workers<sup>191</sup> described a simple one-pot hydrothermal synthesis procedure for the preparation of an effective nitrogen-doped holey graphene (NHG), in which graphene oxide was served as a starting material, NH<sub>3</sub> as a nitrogen source, and hydrogen peroxide as etching agent (Fig. 6). During the formation of this carbocatalyst, several reactions could happen. GO nanosheets were self-assembled, reduced, chemically etched, and simultaneously doped with N.

This carbocatalyst with high N loading, unique hierarchical porous structure, large specific surface area, and good hydrophilicity exhibited an excellent catalytic activity for the reduction of five organic dyes (MB, RhB, CR, MO, and 4-NP) in the presence of NaBH<sub>4</sub> as a reductant in aqueous solution at ambient temperature. The authors also extended the application of the NHG to the hydrogenation of different substituted nitrobenzenes to study its applicability. These reactions were performed using NaBH<sub>4</sub> in H<sub>2</sub>O/EtOH mixture at ambient temperature and provided the corresponding anilines in superb yields (Scheme 5). In 4-NP reduction, the catalyst delivered a TOF higher than those of the many noble-metal-based catalysts, commercial Pd/C, and other previously reported carbocatalysts.

Yuan *et al.*<sup>192</sup> reported sol-gel routes to synthesize two N-doped porous carbon materials (NC-1 and NC-2) using sucrose and citric acid as carbon precursors and *in situ*-formed



R = H, 4-Me, 3-Me, 2-Me, 4-OMe, 4-NH<sub>2</sub>, 2-NH<sub>2</sub>, 4-CHO, 4-NC, 2-NO<sub>2</sub>, 4-F, 4-Cl, 4-Br

Scheme 7 Reduction of nitrobenzenes catalyzed by P-CNT.



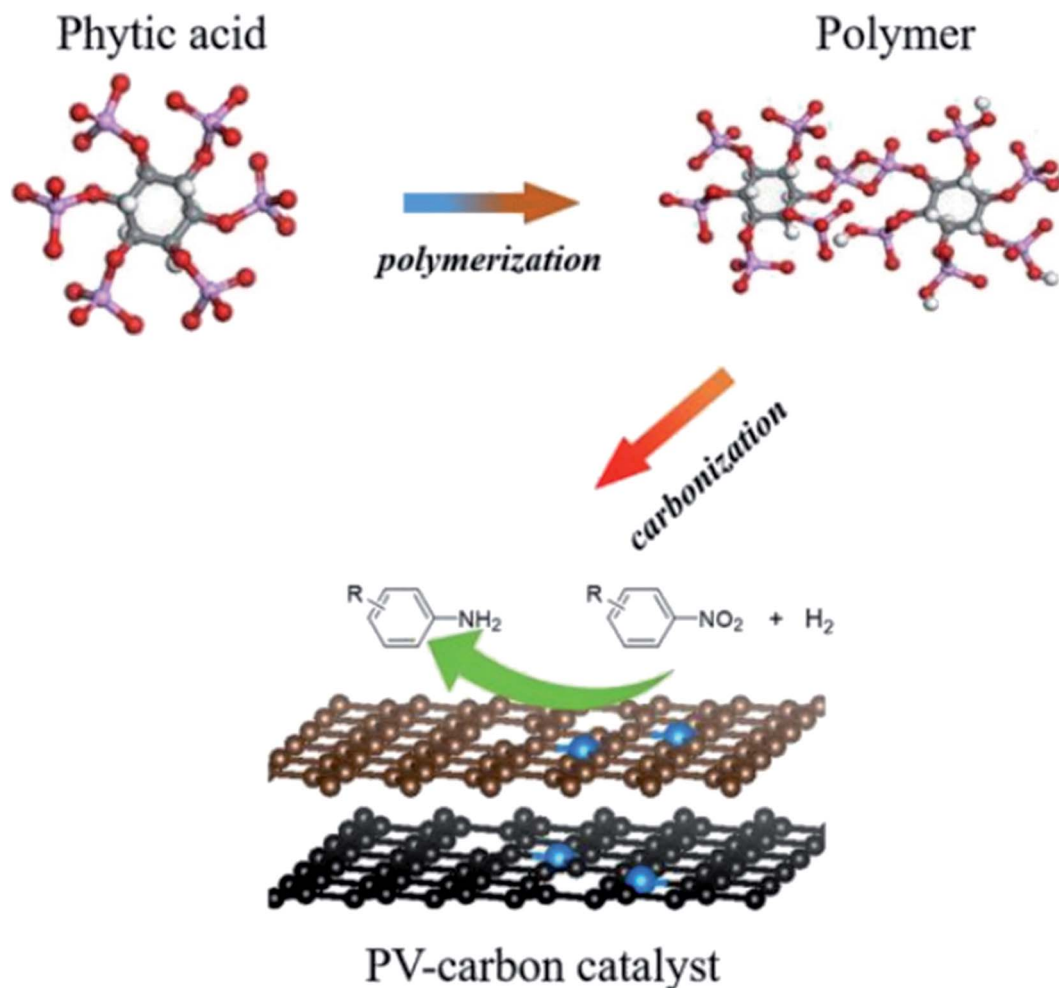
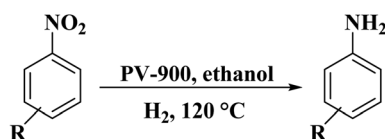


Fig. 9 Preparation of PV-carbon catalyst. Reprinted with permission from ref. 198. Copyright 2017 John Wiley and Sons.

aluminophosphate framework as a template (1 and 2 are the P/Al ratios in the starting CA/AlPO composite). These materials acted as highly effective metal-free catalysts for the hydrogenation of nitrobenzene in an aqueous solution using sulfide and showed much superior catalytic efficiency in comparison with graphite oxide or carbon black catalysts reported in the literature. In addition, NC-2 displayed better removal performance compared with NC-1 material. Also, Both NC-1 and NC-2 were reused for more than five cycles. The presence of numerous nitrogen- and oxygen-containing functional groups on the surface of the N-doped carbon improved their catalytic activity. Furthermore, other features of these catalysts such as tunable surface polarity, enhanced electron transfer ability, and

large surface area, were key parameters in increasing their catalytic performance.

In 2017, a well-defined 3-D N-doped graphene foam (3D-NGF) was reported by Liu *et al.*<sup>193</sup> For the preparation of 3D-NGF, the achieved graphene oxide was spread in H<sub>2</sub>O by sonication and frozen with liquid N. In the following, the resultant material was processed in a vacuum freeze-drying apparatus for 2 days to prepare GO foam. Finally, the GO form was treated with the mixture gas of 50% NH<sub>3</sub> and 50% Ar flowing at 750 °C for 2 h. The 3D-NGF demonstrated high catalytic activity and excellent durability toward the reduction of *p*-nitrophenol to *p*-aminophenol because of the 3D foam-like structure as well as the synergistic effect between the nitrogen-doping, leading to



R = 4-CHO, 4-CO<sub>2</sub>H, 2-Cl, 4-Cl, 3-Cl, 4-F, 4-Br, 4-Me, 4-OMe, 4-OH, 3-OH, 4-CH<sub>2</sub>OH, 4-C≡CH

Scheme 8 Reduction of nitroarene compounds catalyzed by PV-900.



Table 2 Hydrogenation of nitroarenes using B-OLC-2 and B-CNTs-2

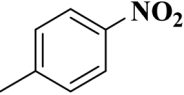
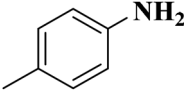
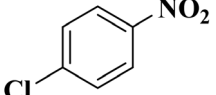
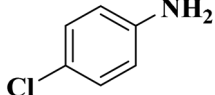
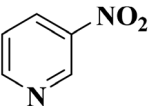
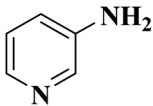
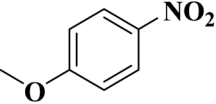
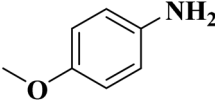
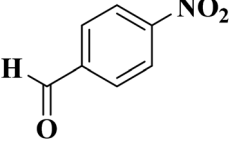
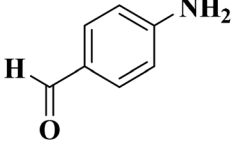
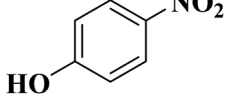
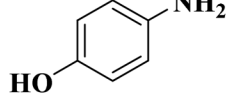
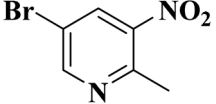
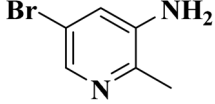
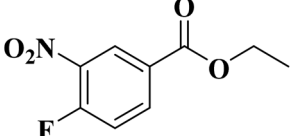
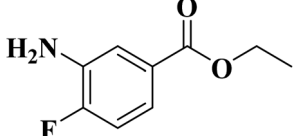
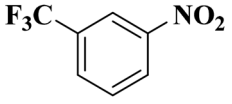
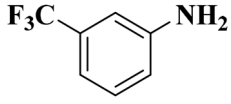
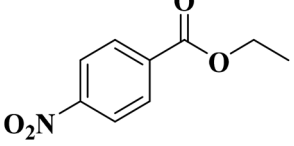
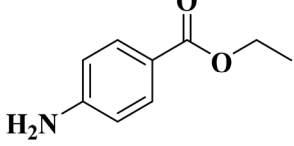
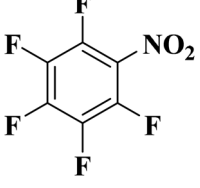
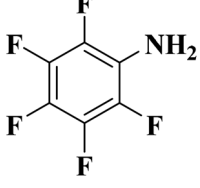
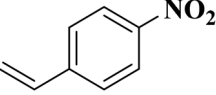
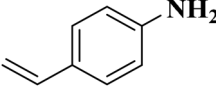
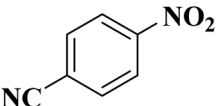
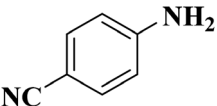
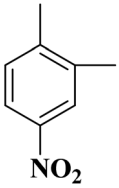
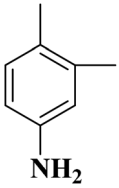
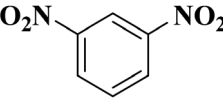
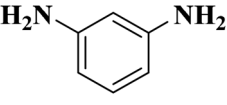
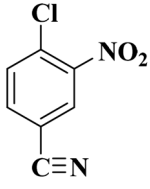
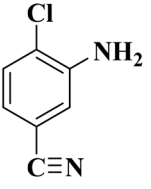
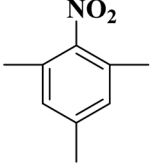
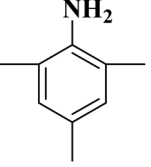
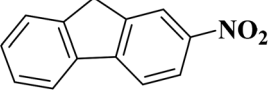
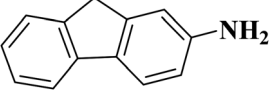
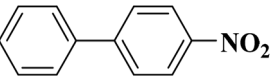
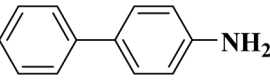
| Substrate   | Product   | Catalyst | Con. (%) | Sel. (%) |
|---|---|----------|----------|----------|
|    |    | B-OLC-2  | >99      | 96.5     |
|   |   | B-CNTs-2 | >99      | 97.3     |
|    |    | B-OLC-2  | >99      | 94.5     |
|   |   | B-CNTs-2 | >99      | 96.3     |
|    |    | B-OLC-2  | >99      | 93.0     |
|   |   | B-CNTs-2 | >99      | 94.9     |
|    |    | B-OLC-2  | >99      | 96.2     |
|   |   | B-CNTs-2 | >99      | 97.1     |
|    |    | B-OLC-2  | >99      | 96.8     |
|   |   | B-CNTs-2 | >99      | 97.4     |
|   |   | B-OLC-2  | >99      | 95.4     |
|   |   | B-CNTs-2 | >99      | 93.9     |
|  |  | B-OLC-2  | >99      | 93.2     |
|   |   | B-CNTs-2 | >99      | 92.9     |
|  |  | B-OLC-2  | >99      | 89.02    |
|   |   | B-CNTs-2 | >99      | 90.3     |
|  |  | B-OLC-2  | >99      | 94.2     |
|   |   | B-CNTs-2 | >99      | 93.1     |
|  |  | B-OLC-2  | >99      | 89.2     |
|   |   | B-CNTs-2 | >99      | 90.3     |
|  |  | B-OLC-2  | >99      | 91.9     |
|   |   | B-CNTs-2 | >99      | 90.2     |
|  |  | B-OLC-2  | >99      | 88.4     |
|   |   | B-CNTs-2 | >99      | 90.9     |



Table 2 (Contd.)

| Substrate   | Product   | Catalyst | Con. (%) | Sel. (%) |
|---|---|----------|----------|----------|
|    |    | B-OLC-2  | >99      | 92.2     |
|   |   | B-CNTs-2 | >99      | 91.2     |
|    |    | B-OLC-2  | >99      | 96.9     |
|   |   | B-CNTs-2 | >99      | 97.1     |
|    |    | B-OLC-2  | >99      | 96.7     |
|   |   | B-CNTs-2 | >99      | 97.1     |
|    |    | B-OLC-2  | >99      | 90.2     |
|   |   | B-CNTs-2 | >99      | 90.6     |
|   |   | B-OLC-2  | >99      | 96.1     |
|   |   | B-CNTs-2 | >99      | 95.3     |
|  |  | B-OLC-2  | >99      | 97.2     |
|   |   | B-CNTs-2 | >99      | 97.0     |
|  |  | B-OLC-2  | >99      | 97.9     |
|   |   | B-CNTs-2 | >99      | 98.0     |

change in electronic property. Also, the 3D structure can efficiently inhibit the agglomeration of the graphene, and thus provides an effective interface for the hydrogenation to take place.

Dai and colleagues<sup>194</sup> developed a hydrothermal strategy for the fabrication of N-doped reduced graphene oxide meshes from pristine GO sheets in the presence of  $\text{NH}_4\text{OH}$  as a nitrogen source at elevated temperature (Fig. 7). The N-RGO meshes functioned as an active catalyst to reduce 4-nitrophenol.

These N-RGO meshes demonstrated new catalytic behaviors of dramatically increased catalytic efficiency, adjustable catalytic kinetics and reusability, and strikingly reduced activation energy. Such catalytic features were attributed to the synergetic effects between graphitic N atoms and structural defects resulting from the selective etching of nanopores. Also, the N-RGO meshes were capable to conduct reactions in continuous flow.

In 2017, Wang and Chen<sup>195</sup> used the N-doped carbon (N-C) catalytic system derived from ZIF-8 as a precursor and

sacrificial agent for the reduction of 4-nitrophenol to 4-aminophenol (Fig. 8). Compared to some of the previously metal catalysts, N-C showed good performance, high durability, recyclability, and minimal pollution. The N-C catalysts synthesized through carbonization at various temperatures possessed diverse catalytic performance as well as different N amounts. Among them, N-C800 with the highest pyridine nitrogen amount displayed superior catalytic performance.

In 2017, Wang and co-workers<sup>196</sup> developed a new protocol to prepare sulfurized graphene (SG) nanomaterials through a ball-milling approach. The activity of SG with a uniform dispersion of S and flake-like morphology was tested in the hydrogenation of *p*-nitrophenol to *p*-aminophenol in the attendance of sodium borohydride as the reductant (Scheme 6). The catalytic mechanism of SG was examined by density functional theory (DFT). The effects of the kinetic parameters including reaction temperatures, catalyst amounts, initial reducer concentrations, and various initial *p*-NP concentrations were investigated.





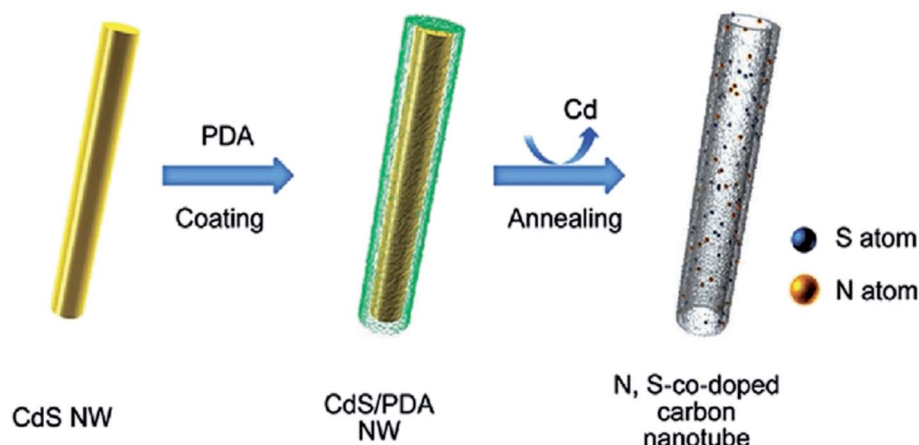


Fig. 10 Preparation of S,N co-doped hollow carbon nanotubes. Reprinted with permission from ref. 200 Copyright 2016 John Wiley and Sons.

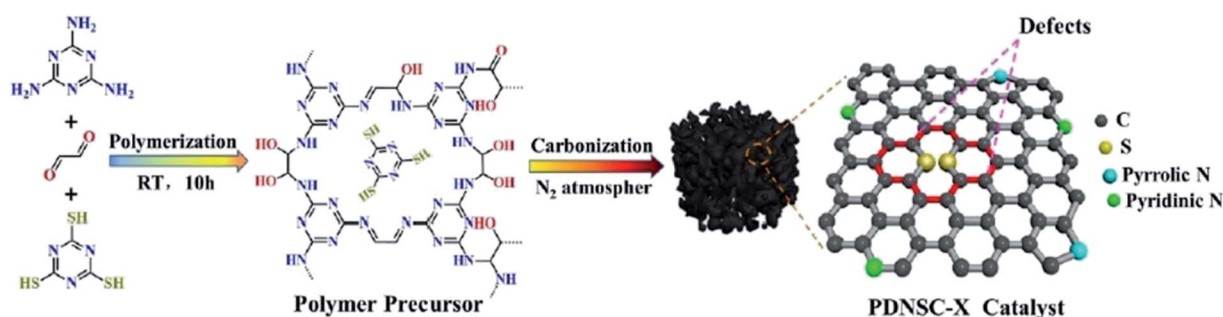
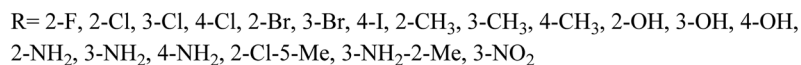
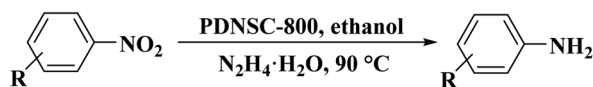


Fig. 11 Preparation of PDNSC-X catalyst. Reprinted with permission from ref. 201. Copyright 2020 Royal Society of Chemistry.



Scheme 9 Hydrogenation of nitrobenzenes using PDNSC-800.

Moreover, the thermodynamic factors such as activation entropy and enthalpy were calculated.

The use of phosphorus-doped carbon nanotubes (P-CNT) as a catalyst in the reduction of nitrobenzene to aniline using H<sub>2</sub> as a reducer was described by Chen and co-workers<sup>197</sup> in 2019.

Furthermore, diversely functionalized nitroarenes with broad industrial interests were successfully converted into relevant products with superb yields and selectivities (Scheme 7). P-CNT was synthesized by pyrolysis a mixture of CNT, Ph<sub>4</sub>PCl, and K<sub>2</sub>CO<sub>3</sub> at 900 °C under N<sub>2</sub> atmosphere for 2.0 h. Besides, recycling tests of the P-CNT displayed that the catalyst was highly durable and maintained its activity and selectivity for up to eight runs. In addition to reduction, catalytic transfer hydrogenation of aniline was performed with P-CNT by applying various hydrogen sources such as formic acid/triethyl

amine (HCOOH/Et<sub>3</sub>N), carbon monoxide/water (CO/H<sub>2</sub>O), and hydrazine hydrate (N<sub>2</sub>H<sub>4</sub>·H<sub>2</sub>O).

In another study, polymerization and carbonization of phytic acid were described by Zou and co-workers<sup>198</sup> to fabricate carbon catalyst with an adjustable concentration of P-dopant and lattice defect (Fig. 9). The as-prepared catalyst (PV-900) exhibited excellent performance, outstanding selectivity, and durability in the reduction of nitroarene compounds (Scheme 8), much higher than nickel, metal-oxide, and carbon-based catalysts which were recently reported. DFT calculations indicated that the combination of lattice defect and P-dopant in carbon can change the band structure as a metal-like and cause remarkable electron delocalization, and thus easily activate both nitro group and H<sub>2</sub>. Additionally, the reduction efficiency was linearly dependent on the defect concentration and P-doping.

Su *et al.*<sup>199</sup> synthesized two kinds of boron-doped carbon materials (carbon nanotubes (B-CNTs) and onion-like carbon (B-OLC)) through high-temperature carbonization of acid-treated CNTs or nanodiamond and boron acid as B precursor. The catalytic performances of the catalysts were surveyed in the hydrogenation of nitroarenes (Table 2) and compared with pristine CNTs and OLC samples. The results showed that substitutional boron species  $BC_3$  played an important role in increasing the catalytic activity and efficient application of hydrazine hydrate.

Song and colleagues<sup>200</sup> developed a “solid dual-ions-transformation reaction” strategy to prepare environmentally friendly S,N co-doped hollow carbon nanotubes (Fig. 10). The procedure used for the fabrication of S,N co-doped hollow carbon nanotubes involved three steps: the preparation of CdS nanowires as both source of sulfur and hard template; *in situ* self-polymerization of dopamine on the surface of CdS (PDA acted as the sources of N and C as well as the reductant); and carbonization. Sulfur and nitrogen amount in the final materials could be simply adjusted by altering the carbonization

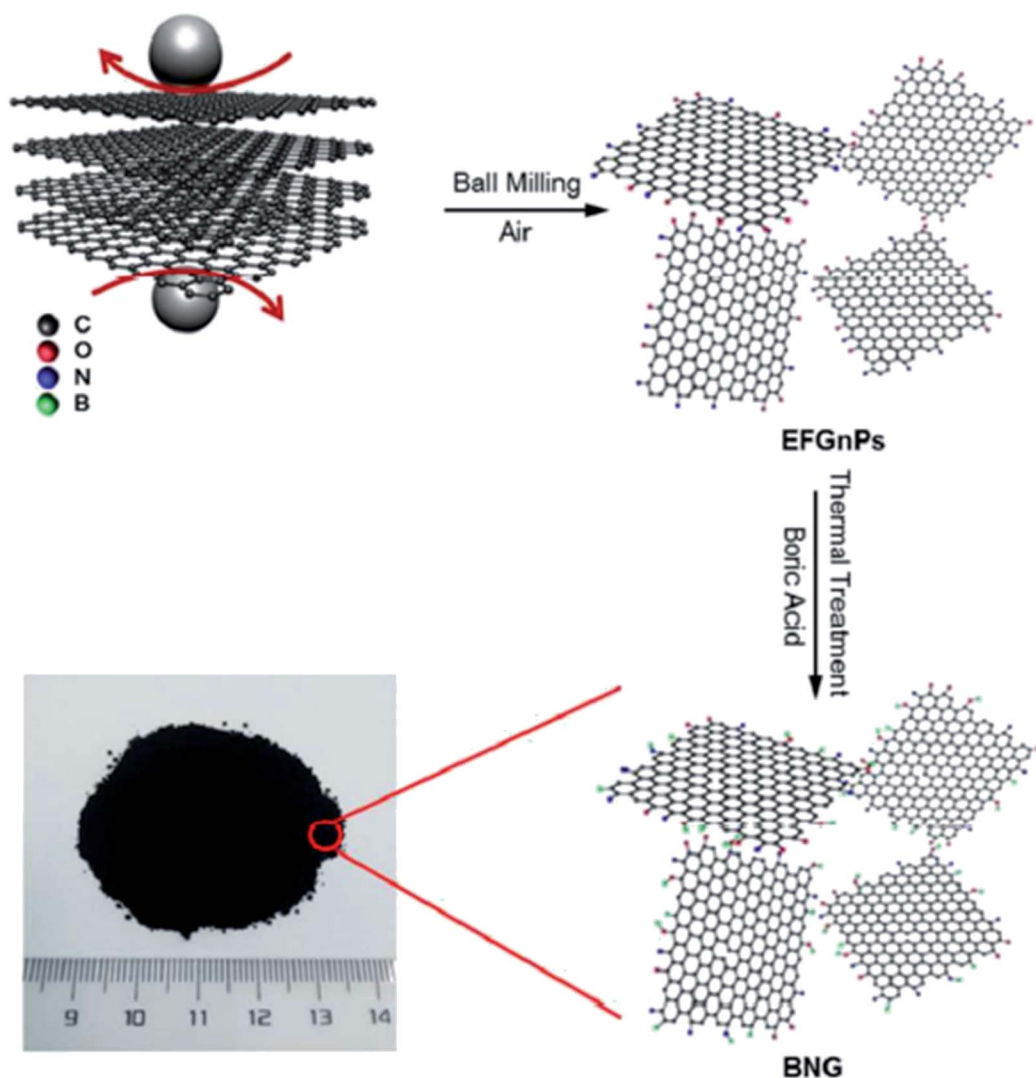
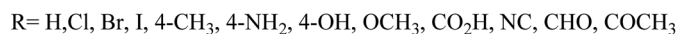
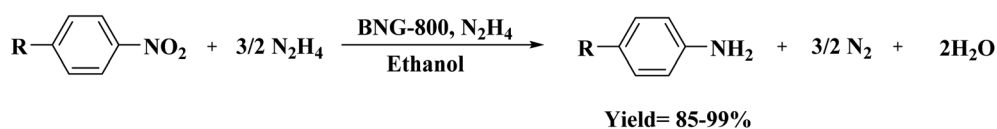


Fig. 12 Preparation of BNG. Reprinted from ref. 202. Royal Society of Chemistry.



Scheme 10 Hydrogenation of nitroarenes catalyzed by BNG-800.



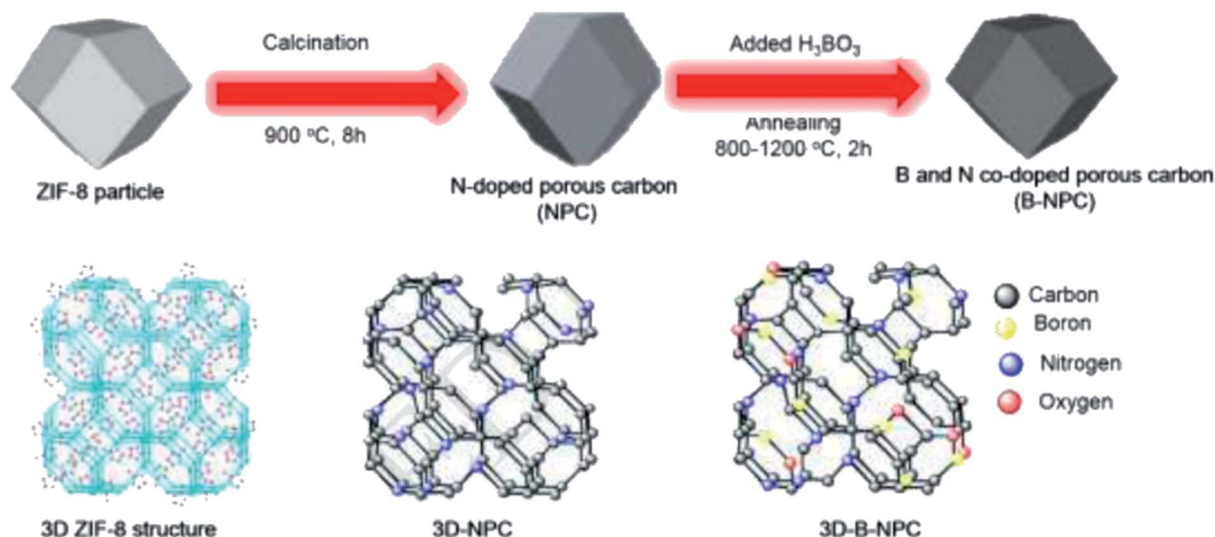
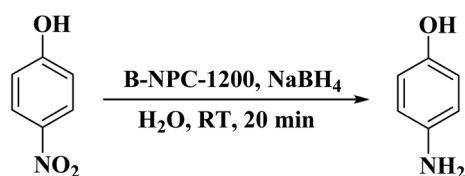


Fig. 13 Preparation of B-NPC. Reprinted with permission from ref. 203. Copyright 2019 Elsevier.



Scheme 11 Reduction of p-NP catalyzed by B-NPC-1200.

temperature. The catalytic activity of S,N co-doped carbon nanotubes was evaluated in the hydrogenation of 4-amino-phenol at ambient temperature using  $\text{NaBH}_4$ .

In 2020, a convenient two-steps method to fabricate polymer-derived N,S co-doped carbons (PDNSC-X) was offered by Long

*et al.*<sup>201</sup> The starting material was prepared from polymerization of trithiocyanuric acid, glyoxal, and melamine. Then, the pyrolysis of synthesized polymer containing numerous S and N active species as a precursor at four different temperatures (600, 700, 800, and 900 °C) under  $\text{N}_2$  atmosphere afforded PDNSC-X materials (Fig. 11). PDNSC-800 displayed outstanding catalytic performance and high selectivity toward the hydrogenation of a broad variety of functionalized nitrobenzenes (Scheme 9) as well as the selective oxidation of ethylbenzene due to the abundant N- and S-containing active sites, a hierarchically porous structure, synergistic effects of a high surface area, and defect formation. In addition, the PDNSC-800 catalyst exhibited high durability and reusability in both reactions even after eight runs. Also, this study clarified the relationship between the

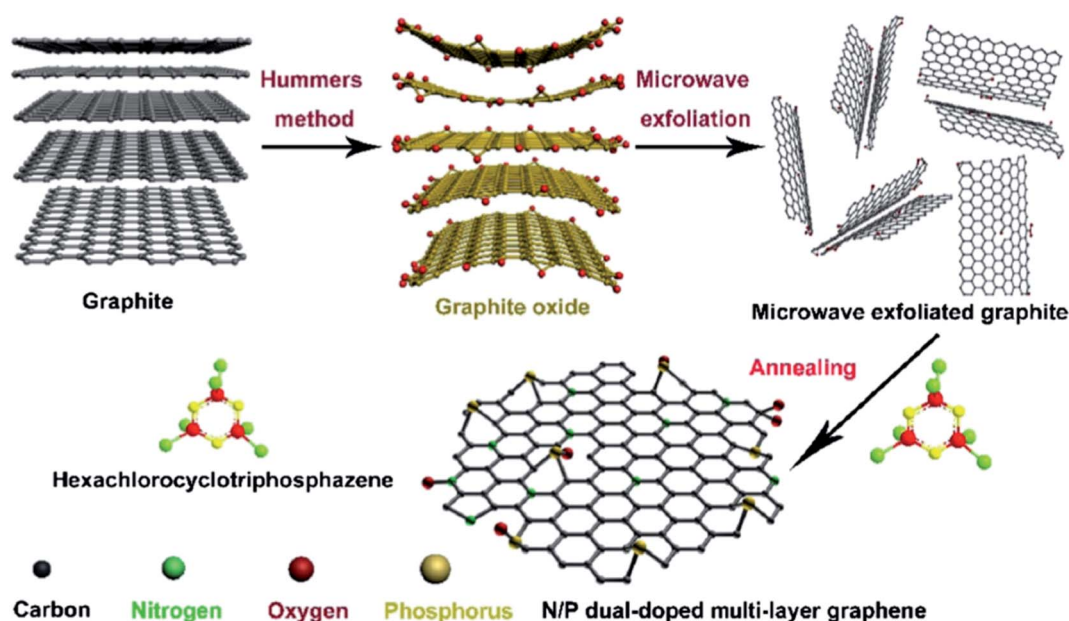
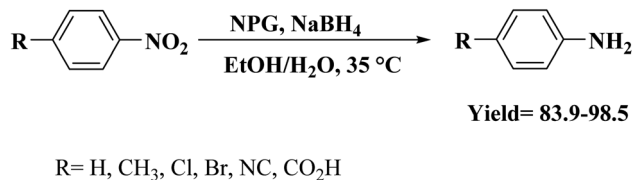
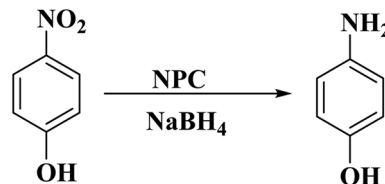


Fig. 14 Preparation of NPG. Reprinted with permission from ref. 204. Copyright 2018 Elsevier.



Scheme 12 Hydrogenation of nitroarenes catalyzed by NPG.



Scheme 13 Reduction of p-NP in the presence of NPC.

different doped atoms in N,S co-doped catalysts and superb selectivity in non-metallic catalytic synthesis.

In 2018, Li *et al.*<sup>202</sup> employed ball-milling and thermal methods for the preparation of B and N co-doped graphene-like carbon (BNG) materials (Fig. 12). To prepare BNG catalysts, initially, the edge-selectively functionalized graphene nanoplatelets (EFGnPs) were synthesized using ball milling of the pure graphite, and then the obtained EFGnPs and boric acid were pyrolyzed in various temperatures. The catalytic performance of these materials was tested in the reduction of 4-chloronitrobenzene to 4-chloroaniline and among them, BNG-800 was the best catalyst (was much more active than other catalysts). Authors found that the type of B species possessed a great influence on the reaction and the BNG bearing the most B/N showed the best catalytic efficiency, demonstrating that the doped B/N in BNG was one of the important active centers in promoting this reaction.

The scope of the reaction was explored for a broad range of functionalized nitroarenes; high levels of yield were observed for the corresponding anilines under the optimized reaction conditions (Scheme 10).

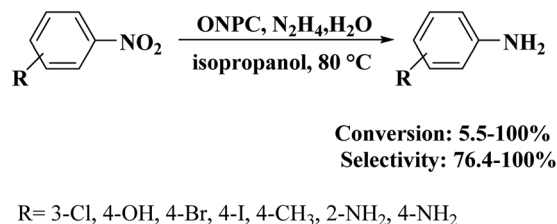
Also, the BNG-800 could be easily and effectively reused for six successive cycles without the formation of dehalogenation products for halogen-substituted nitroarenes.

In 2019, Chung and co-workers<sup>203</sup> reported the synthesis of three-dimensional boron and nitrogen heteroatom-doped porous carbons (3DBNPCs) through carbonization of the mixture of nitrogen-doped porous carbons (NPC) (derived from

ZIF-8) and boric acid at different temperatures (Fig. 13). As fabricated B-NPC-1200 exhibited superior catalytic prowess in the hydrogenation of p-NP (Scheme 11) with a high reaction rate constant and low activation energy. The doping of boron atoms into nitrogen-doped 3D porous carbon considerably improved the electrical conductivity and the catalytic activity of B-NPC-1200. Also, the synergistic effects between oxygen, boron, and nitrogen atoms could create the strongly active sites that were responsible for the lowering of the activation energy in the structure of the catalyst.

The B-NPC-1200 was further applied for the reduction of various nitro aromatics. Besides, the catalyst could be reused in five successive cycles without an obvious decrease in its activity. The authors suggested that the content and type of boron precursor can influence the structure of catalyst including properties and morphologies.

In 2018, Xi and coworkers<sup>204</sup> described an effective and facile route to prepare N,P-dual-doped graphene (NPG) carbocatalyst.



Scheme 14 Hydrogenation of nitroarenes catalyzed by ONPC.

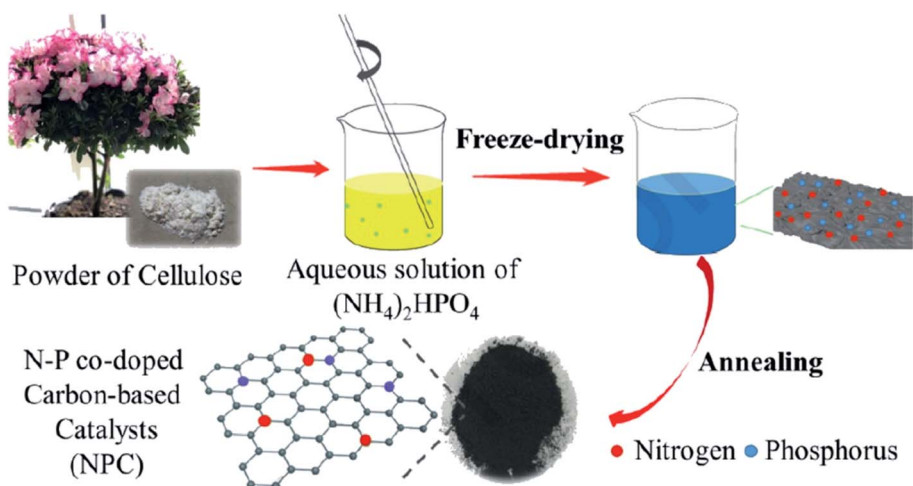


Fig. 15 Preparation of NPC. Reprinted with permission from ref. 186. Copyright 2020 Elsevier.





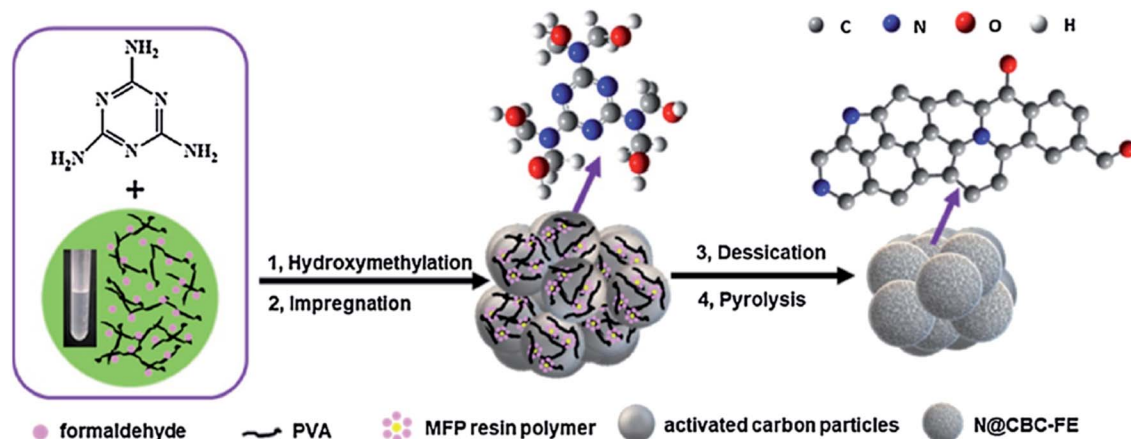


Fig. 16 Preparation of N@CBC-FE catalysts. Reprinted with permission from ref. 206. Copyright 2021 Elsevier.

The synthesis process consisted of oxidation of graphite powders, microwave exfoliation of graphite oxide, and finally, annealing of microwave-exfoliated graphite (MEG) and hexachlorocyclotriphosphazene (HCCP) mixture under an inert atmosphere at 700 °C (Fig. 14). HCCP functioned as both P and N sources. NPG showed excellent efficiency, selectivity, durability, and good reusability toward hydrogenation of 4-NP in aqueous media.

The catalytic performance was higher compared with other carbocatalysts based on graphene and even similar to that of commercial Pd/C (5%) and many previously reported noble metal-based catalysts.

Furthermore, the application of NPG catalyst could be extended to the hydrogenation of other substituted nitroarenes (Scheme 12).

Recently, Pu and co-workers<sup>186</sup> reported the synthesis of a metal-free catalyst containing nitrogen and phosphorus co-doped carbon (NPC) material (Fig. 15). The abundant and benign  $\alpha$ -cellulose crystallite served as a carbon source, while ammonium phosphate supplied the nitrogen and phosphorus components. The sample was fabricated through the mixing of precursors, freeze-drying followed by pyrolyzing under nitrogen at 800 °C. The catalytic efficiency of the heterogeneous cellulose-derived N/P-doped carbon material with flake-like morphology was assessed for the reduction of p-NP (Scheme 13), affording high TOF of  $2 \times 10^{-5}$  with an apparent kinetic rate constant of  $0.0394 \text{ min}^{-1}$ , activation energy of  $21.55 \text{ kJ mol}^{-1}$ , and excellent yield because of the synergistic effect of phosphorus and nitrogen dopants.

Structural engineering of carbon-based materials is an innovative method to adjust their chemical and physical

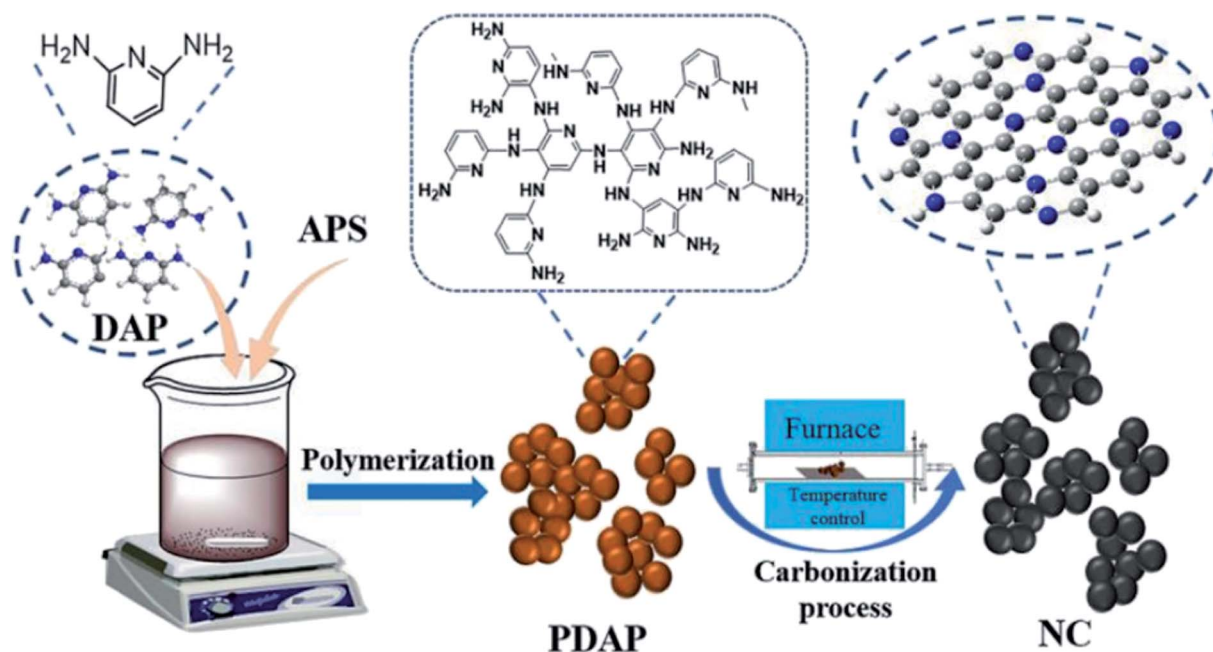


Fig. 17 Preparation of NC. Reprinted with permission from ref. 207. Copyright 2021 Elsevier.

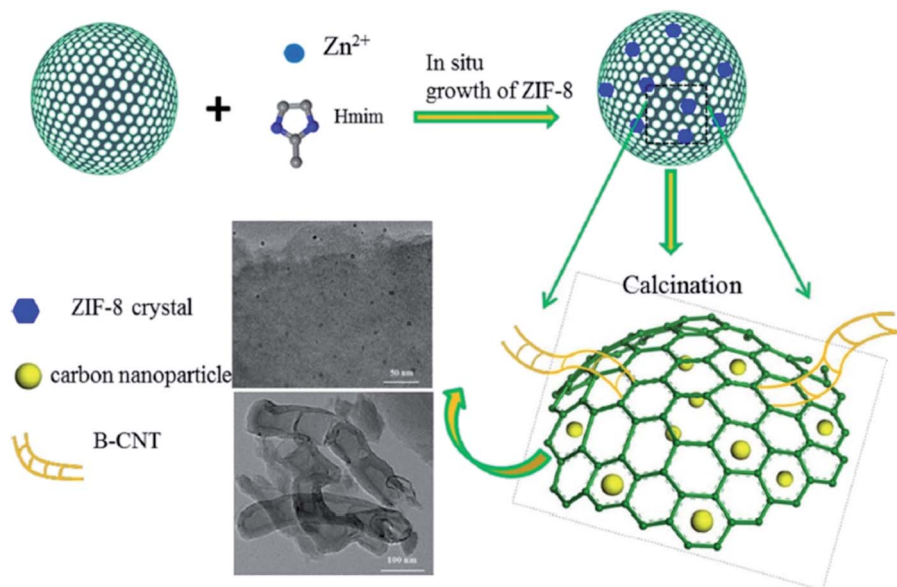


Fig. 18 Preparation of ZIF-8/SAC composite. Reprinted with permission from ref. 209. Copyright 2018 Springer Nature.

features, which are directly attributed to their catalytic behaviors.

An environmentally benign and inexpensive procedure was disclosed to obtain oxygen and nitrogen co-doped porous carbon (ONPC) using coal tar- and residual oil-derived asphaltene as starting material, by Shen and colleagues<sup>205</sup> in 2018. Firstly, the synthesized asphaltene as parent carbon was oxidized by  $\text{HNO}_3$  to dope O groups and next activated using

potassium hydroxide combined with urea to introduce N species. The resulting ONPC was able to catalyze the hydrogenation of nitroarenes to corresponding anilines in the presence of hydrazine hydrate (Scheme 14). This catalyst indicated a significantly better catalytic activity relative to carbon black, activated carbon (AC), and un-doped porous carbon (PC), owing to co-doping of two different atoms (O and N), developed pore structure, and huge surface area. Experimental studies using

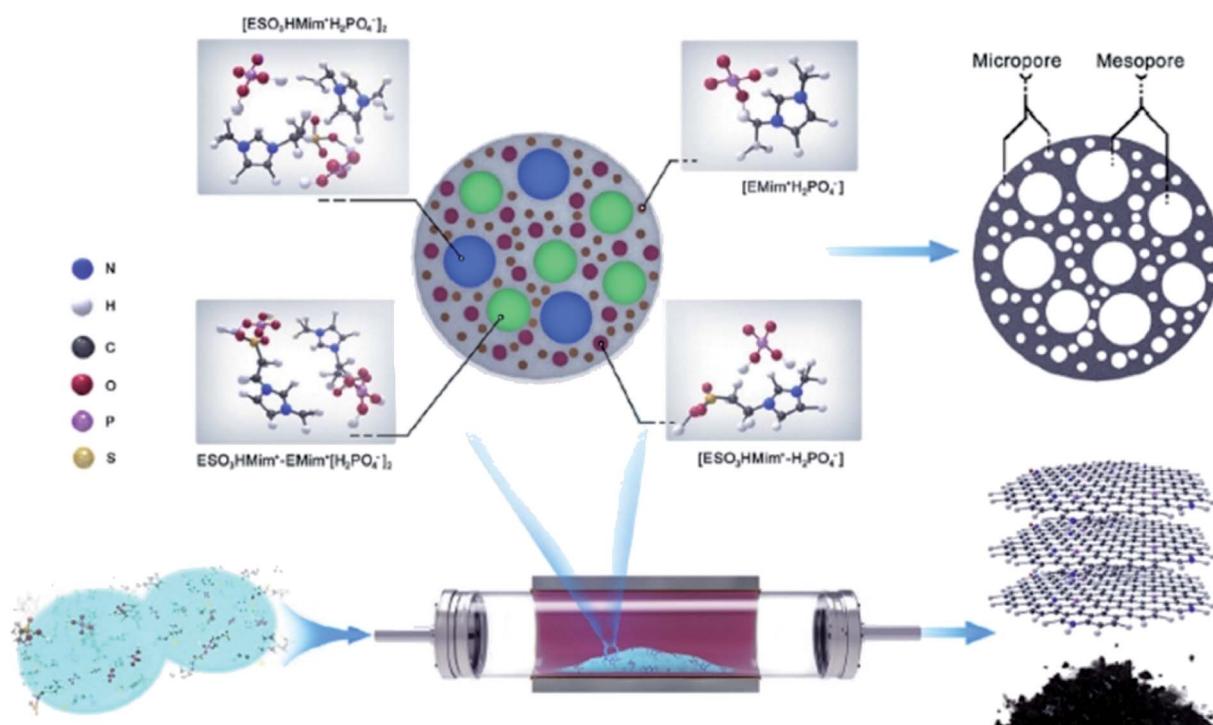


Fig. 19 Preparation of NP-C600. Reprinted with permission from ref. 213. Copyright 2019 Elsevier.



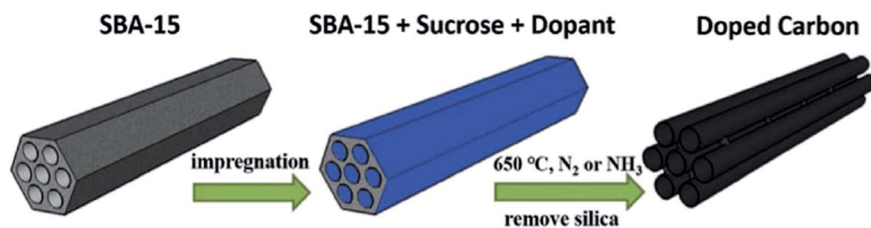


Fig. 20 Preparation of S and N co-doped mesoporous carbon. Reprinted with permission from ref. 215. Copyright 2018 Elsevier.

model catalysts confirmed that C=O groups were more favorable oxygen active species for the reduction of nitrobenzene. When N atoms were introduced into PC, the generated nitrogen species synergistically cooperated with oxygen groups, resulting in high catalytic activity.

**2.3.2 Hydrochlorination reactions.** Pérez-Ramírez and co-workers<sup>167</sup> presented an innovative method to synthesize N-doped carbons derived from polyaniline with adjustable electrical conductivity at defined nitrogen distribution and content and porous properties. Using these model catalysts in hydrochlorination of acetylene, authors provided insights into the reaction mechanism and the active sites and revealed key

catalytic descriptors in this reaction: (1) high electrical conductivity presumably influences the surface diffusion of adsorbed species, and (2) the adsorption of the substrates increases with increasing content of N species of pyrrolic. To achieve maximum catalytic efficiency, the interplay between these two properties must be attentively controlled because enhancing the electrical conductivity results in a decreased nitrogen content.

In a very recent study, Zhang *et al.*<sup>206</sup> developed N-doped activated carbon-based catalysts for acetylene hydrochlorination through a melamine/formaldehyde/polyvinyl alcohol (PVA) coating pyrolysis approach (Fig. 16) and

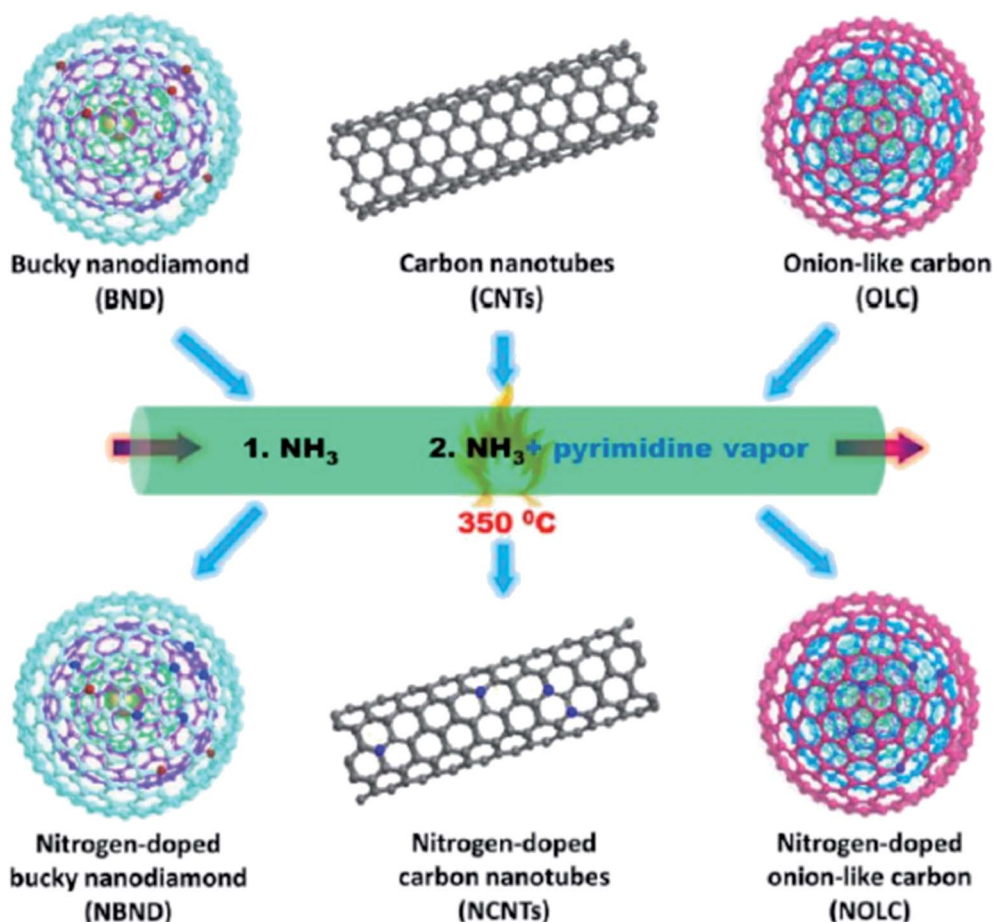


Fig. 21 Preparation of nitrogen-doped nanocarbon (NDN) materials. Reprinted with permission from ref. 217. Copyright 2019 American Chemical Society.



investigated the effects of the synthesis parameters, such as the calcination temperature of the precursors, mass ratio of AC to melamine, the content of PVA, and the molar ratio of formaldehyde to melamine. The results of various analyses demonstrated that N species of graphitic-N and pyridinic-N and defect sites were the main reasons for high catalytic efficiency with a conversion of acetylene up to 75% and gas hourly space velocity of  $50 \text{ h}^{-1}$  under  $220^\circ\text{C}$  in 120 h. Also, the numerous mesopores of catalyst retarded the process of deactivation and accelerated the reactants transfer.

Recently, a simple method for the preparation of a series of carbon materials with rich C defects and high nitrogen content was developed by Zhu and colleagues<sup>207</sup> (Fig. 17). These materials were synthesized through polymerization of diaminopyridine by ammonium persulfate and followed by pyrolysis in different temperatures and were employed as a catalyst for hydrochlorination of acetylene. NC-800 displayed outstanding activity and durability with acetylene conversion of 98%,  $\text{C}_2\text{H}_2$  GHSV =  $30 \text{ h}^{-1}$  under  $220^\circ\text{C}$ . The exceptional catalytic performance of NC-800 was related to strong  $\text{C}_2\text{H}_2$  and HCl adsorption, a high defect amount, a large specific surface area and a good level of active pyridine and pyrrole N contents.

Li and co-workers<sup>208</sup> fabricated a series of nitrogen-doped carbon materials derived from ZIF-8 by adding melamine to tune the N content. The catalytic application of these samples was investigated in acetylene hydrochlorination and the optimized  $\text{Z}_4\text{M}_1$  with the appropriate pore structure and the largest specific surface areas exhibited the highest acetylene conversion under  $180^\circ\text{C}$  and,  $\text{C}_2\text{H}_2$  GHSV of  $50 \text{ h}^{-1}$ , indicating a promising non-metallic catalyst for this reaction. According to

TG analysis, the authors suggested that coke deposition was a reason for the deactivation of the catalysts, and the coke deposition gently enhanced with the increasing content of N.

Li and co-workers<sup>209</sup> utilized MOF-derived N-doped carbon composites as efficient catalysts in the acetylene hydrochlorination and the optimal 17% ZIF-8/SAC afforded VCM in good yield and high selectivity. These catalysts were prepared through *in situ* preparation of ZIF-8 in the pores of spherical activated carbon (SAC) (with different contents), followed by calcination at  $950^\circ\text{C}$  to tune the morphology and catalytic performance (Fig. 18). Bamboo-shaped CNTs with a mean diameter of 40–80 nm appeared on the modified SAC surface could modify the porosity of composites, preventing the generation of coke deposition and well-dispersed nanoparticles with a mean size around 10.50 nm could simply form more active centers and efficiency increase the catalytic performance.

Also, results of TGA and TPD confirmed that the optimal 17% ZIF-8/SAC could increase the adsorption of the reactants as well as prevent the product adsorption, thereby leading to the reduction in the amount of coking deposition.

In 2017, Wang *et al.* utilized the ZIF-8-derived N-doped carbon catalyst calcined at  $1000^\circ\text{C}$  for the acetylene hydrochlorination reaction.<sup>210</sup> Catalyst showed excellent activity and outstanding durability (92% acetylene conversion was observed with a slight decrease during the 200 h test under atmospheric pressure at  $220^\circ\text{C}$ ). Theoretical calculations and experimental studies indicated that neighboring C atoms of pyridinic N atoms were active centers and the main reason for the deactivation of catalyst was coke deposition covering pyridinic N.

Table 3 Oxidation of phenols to relevant *p*-benzoquinones using NBND

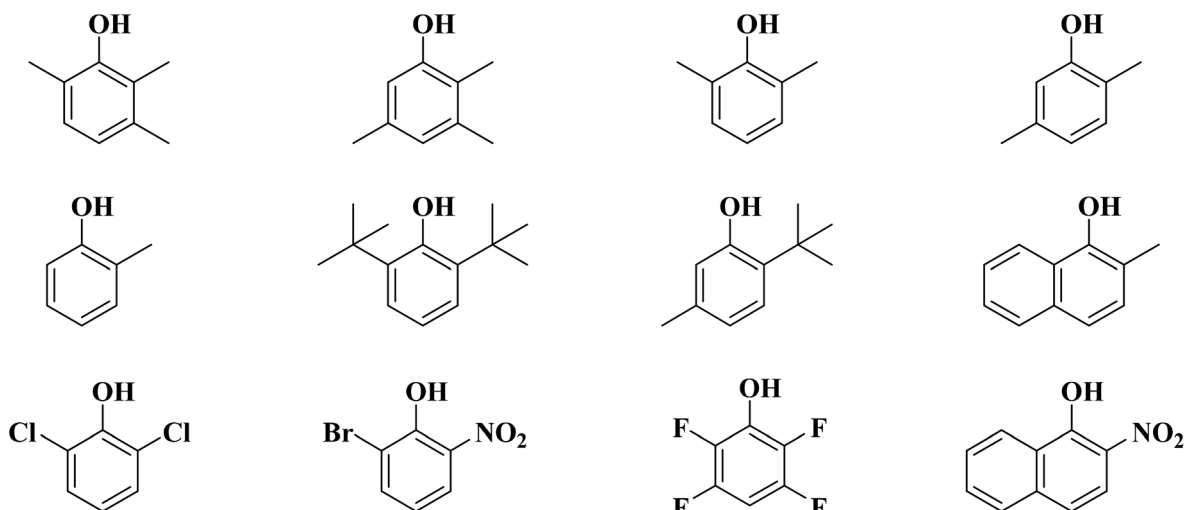
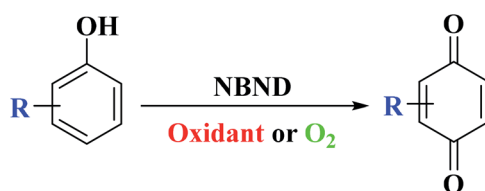
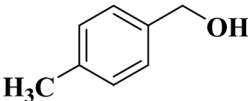
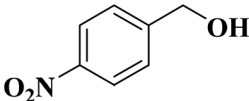
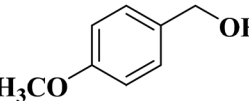
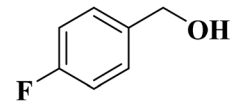
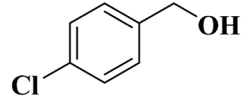
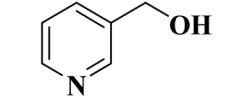
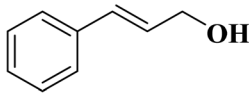
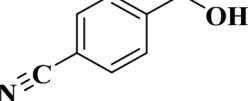
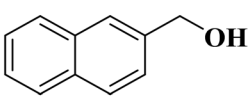
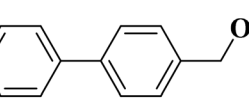
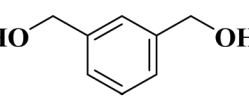
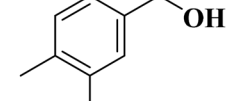
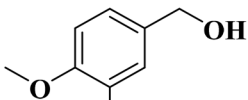
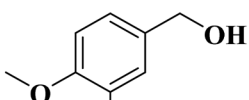
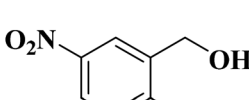
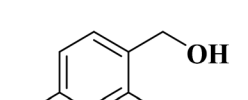
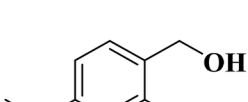
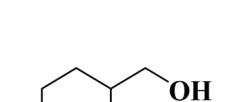






Table 4 Oxidation of alcohols to relevant aldehydes using NBND

| $\text{R-OH} \xrightarrow[\text{Oxidant or O}_2]{\text{NBND}} \text{R=O}$          |  |   |  |
|--|--|---|--|
|   |   |   |   |
|   |   |   |   |
|   |   |   |   |
|   |   |   |   |
|  |  |  |  |

Recently, Qi' group<sup>211</sup> proposed several sulfur-doped spherical activated carbon (SAC) materials with selecting phenyl disulfide as the S source. The performance evaluation of these catalysts was performed in the acetylene hydrochlorination reaction and 9% S/B-SAC displayed preferable catalytic efficiency, in comparison to the blank carrier under 180 °C and GHSV (C<sub>2</sub>H<sub>2</sub>) of 90 h<sup>-1</sup>.

The characterization data indicated that the presence of S dopants increased the capability of reactants' adsorption and prevented the generation of coke deposition. In addition, the DFT study demonstrated that the incorporation of S atoms altered charge density created more active centers on a carrier, and accelerated the electron transfer between reactants and carrier surface.

In 2015, Zhu and colleagues<sup>212</sup> designed a metal-free catalyst for the hydrochlorination of acetylene.

Boron and nitrogen dual doped on graphene oxide (B, N-G) catalyst was obtained by calcination of pre-made B-G intermediate under 20% NH<sub>3</sub>/Ar at 900 °C. This catalyst displayed acetylene conversion considerably superior compared to N- or B-doped graphene and a little lower than that of Hg and Au catalysts.

TPD experiments and DFT calculations indicated that the synthetic effect of N and B codoping could facilitate the adsorption of HCl, which is the rate-determining step in this reaction.

In 2019, Zhao and his research team<sup>213</sup> described the use of N,P-codoped carbon-based materials toward hydrochlorination of acetylene. For the preparation of these catalysts, modified ionic liquids (ILs) such as 1-ethyl-3-methylimidazolium dicyanamide [EMim]<sup>+</sup>N(CN)<sub>2</sub><sup>-</sup> and 1-ethylsulfonate-3-methylimidazolium dihydrogen phosphate [ESO<sub>3</sub>HMim<sup>+</sup>H<sub>2</sub>PO<sub>4</sub><sup>-</sup>] were employed as nitrogen and phosphorus sources, respectively (Fig. 19).

The utilization of task-specific ILs can facilitate the uniform introduction of heteroatoms over the entire carbon-based samples.

The outstanding and catalytically beneficial chemical and physical properties can be created in the fabricated carbon-based materials because of the formation of defects as well as uneven charge distribution caused by the presence of various heteroatoms.

The catalytic efficiency of these new N,P-codoped carbon-based catalysts was higher compared to the HgCl<sub>2</sub> catalysts and comparable to that of Au-based catalysts.

Table 5 Oxidation of alkanes using M-G-1.5-800

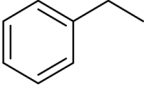
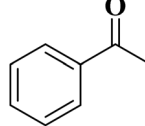
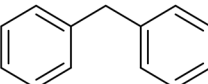
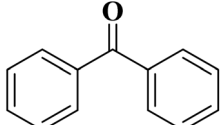
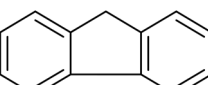
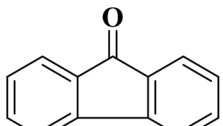
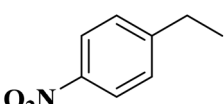
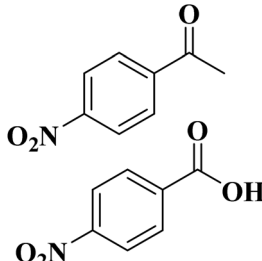
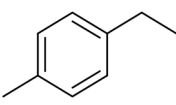
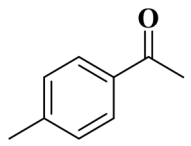
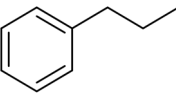
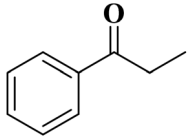
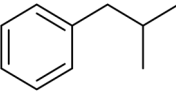
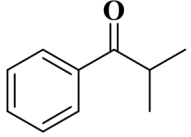
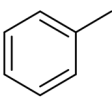
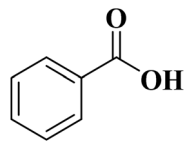

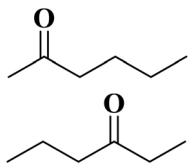
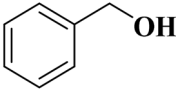
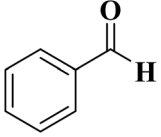
| Substrate   | Product  | Conv./% | Yield/% |
|---|--|---------|---------|
|    |             | 93.8    | 91.2    |
|    |             | 97.6    | >99     |
|    |             | >99     | >99     |
|    | <br>5.1 : 1 | 98.7    | >99     |
|  |           | 89.5    | 60.0    |
|  |           | 85.4    | 82.6    |
|  |           | 73.9    | 51.8    |
|  |           | 51.4    | 48.7    |



Table 5 (Contd.)

| Substrate   | Product  | Conv./% | Yield/% |
|---|--|---------|---------|
|  | <br>1.3 : 1 | —       | 26.3    |
|  |             | 12.3    | 9.8     |

DFT calculations and experimental results confirmed that P atoms bonded with N in the pyridine structure were responsible for the preferable catalytic activity of the NP-C600 catalyst.

In 2017, Zhu *et al.*<sup>214</sup> used  $(\text{NH}_4)_2\text{S}_2\text{O}_8$  (APS) and *p*-phenyldiamine (pPD) as the sulfur and nitrogen sources to construct several S and N dual-doped carbon materials with various molar ratios of the pPD/APS to catalyze acetylene hydrochlorination. The authors concluded that the pyrrolic nitrogen amount in the catalysts changes with the addition of various S amounts, leading to differences in the catalytic performance. The co-doping of S with N in the catalysts provided the synergistic effect for acetylene hydrochlorination. Also, TPD experiments and DFT calculations revealed that the doping of the S and N-doped carbon catalysts enhanced the adsorption ability of  $\text{C}_2\text{H}_2$ .

In 2017, a hard templating approach was utilized by the research group of Li<sup>215</sup> for the preparation of a sulfur and

nitrogen dual-doped mesoporous carbon using sucrose as the precursor of carbon and thiourea as precursors of sulfur and nitrogen in the presence of SBA-15 as the template (Fig. 20). Acetylene hydrochlorination reaction was selected to survey the catalytic efficiency of the resulting material. The authors found that doping of sulfur could effectively improve the pyridinic N content and hence showed increased acetylene conversion relative to the nitrogen-doped carbon catalyst. Based on the  $\text{C}_2\text{H}_2$  TPD results and high-resolution XPS data, carbon atoms bonded to pyridinic nitrogen were active centers of catalyst for the reaction.

In addition, high nitrogen level, mesoporous structure, and large specific surface area derived from SBA-15 resulted in superb catalytic durability and preferable catalytic activity of the co-doped catalyst processed in  $\text{NH}_3$ .

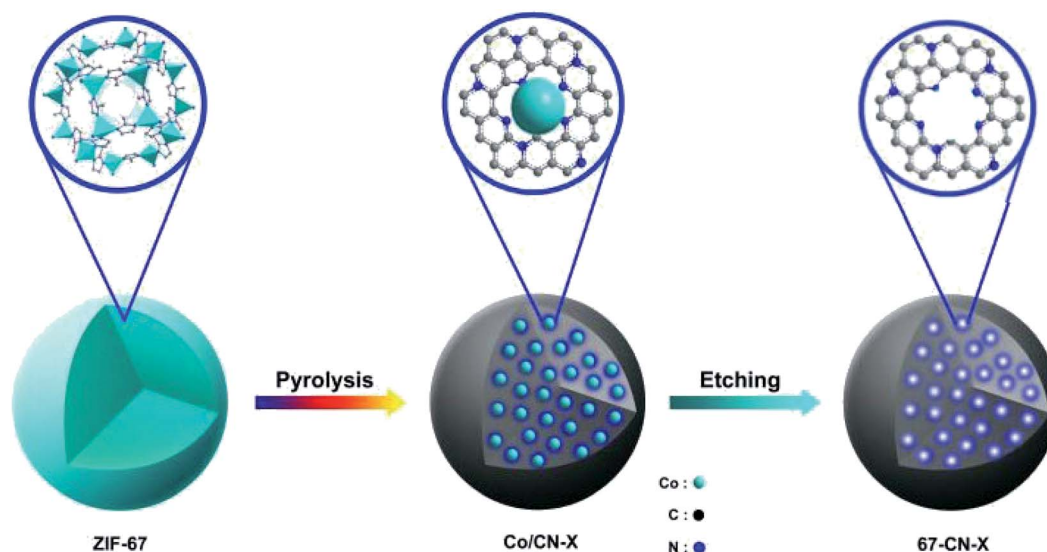
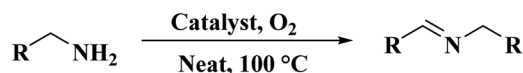
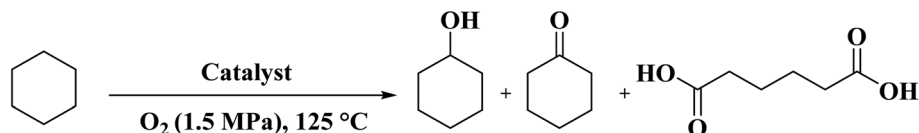


Fig. 22 Synthesis of N-doped carbons. Reprinted with permission from ref. 222. Copyright 2016 Royal Society of Chemistry.

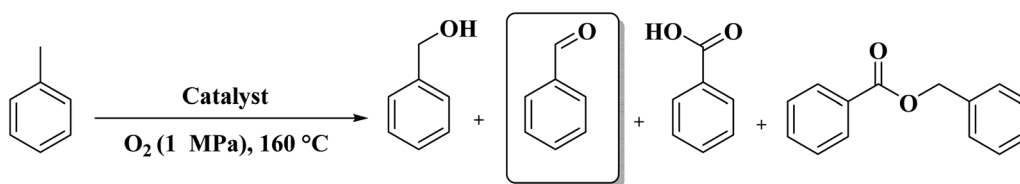


R = Ph, 4-MeC<sub>6</sub>H<sub>4</sub>, 3-MeC<sub>6</sub>H<sub>4</sub>, 2-MeC<sub>6</sub>H<sub>4</sub>, 4-FC<sub>6</sub>H<sub>4</sub>, 4-ClC<sub>6</sub>H<sub>4</sub>, 2-pyridyl, cyclohexyl, C<sub>6</sub>H<sub>13</sub>

Scheme 15 Oxidative coupling of amines.



Scheme 16 Oxidation of cyclohexane using carbon materials.



Scheme 17 Aerobic toluene oxidation using carbon materials.

**2.3.3 Oxidation reactions.** In 2019, Yu and his research team<sup>216</sup> fabricated N-doped carbon nanotubes by wrapping CNTs with a N-doped carbon layer using pyridine as N sources through the chemical vapor deposition (CVD) technique. NCNTs were applied for the epoxidation of styrene by *tert*-butyl hydroperoxide (TBHP) as an oxidant. When the nitrogen

content was lower than 3.51%, a remarkable catalytic activity was observed, while at higher nitrogen contents, activity decreased. The authors justified this behavior with density functional theory calculations.

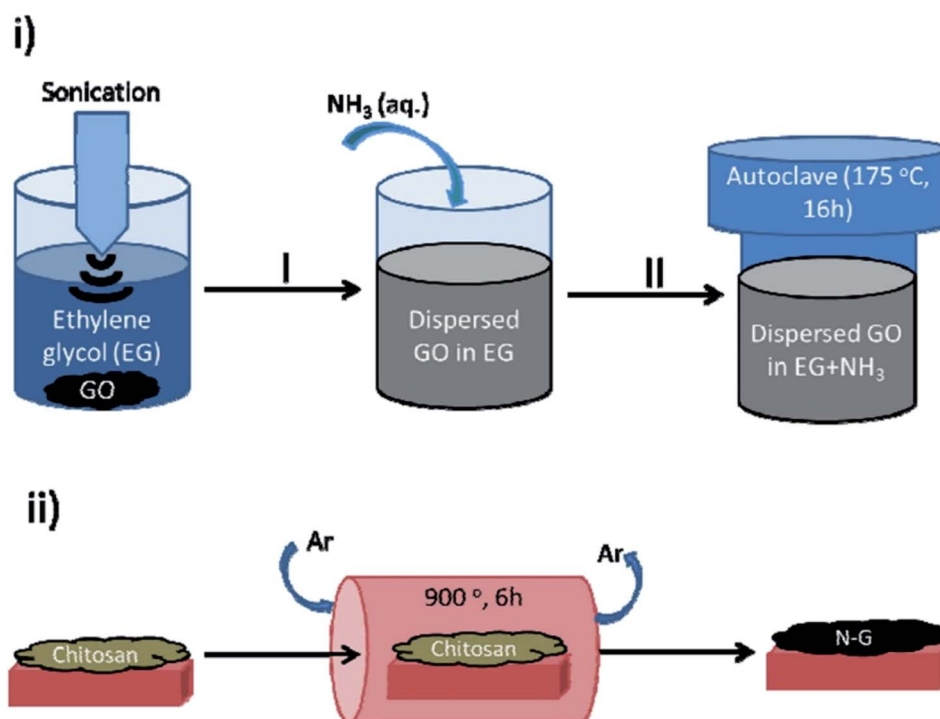
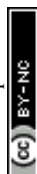


Fig. 23 Preparation of (i) NH<sub>2</sub>-rGO(x) and (ii) N-G samples. Reprinted with permission from ref. 223. Copyright 2017 Royal Society of Chemistry.





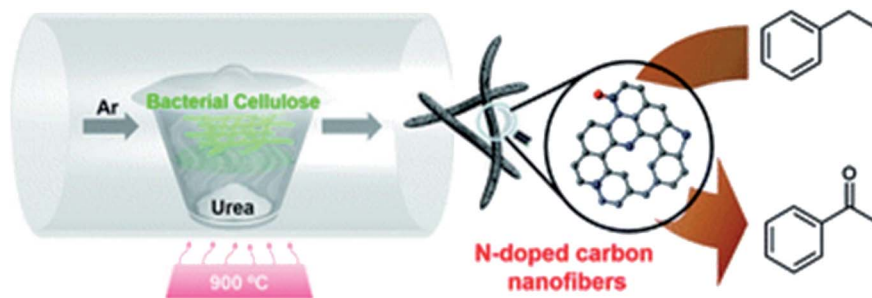


Fig. 24 Preparation of NCNF. Reprinted with permission from ref. 224. Copyright 2019 Royal Society of Chemistry.

Table 6 Oxidation of arylalkanes using NCNF as the catalyst

| $\text{R}^1\text{---}\text{R}^2 \xrightarrow[\text{H}_2\text{O}, 80\text{ }^\circ\text{C}]{\text{Catalyst, TBHP}} \text{R}^1\text{---}\text{C}(=\text{O})\text{---}\text{R}^2 + \text{R}^1\text{---}\text{C}(\text{OH})\text{---}\text{R}^2$ |         |          |          |
|--|---------|----------|----------|
| Substrate  | Product | Con. (%) | Sel. (%) |
|  |         | 78       | 4 : 1    |
|  |         | 96       | 99       |
|  |         | 97       | 99       |
|  |         | 99       | 1 : 2.85 |
|  |         | 99       | 99       |
|  |         | 99       | 99       |
|  |         | 96       | 20       |

When  $N_G$  and  $N_P$  were quite close, a synergistic effect was displayed between them, which was unbeneficial for the catalytic performance because of the very high energy barriers.

Lin and colleagues<sup>217</sup> reported an effective and simple CVD-like method to synthesize four N-doped nanocarbon (NDN) catalysts (including nitrogen-doped onion-like carbon (NOLC), nitrogen-doped oxidized bucky nanodiamond (NOBND), nitrogen-doped CNTs (NCNTs), and nitrogen-doped bucky nanodiamond (NBND)) with enriched pyridinic nitrogen configuration and without any graphitic N species (Fig. 21). Both the ammonia gas and pyrimidine vapor were employed as the N precursors at a relatively low calcination temperature. NBND showed high catalytic prowess towards the oxidation of phenols (Table 3) and complicated alcohols (Table 4) with  $H_2O_2$ ,  $O_2$ , or TBHP as oxidants. The authors also indicated the activation mechanisms and potential roles of N species using aromatic molecules with single N species as probe catalysts. They found that pyridinic nitrogen species played a key role in catalytic reactions.

Wang *et al.*<sup>218</sup> reported the preparation of a series of nitrogen-doped graphene materials and their catalytic performance as metal-free catalysts for oxidation of organic pollutants (p-hydroxyl benzoic acid (PHBA), furfuryl alcohol (FFA), and phenol) through activation of peroxymonosulfate (PMS). N-doped graphenes were fabricated by pyrolyzing MIL-100 (Fe) in the presence of three various nitrogen precursors (urea, melamine, and dicyandiamide) and subsequent acid digestion to eliminate Fe. The specific surface area of catalysts and N doping were important factors affecting the activity of pollutants removal. The mechanism was studied by both quenching experiments (EtOH and  $NaN_3$  as the radical scavengers) and electron paramagnetic resonance (EPR, 2,2,6,6-tetramethyl-4 piperidinol, and 5,5-dimethyl-1-pyrroline N-oxide as the trapping agents). Also, furfuryl alcohol and benzoic acid were used as probing reagents for singlet oxygen and hydroxyl/sulfate radicals, respectively. Overcomes affirmed that singlet oxygen was formed and influenced the degradation of the pollutant on

N-doped graphene instead of hydroxyl/sulfate radicals regardless of N precursors.

By employing fructose, glucose, and 5-hydroxymethylfurfural (5-HMF) as inexpensive and widely available precursors, the Wen group<sup>219</sup> prepared the three kinds of N-doped graphene-like carbon (NG) catalysts *via* a pyrolysis process. Among them, when 5-HMF was utilized, a thin-layered structure with a large lateral dimension was obtained. Also, the NG derived from 5-HMF demonstrated better efficiency in epoxidation reactions than those of the conventional carbon catalysts and its performance was even comparable to that of a cobalt catalyst.

EPR, TEM, and XPS analyses displayed that the increased catalytic performance arose from the activation ability both for  $O_2$  and alkene, which could be ascribed to the graphitic N species and graphitic layered structure.

Sun and co-workers<sup>220</sup> utilized a simple route for the preparation of nitrogen-doped reduced graphene oxide (N-rGO) through simultaneous reduction and introduction of nitrogen on GO using ammonium nitrate as N precursor at various temperatures from 300 to 400 °C. The performances of these metal-free N-rGO materials as green catalysts were studied in the aqueous oxidation of phenol solutions by catalytic activation of peroxymonosulfate (PMS).

Characterization data showed that the chemical compositions and crystal/micro-structures of samples are dependent on the thermal annealing temperature. Authors concluded that the improvement of phenol degradation using N-rGO at calcination temperatures between 300 and 325 °C was due to the N heteroatom, whereas these improved performances for N-rGO at calcination temperatures between 350 and 400 °C were due to both relatively high specific surface area and N heteroatoms.

Using melamine and biomass (such as lignin, glucose, and cellulose) as the nitrogen and carbon sources, and the mixture of KCl/ZnCl<sub>2</sub> as the solvent and porogen, Liu group<sup>221</sup> fabricated a series of mesoporous nitrogen-doped carbons (NDCs) with specific surface area up to 1800 m<sup>2</sup> g<sup>-1</sup> and N content up to 11.9% based on a "Salt Templating" synthesis method. The M-

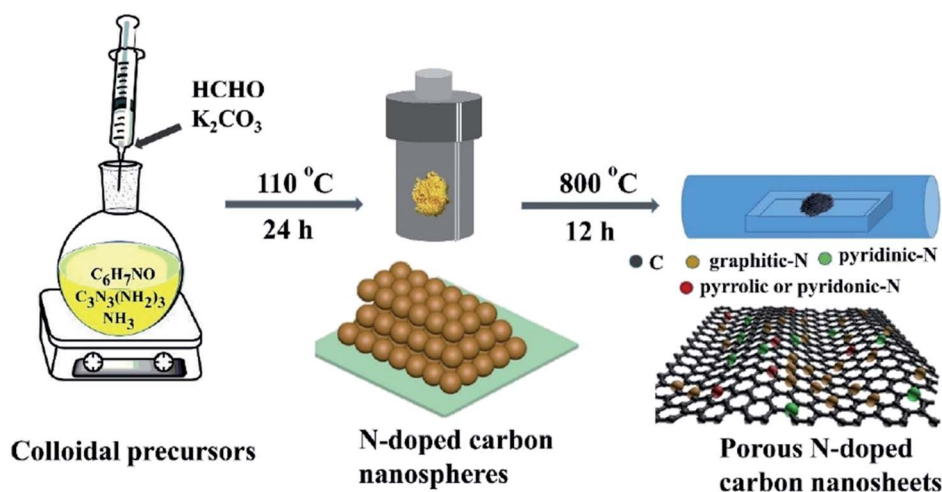
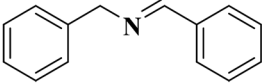
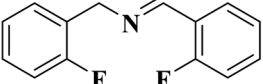
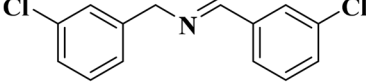
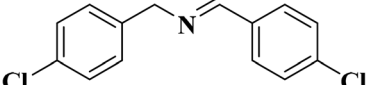
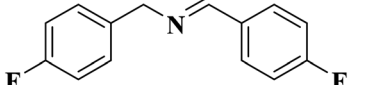
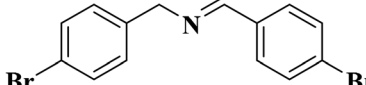
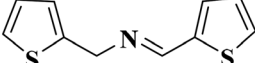
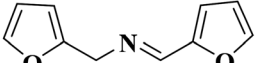
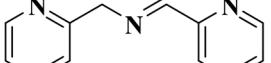
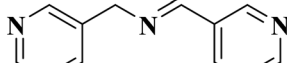
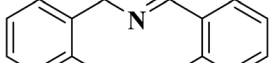

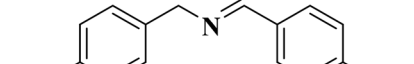
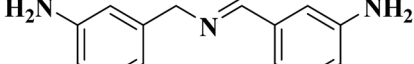
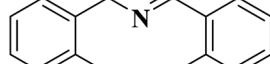
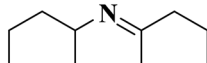
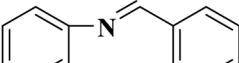
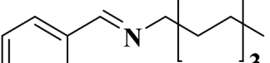
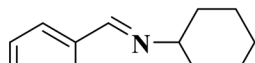
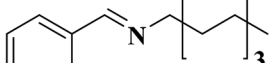
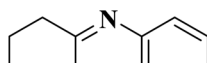
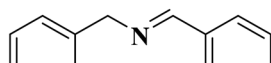
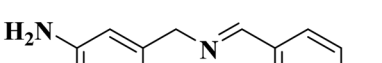
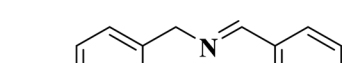


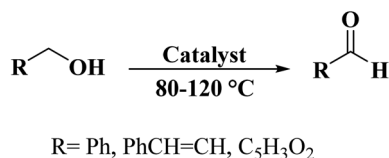
Fig. 25 Preparation of NC-800. Reprinted with permission from ref. 225. Copyright 2019 Royal Society of Chemistry.



Table 7 The imines synthesis of different amines using NC-800

| $\text{R}_1\text{-NH}_2 + \text{R}_2\text{-NH}_2 \xrightarrow[\text{D:W=1:0.5, 120 }^\circ\text{C}]{\text{NC-800, air/O}_2} \text{R}_1\text{-N}=\text{R}_2$ |  |  |
|---|--|--|
| <br>8 h, 99.9%   | <br>8 h, 99.9%    | <br>8 h, 80.5%    |
| <br>9 h, 96.0%   | <br>9 h, 97.0%    | <br>9 h, 80.9%    |
| <br>10 h, 91.0%  | <br>10 h, 99.9%   | <br>8 h, 99.9%    |
| <br>8 h, 93.0%   | <br>10 h, 65.0%   | <br>8 h, 92.0%    |
| <br>8 h, 81.0%   | <br>8 h, 29.0% | <br>8 h, 45.5%  |
| <br>12 h, 56.0%  | <br>10 h, 99.9% | <br>10 h, 49.0% |
| <br>12 h, 56.8%  | <br>10 h, 64.0% | <br>12 h, 30.0% |
| <br>10 h, 45.0%  | <br>10 h, 20.0% | <br>10 h, 27.0% |





**Scheme 18** Aerobic oxidation of alcohols using the nitrogen-doped AC catalysts.

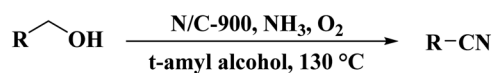
G-1.5-800 (G = glucose, 1.5 = mass ratio of melamine to glucose, and 800 = calcination temperature) with nitrogen loading of 11.4% indicated high activity toward alkanes oxidation in the presence of *tert*-butyl hydroperoxide (TBHP) as the oxidant in the aqueous phase (Table 5). In addition, NDCs were applied as ideal supports to stabilize noble metal nanoparticles (*e.g.*, Rh, Ru, Pt, and Pd).

A facile two-step synthetic method including pyrolysis-etching of ZIF-67 was reported by Li and Wang<sup>222</sup> for the preparation of highly graphitized N-doped mesoporous carbon

materials (Fig. 22). High contents of sp<sup>2</sup>-bonded carbons, large pore volumes, and specific surface areas, and abundant mesopores were realized after chemical etching of the *in situ* generated Co nanoparticles. Also, the sizes of mesopores could be controlled through the adjustment of pyrolysis temperature. These N-doped carbons as metal-free catalysts exhibited effective catalytic activities and strong durability in several oxidation reactions like the oxidative coupling of amines (Scheme 15), aerobic oxidation of cyclohexane (Scheme 16) as well as toluene (Scheme 17).

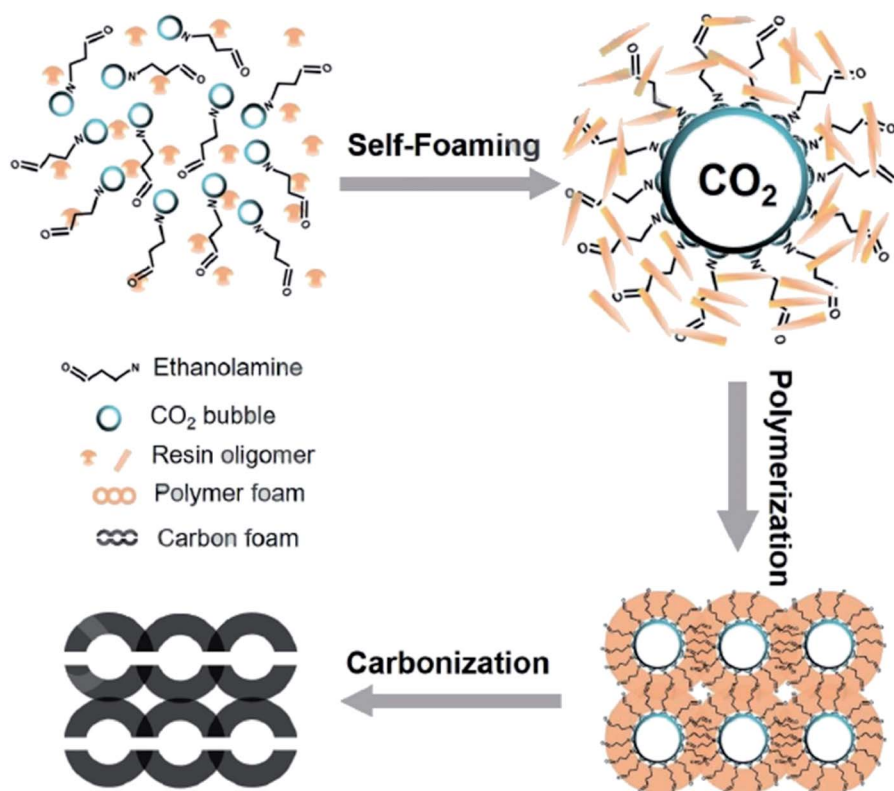
Characterization results suggested that the uniform distribution of doped graphitic-type N and the available mesopores created by etching were responsible for the outstanding efficiency of these catalysts.

In 2017, Rizescu and co-workers<sup>223</sup> reported two different types of N-containing graphenes. One of the types was prepared through simultaneous reduction of graphene oxide (GO) as starting material and amination with ammonia at three various concentrations. The second type was fabricated by pyrolysis of chitosan at 900 °C under an inert atmosphere (Fig. 23). The



R = 1-naphtyl, 4-OMeC<sub>6</sub>H<sub>4</sub>, 2,4-(OMe)<sub>2</sub>C<sub>6</sub>H<sub>3</sub>, 3,4-(Me)<sub>2</sub>C<sub>6</sub>H<sub>3</sub>, 4-MeC<sub>6</sub>H<sub>4</sub>, 3-MeC<sub>6</sub>H<sub>4</sub>, 2-MeC<sub>6</sub>H<sub>4</sub>, 4-BrC<sub>6</sub>H<sub>4</sub>, 4-ClC<sub>6</sub>H<sub>4</sub>, 4-FC<sub>6</sub>H<sub>4</sub>, 4-CF<sub>3</sub>C<sub>6</sub>H<sub>4</sub>, 2-thienyl, C<sub>7</sub>H<sub>15</sub>

**Scheme 19** Synthesis of nitriles in the presence of *meso*-N/C-900.

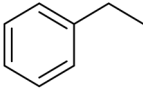
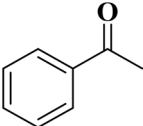
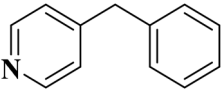
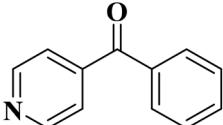
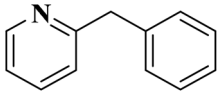
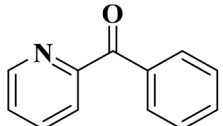
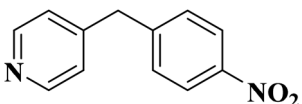
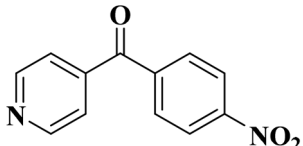
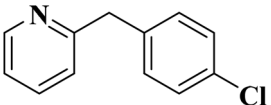
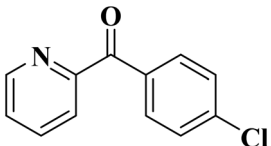


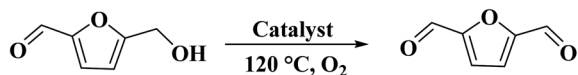
**Fig. 26** Preparation of foam-like carbon monoliths. Reprinted with permission from ref. 229. Copyright 2020 Elsevier.





Table 8 Oxidation of ethylbenzene and pyridine compounds using N-doped carbon foam<sup>a</sup>

| Substrate   | Product  | Conversion (%) | Selectivity (%) |
|---|--|----------------|-----------------|
|  |   | 93             | 91              |
|  |   | 84             | >99             |
|  |   | 64             | >99             |
|  |   | >99            | >99             |
|  |  | 24             | >99             |

<sup>a</sup> TBHP as oxidant, H<sub>2</sub>O as solvent at 80 °C.

Scheme 20 Aerobic oxidation of HMF using N-doped porous carbon-700.

performance of these two N-doped Gs was tested for the selective wet oxidation of glucose to succinic acid. These protocols afforded good selectivities and excellent glucose conversions under O<sub>2</sub> pressure at 160 °C.

Graphenic-type N atoms on graphene were responsible for these performances. Notably, catalysts could be reused for four runs without any decline in selectivity and conversion of the process.

In 2019, Cao and his research team<sup>224</sup> demonstrated the preparation of the N-doped carbon nanofibers (N-CNF) *via* one-step carbonization of urea and bacterial cellulose as low-cost raw materials (Fig. 24).

The obtained N-doped carbon nanofibers indicated excellent selectivity, activity, and good reusability for oxidation of arylalkanes in aqueous solution in the presence of *tert*-butyl

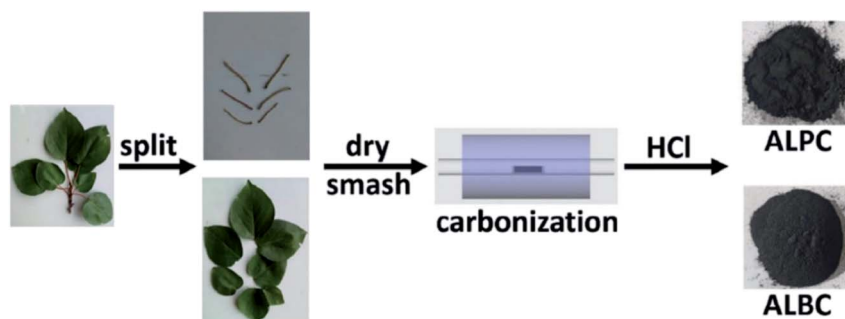
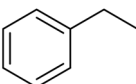
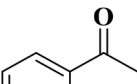
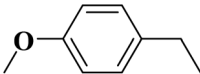
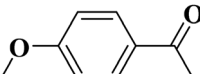
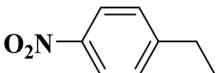
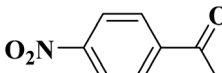
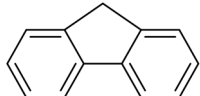
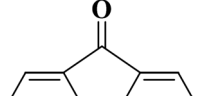
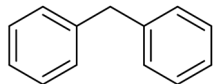
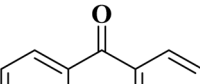
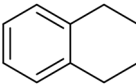
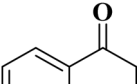
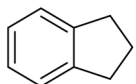
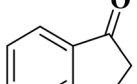


Fig. 27 Preparation of ALPC and ALBC. Reprinted with permission from ref. 231. Copyright 2020 Springer Nature.

Table 9 Oxidation of different aromatic alkanes catalyzed by ALPC<sup>a</sup>

| Substrate   | Product   | Con. (%) | Sel. (%) |
|---|---|----------|----------|
|    |    | 93       | 99       |
|    |    | 15       | 94       |
|    |    | 54       | 98       |
|    |    | 25       | 98       |
|    |    | 65       | 98       |
|    |    | 83       | 93       |
|  |  | 81       | 89       |

<sup>a</sup> ALPC as a catalyst, TBHP as an oxidant at 80 °C.

hydroperoxide (TBHP) (Table 6), because of the great nitrogen content, large specific surface area, as well as interconnected nanofibrous structure. Moreover, the catalytic performance of N-CNF was well maintained even when O<sub>2</sub> was used as an oxidant.

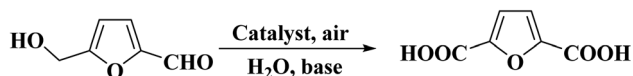
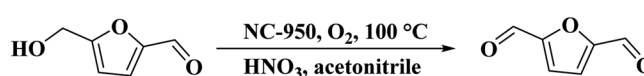
A porous multifunctional and environmentally friendly N-doped carbon catalyst for the oxidation of amines and transfer hydrogenation of nitriles was developed by Li *et al.*<sup>225</sup> (Fig. 25) and diverse substrates were efficiently transformed to the relevant products under the mild conditions using 15 mg NC-800 (Table 7) due to the outstanding surface area and abundant active sites. In particular, this catalyst retained the initial catalytic efficiency at least seven times, which is comparable with metal catalysts. According to experimental and

characterization data, the authors concluded that graphite-N atoms are the main active site in NC-800.

Via treatment of activated carbon (AC) with hydrogen peroxide and ammonia, several N-doped carbons were synthesized by Arai *et al.*<sup>226</sup> The nature and content of species of nitrogen were investigated by XPS analysis to determine the genesis of active species. Graphitic-N species were remarkable to form active sites on the surface of activated carbon.

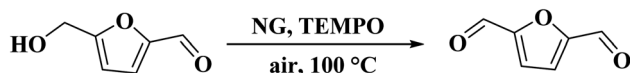
These catalysts were found to be efficient for the oxidation of alcohols like 5-(hydroxymethyl)-2-furaldehyde, cinnamyl alcohol, and benzyl alcohol (Scheme 18) and, in some cases, even more, selective than those of conventional carbon-supported Ru and Pt catalysts.

An attractive catalytic application of nitrogen- and oxygen-doped activated carbon was also disclosed by the same

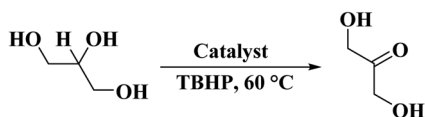
Scheme 21 Oxidation of HMF catalyzed by PCN<sub>x</sub>.

Scheme 22 Oxidation of HMF over NC-950.





Scheme 23 Oxidation of HMF catalyzed by NG.



Scheme 24 Oxidation of glycerol catalyzed by N-CNTs.

research team.<sup>227</sup> N-doped AC could catalyze the hydrogenation of nitrobenzene using hydrazine but not phenylacetylene. Phenylacetylene hydrogenation could take place when nitrobenzene existed in the reaction mixture. The authors believed that synergistic effects between nitrogen and/or oxygen species of surface and nitrobenzene could accelerate the adsorption of phenylacetylene and thus allowed its hydrogenation.

A hard templating method was applied by Gao *et al.*<sup>228</sup> for the preparation of nitrogen-doped nanocarbons with a mesoporous structure and a large surface area using polypyridyl ligand 4,5-diazafluorene-9-one azine (DAA) as carbon and nitrogen precursor in the presence of SiO<sub>2</sub>. The achieved *meso*-N/C-900 indicated good efficiency, selectivity, and reusability toward the aerobic oxidative preparation of nitriles from various alcohols by aqueous ammonia (Scheme 19) due to the efficient pyridinic/pyrrolic-N doping as well as the available mesopores.

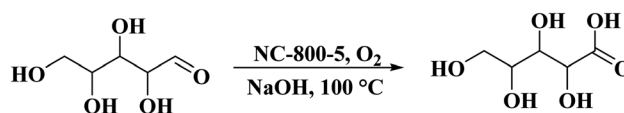
In 2019, Wang and co-workers<sup>229</sup> reported the fabrication of an N-doped and nanofiber-based porous carbon foam through a simple and effective self-foaming method, followed by the carbonization process (Fig. 26). In this method, formaldehyde and resorcinol were utilized as carbon sources and CO<sub>2</sub>-rich ethanolamine (EAC) served as the polymerization catalyst, N source, and foaming agent.

EAC played a critical role in initiating polymerization on the interfaces of bubbles as well as in the release. The hierarchical

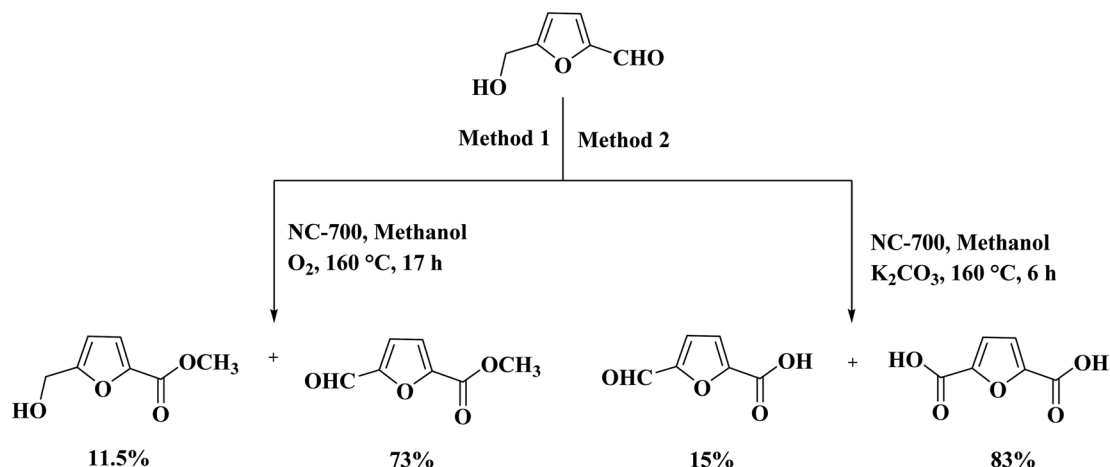
porous structures provided accessible active sites with high surface area sites while doping with nitrogen changed the electronic properties of the carbon. The N-doped carbon foam was able to catalyze the selective oxidation of C–H in ethylbenzene and benzyl pyridines under atmospheric pressure in water in the presence of *tert*-butyl hydroperoxide (TBHP) as an oxidant (Table 8). Also, the synthesized carbon foam exhibited good catalytic activity in the scale-up test.

The use of N-doped porous carbons, as catalysts in the selective aerobic oxidation of 5-hydroxymethylfurfural (HMF), was described by Wang and co-workers<sup>230</sup> in 2019. To prepare these materials, chitosan as a natural N-containing macromolecule was pyrolyzed in the presence of K<sub>2</sub>CO<sub>3</sub> as an activator at temperatures ranging from 600 to 900 °C. The N-doped porous carbon at 700 °C exhibited the best catalytic efficiency, affording 2,5-diformylfuran (DFF) in excellent yield and selectivity under 2.0 MPa O<sub>2</sub> at 120 °C, for 7.5 h (Scheme 20). Based on the XPS data, graphitic N atoms on the catalyst's surface were essential for the activation of O<sub>2</sub> to generate radicals of oxygen that simplified the oxidative dehydrogenation of HMF.

Sun and co-workers<sup>231</sup> synthesized two nitrogen-doped porous carbon materials through direct carbonization of the petioles and blades of apricot leaves at 800 °C for 2 h under N<sub>2</sub> flow without adding nitrogen precursors (denoted as ALPC and ALBC) (Fig. 27). Characterization results indicated that as-obtained compounds were similar in graphitization degree and element composition, but differ significantly in pore volume and surface area. Such differences can arise from the different contents of proteins, vascular bundles, and inorganic salts in blades and petioles. The catalytic behavior of ALPC and ALBC was evaluated in the oxidation of ethylbenzene and ALPC



Scheme 26 Oxidation of D-xylose in the presence of NC-800-5.



Scheme 25 Oxidation of 5-HMF using NC-700.

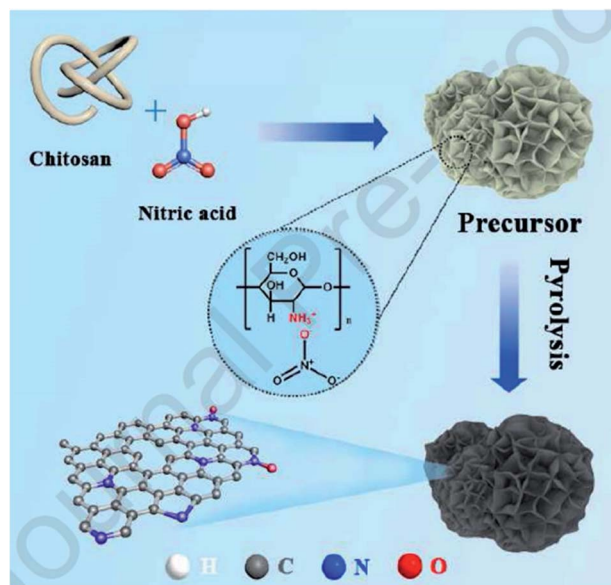


Fig. 28 Preparation of NC catalysts. Reprinted ref. 237. Elsevier.

showed higher catalytic activity owing to the high surface area, and high mean pore size, as well as doped N species. Additionally, the catalytic performance of ALPC was also investigated in the oxidation of different aromatic alkanes and products obtained with high selectivities and diverse yields (Table 9). Furthermore, the ALPC could be used for 5 cycles with a negligible reduction in efficiency presumably owing to the loss of catalyst during the recycling process. The authors noted that the carbon catalysts derived from the blades and petioles of parasol tree leaves and poplar leaves showed the same difference in reaction. These results can provide guidance for preparing carbon materials from leaves.

Verma *et al.*<sup>232</sup> reported an effective, sustainable, and inexpensive chitosan-derived porous carbon nitride (PCN<sub>x</sub>) catalyst

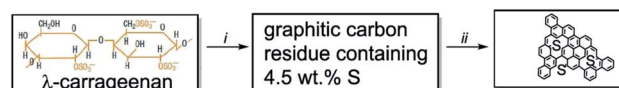


Fig. 30 Preparation of (S)G. Reprinted with permission from ref. 92. Copyright 2015 Elsevier.

originated from marine waste for selective oxidation of 5-hydroxymethyl-furfural (HMF). The reaction was carried out at 70 °C under ambient air pressure and 2,5-furandicarboxylic acid (FDCA) was attained in high yield (Scheme 21). The graphitic N in the catalyst activated the oxygen and played a main role in the hydrogenation. Additionally, the PCN<sub>x</sub> showed high reusability, and no remarkable decrease of efficiency was observed during the five consecutive runs.

Chitosan as a renewable, abundant, and inexpensive precursor was applied by Zhang and colleagues<sup>233</sup> for the manufacturing of nitrogen-doped carbon materials. Also, to increase the nitrogen loading, urea as a commercially available, nitrogen-enriched, and cheap co-precursor was added. The catalytic performance of these materials was largely dependent on the surface area and the type of N species. The NC-950 indicated the best catalytic efficiency for the nitric acid-mediated oxidation of 5-hydroxymethylfurfural (HMF) into 2,5-diformylfuran (DFF) at 100 °C in the presence of molecular oxygen as the terminal oxidant (Scheme 22). The control tests demonstrated that firstly, HNO<sub>3</sub> accelerated reaction, and O<sub>2</sub> was used as a secondary oxidant for recovery of HNO<sub>3</sub>. Additionally, the designed material retained its activity and selectivity for six consecutive recycles.

In 2016, Sun and co-workers<sup>89</sup> used a facile pyrolysis method to fabricate high-quality N-doped graphene (NG) nanomaterials using urea as a nitrogen precursor, glucose as a carbon precursor, and ferric chloride as both a catalyst and a template. A relatively high nitrogen doping level and a low oxygen content

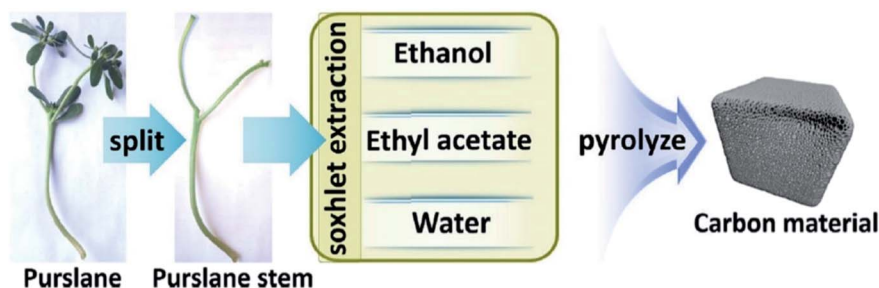
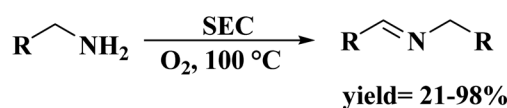


Fig. 29 Preparation of nitrogen-doped foam-like carbon catalysts. Reprinted with permission from ref. 238. Copyright 2021 Springer Nature.

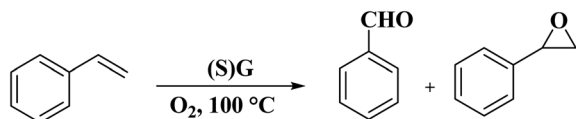


R = 4-ClC<sub>6</sub>H<sub>4</sub>, 2-ClC<sub>6</sub>H<sub>4</sub>, 4-MeC<sub>6</sub>H<sub>4</sub>, 2-MeC<sub>6</sub>H<sub>4</sub>, 4-COMeC<sub>6</sub>H<sub>4</sub>, 2-furyl, 2-pyridyl, C<sub>5</sub>H<sub>11</sub>, hexyl

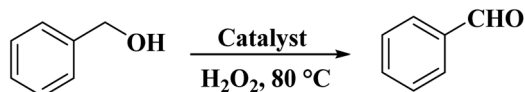
Scheme 27 Oxidative coupling of amines catalyzed by SEC.







Scheme 28 Aerobic oxidation of styrene catalyzed by (S)G.



Scheme 29 Oxidation of benzylic alcohol catalyzed by SG.

were obtained at a moderate temperature. The achieved NG effectively catalyzed phenol oxidation by activation of peroxymonosulfate (PMS). Electron paramagnetic resonance (EPR) spectrums showed that both  $\cdot\text{OH}$  and  $\text{SO}_4^{\cdot-}$  were formed during oxidation processes and played key roles in the oxidation of phenol solutions.

Hou and his research team<sup>234</sup> introduced several nitrogen-doped graphenes with different types and amounts of nitrogen through thermal treatment of GO under ammonia flow and their applications were demonstrated in aerobic oxidation of 5-hydroxymethyl-furfural (HMF) using 2,2,6,6-tetramethylpiperidin-oxyl (TEMPO) as co-catalyst. An excellent HMF conversion and very good selectivity of 2,5-diformylfuran (DFF) were provided at 100 °C under air pressure for 6 h (Scheme 23). Based on XPS results and other control tests, the authors found that the graphitic N atoms activated molecular oxygen. They also concluded that the synergistic effect of NG, TEMPO, and molecular oxygen was the reason for the improved catalytic activity. In addition, the apparent activation energy of N-doped graphene for oxidation of HMF was much lower than those of conventional metal catalysts supported on active carbon (Au/C, Pd/C, Pt/C, and Ru/C).

In 2017, Villa *et al.*<sup>235</sup> reported the first metal-free catalyst for the oxidation of glycerol to dihydroxyacetone (DHA) in the

presence of TBHP as an oxidant (Scheme 24). Two nitrogen-rich carbon nanotubes were synthesized through catalytic CVD technique at 700 and 800 °C by Fe–Mo–Al catalyst prepared using hydrothermal method and imidazole as nitrogen/carbon feedstocks. Pyridinic nitrogen groups doped in the carbon framework were identified as active centers for the reaction that are probably transformed into pyridine oxime groups generated by edge oxidation of N-doped active carbon by TBHP. The catalyst was found to be recyclable for eight successive runs and provided an environmentally benign method for the transformation of glycerol to DHA.

Quite recently, Xu *et al.*<sup>236</sup> presented the synthesis of cheap N-doped carbon (NC) materials through pyrolysis of a mixture of bamboo sawdust, melamine, and  $\text{K}_2\text{CO}_3$ . The performance of these materials was studied in the selective oxidation of crude 5-hydroxymethyl-furfural (5-HMF) achieved from HFCS-90 into furan-2,5-dicarboxylic acid (FDCA). According to the characterization data and activity tests, the rate of generation of product was greatly dependent on the lattice defects in the carbon framework, the graphitic N content, and the pyrolysis temperature of the catalyst. The NC-700 catalyst afforded full HMF conversion and 83% FDCA yield under the optimized reaction conditions (2 MPa  $\text{O}_2$ , 160 °C, and 6 h) (Scheme 25).



Fig. 32 Preparation of M Cel-PC4(800) and catalytic application in oxidation of benzyl alcohol. Reprinted with permission from ref. 241. Copyright 2018 Royal Society of Chemistry.

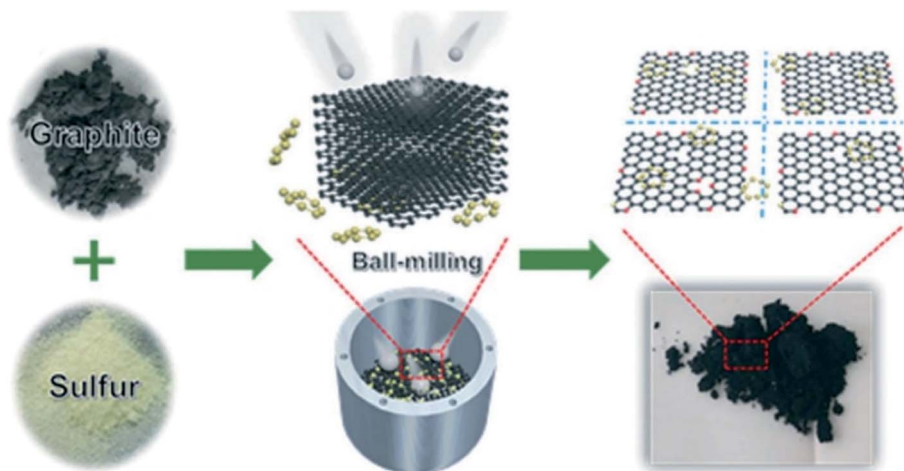


Fig. 31 Preparation of SG. Reprinted with permission from ref. 240. Copyright 2019 Royal Society of Chemistry.

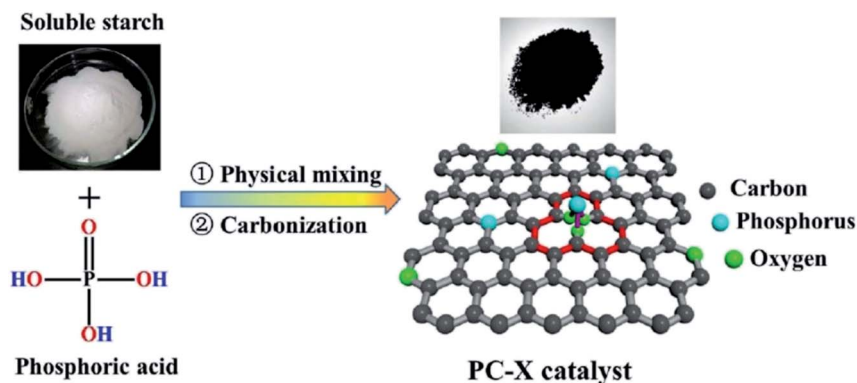
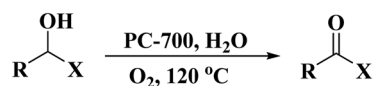


Fig. 33 Preparation of PC-X catalyst. Reprinted with permission from ref. 242. Copyright 2019 Royal Society of Chemistry.



X = H, CH<sub>3</sub>

R = 4-OCH<sub>3</sub>C<sub>6</sub>H<sub>4</sub>, 4-CH<sub>3</sub>C<sub>6</sub>H<sub>4</sub>, 4-ClC<sub>6</sub>H<sub>4</sub>, 4-NO<sub>2</sub>C<sub>6</sub>H<sub>4</sub>, 4-FC<sub>6</sub>H<sub>4</sub>, PhCH=CH, 4-CH<sub>2</sub>OHC<sub>6</sub>H<sub>4</sub>, Ph, 2-furyl, hexyl, C<sub>3</sub>H<sub>7</sub>

Scheme 30 Oxidation of benzyl alcohols over PC-700.

Utilizing chitosan as both C and N sources and HNO<sub>3</sub> as a solvent, Liu *et al.*<sup>237</sup> successfully fabricated N-doped defect-rich carbon materials by carbonization at various temperatures (700, 800, and 900 °C) (Fig. 28). The NC-800-5 (5: the ratio of HNO<sub>3</sub> to chitosan) was an effective heterogeneous catalyst for the oxidation of D-xylose in alkaline aqueous media, under

1 MPa O<sub>2</sub> pressure, at 100 °C, and D-xylic acid could be furnished in moderate yield (57.4%) for 30 min (Scheme 26). DFT calculation revealed that graphitic N species act as active centers and contribute to the interaction between D-xylose molecular and hydroxyl ion, leading to the generation of geminal diols ion. Subsequently, the cleavage of the C–H bond

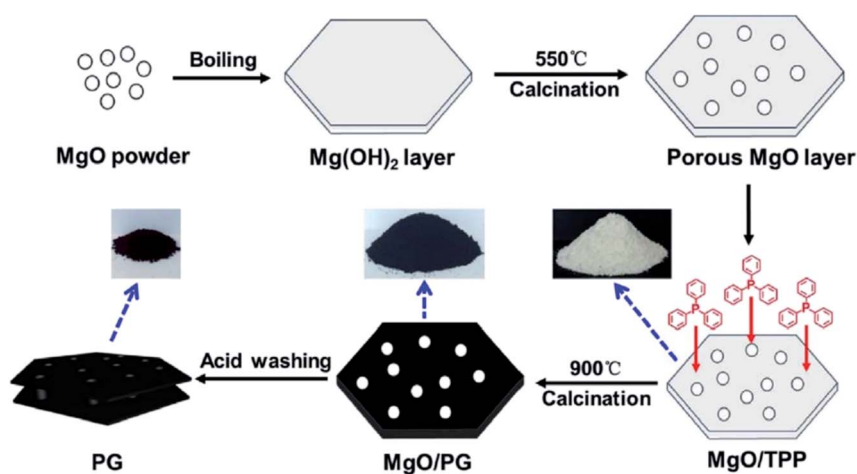
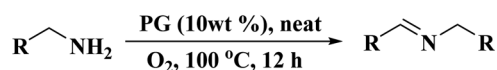


Fig. 34 Preparation of PG. Reprinted with permission from ref. 243. Copyright 2017 Elsevier.



R = 4-FC<sub>6</sub>H<sub>4</sub>, 4-ClC<sub>6</sub>H<sub>4</sub>, 3,4-(Cl)<sub>2</sub>C<sub>6</sub>H<sub>4</sub>, 4-MeC<sub>6</sub>H<sub>4</sub>, 3-MeC<sub>6</sub>H<sub>4</sub>, 2-MeC<sub>6</sub>H<sub>4</sub>, 2-thienyl, hexyl, C<sub>3</sub>H<sub>7</sub>

Scheme 31 Aerobic oxidative coupling of amines in the presence of PG.



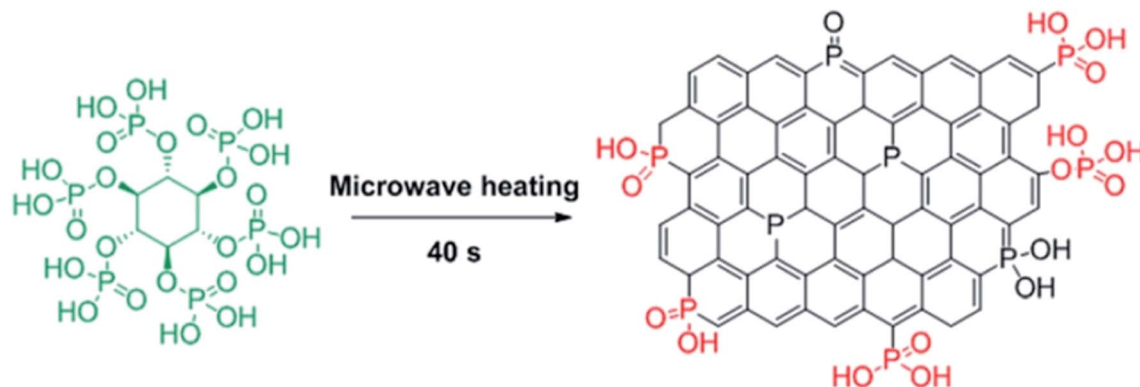
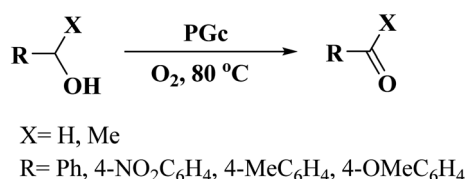


Fig. 35 Preparation of PGc. Reprinted with permission from ref. 244. Copyright 2016 American Chemical Society.



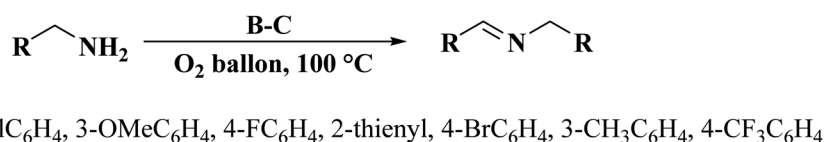
Scheme 32 Aerobic oxidation of benzyl alcohols catalyzed by PGc.

produces the carboxylic group. Additionally, the catalyst showed good durability and reusability after activation treatment.

Very recently, Sun and co-workers<sup>238</sup> selected purslane stem as a precursor to fabricate nitrogen-doped foam-like carbon catalysts by a simple two-steps method of Soxhlet extraction and pyrolysis (Fig. 29). For the preparation of these materials, firstly, the dry samples were treated with water, ethyl acetate, and ethanol by Soxhlet extraction, and then pyrolyzed under flowing nitrogen flow at 700 °C. The polarity of the solvents used in Soxhlet extraction possess is different, hence they extracted

various components from the purslane stem, which possessed considerable influences on the structure and catalytic efficiency of afforded carbon samples. The catalytic ability of these carbon materials was tested in the oxidative coupling of benzylamine and the carbon material derived from the purslane stem pretreated with ethanol (SEC) was found to be the most active catalyst among others because of the many available N-containing active sites, large pore size, and high surface area. Furthermore, diverse amines were transformed into imines using SEC as catalyst under mild conditions (Scheme 27). Also, the SEC showed good durability and could be reused for at least six cycles without a remarkable decrease in activity. In addition, the catalysts synthesized from apricot leaf and celery stem pretreated with ethanol in Soxhlet extraction displayed superior catalytic performance compared with the samples pretreated with water and ethyl acetate.

Dhakshinamoorthy and his research team<sup>92</sup> synthesized S-doped graphene [(S)G] from λ-carrageenan as a natural polysaccharide containing sulfate groups through carbonization at



Scheme 33 Oxidative coupling of amines in the presence of B-C.

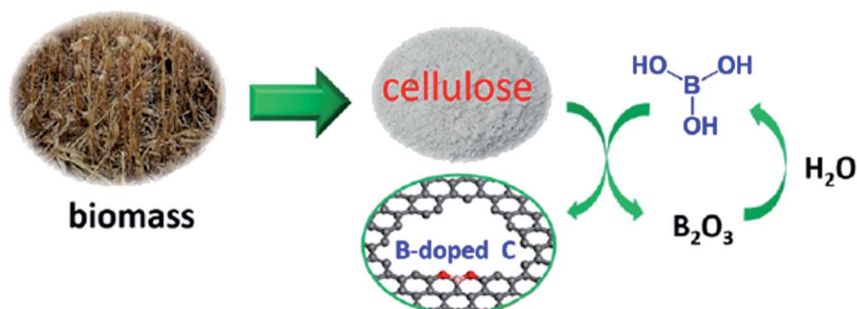


Fig. 36 Preparation of B-doped C. Reprinted with permission from ref. 245. Copyright 2018 American Chemical Society.

1000 °C, followed by exfoliation (Fig. 30). The utilization of carrageenans with lower sulfate amounts and increasing carbonization temperature to 1200 °C led to the failure of S introduction. XPS results confirmed the attendance of two kinds of S species, alike to sulfide and sulfoxide. (S)G catalyzed the aerobic oxidation of styrenes to their desired benzaldehydes along with the formation of a small amount of styrene oxide (Scheme 28). Unlike (S)G, reduced graphene oxide showed no efficiency under identical reaction conditions. The catalyst was used for two runs without a remarkable decrease in selectivity and conversion.

Chemical activation of polythiophene with potassium hydroxide at various carbonization temperatures was reported by Zeng and co-workers<sup>239</sup> for the synthesis of *in situ* S-doped activated carbons with large specific surface areas and developed total pore volumes.

The ACS-800 demonstrated outstanding catalytic performance for oxidation of 4-chlorophenol (4CP) in 1 h with an apparent rate constant much superior compared to AC-800.

The authors pointed out that the removal of acidic functional groups (like carboxyl groups and sulphone groups) and the incorporation of S at an elevated temperature significantly increased the catalytic efficiency of ACS-800. Results showed that carbonization temperature was effective on the textural features, also could improve the surface chemistry of the materials, thereby enhancing the catalytic performances of carbons.

In comparison tests, ACS-800 indicated higher efficiency in activation of persulfate than those of the conventional catalytic systems (multi-walled carbon nanotube, reduced graphene oxide, zero-valent iron (ZVI), Fe<sub>3</sub>O<sub>4</sub>, and Co<sub>3</sub>O<sub>4</sub>). In addition, various peroxides and different aqueous organics were utilized to further assess the catalytic performance of ACS-800. Overcomes presented that ACS-800 activated different peroxides and effectively degraded various types of organic pollutants.

In 2019, Wang and co-workers<sup>240</sup> used sulfurized graphene (SG) as an efficient catalyst for the oxidation of benzyl alcohol in

the presence of H<sub>2</sub>O<sub>2</sub> in a liquid phase reaction system (Scheme 29). SG nanosheets were prepared from the mixture of commercial graphite and sulfur powder through a modified ball-milling strategy (Fig. 31). DFT calculations indicated that the incorporation of the S atoms into the C framework can facilitate excellent catalytic performance by promoting the decomposition of hydrogen peroxide molecules into OH radicals. Moreover, a high-gravity RPB reactor was utilized and the benzyl alcohol conversion was enhanced. Both experimental and CFD simulations displayed that the high gravity level can afford faster surface renewal rate and more turbulent kinetic energy, leading to more effective collision chances between the catalyst and the reactants, finally resulting in better catalytic activity.

In 2018, Chen and co-workers<sup>241</sup> presented the catalytic activities of a series of P-doped carbons (MCell-PCs) in selective oxidation of benzyl alcohol at the atmospheric air as the inexpensive oxidant in the attendance of H<sub>2</sub>O as the green solvent (Fig. 32). The catalysts were prepared through pyrolyzing microcrystalline cellulose (MCell) activated by the H<sub>3</sub>PO<sub>4</sub> at 800 °C for 2 h under flowing nitrogen. The maximum benzaldehyde yield (99.7%) and turnover frequency value were observed with MCell-PC-4(800) (4: weight ratio of MCell to H<sub>3</sub>PO<sub>4</sub>), while the un-doped catalyst only gave a 9.4% yield. According to the experiments and DFT calculations, it was confirmed that the C<sub>3</sub>PO species were the most catalytic active centers.

In 2019, Dong *et al.*<sup>242</sup> reported the design of phosphorus-doped carbon materials by applying easily accessible biomass soluble starch and H<sub>3</sub>PO<sub>4</sub> through a two-steps approach including physical mixing and carbonization (Fig. 33). The obtained PC-700 with a highly porous structure and extremely high surface area efficiently behaved in the aerobic oxidation of benzyl alcohol with a superior TOF value compared to other heteroatom-doped carbons which were previously reported (Scheme 30). Also, this catalyst was applicable for the oxidation of different substrates, such as aliphatic, heterocyclic, alicyclic,

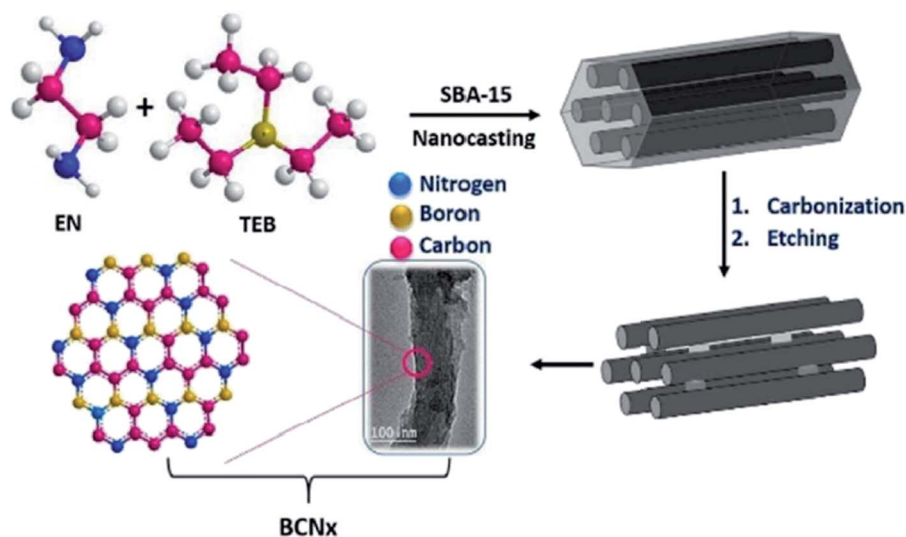


Fig. 37 Preparation of B<sub>x</sub>CN. Reprinted with permission from ref. 247. Copyright 2016 Royal Society of Chemistry.





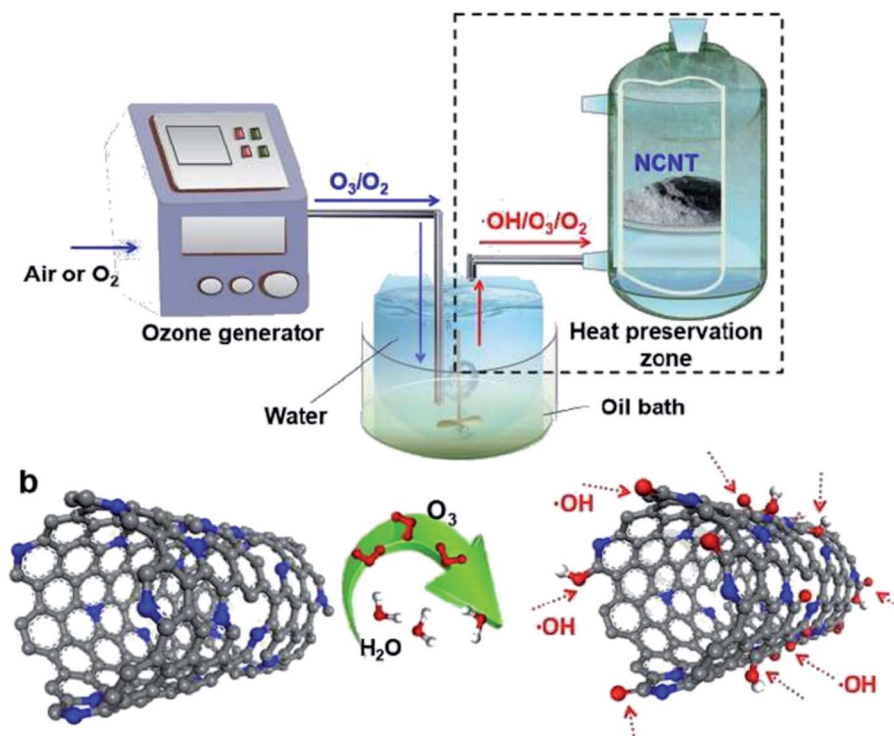
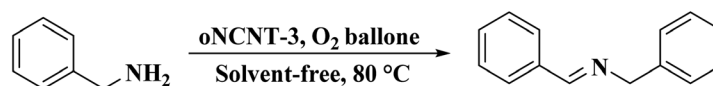


Fig. 38 Preparation of oNCNT. Reprinted with permission from ref. 248. Copyright 2020 Elsevier.



Scheme 34 Oxidative coupling of benzylamine in the presence of oNCNT-3.

and aromatic alcohols. The experimental results and characterization data revealed that the P–O–C species and the defects arising from P–O species doping on catalyst were the active

centers for reaction. Besides, the recycling tests indicated that the PC-700 retained its initial catalytic activity for eight consecutive cycles.

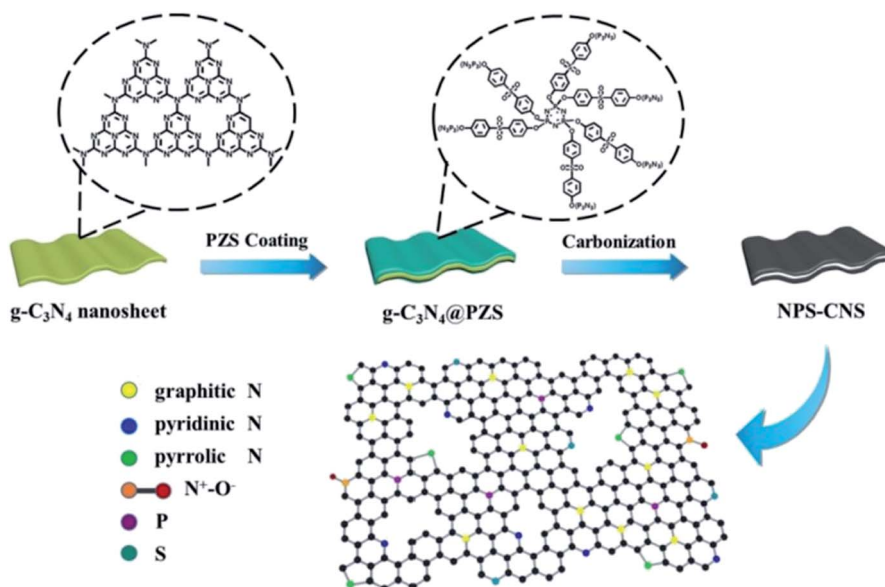
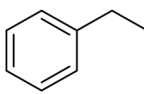
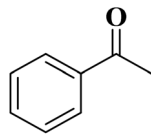
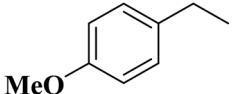
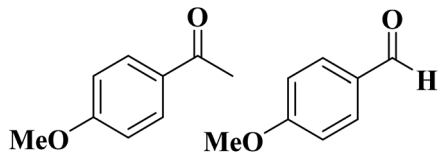
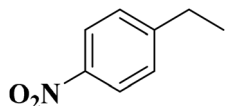
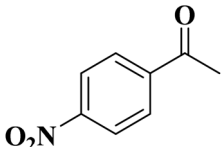
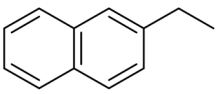
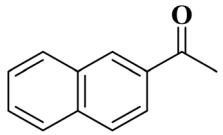
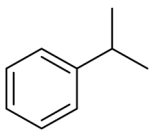
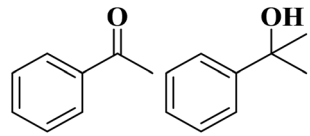
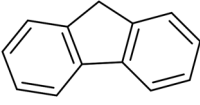
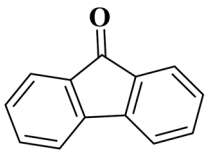
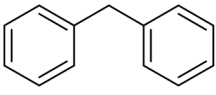
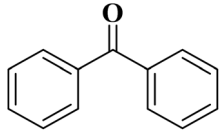


Fig. 39 Preparation of NPS-CNS. Reprinted with permission from ref. 249. Copyright 2016 Royal Society of Chemistry.

Table 10 Oxidation of aromatic alkanes using NPS-CNS-300-1000

$$\text{R}^1\text{CH}_2\text{R}^2 \xrightarrow[\text{H}_2\text{O}, 80^\circ\text{C}]{\text{NPS-CNS-300-1000, TBHP}} \text{R}^1\text{C}(=\text{O})\text{R}^2 + \text{R}^1\text{CH}(\text{OH})\text{R}^2$$

| Substrate   | Product   | Con. (%) | Sel. (%) |
|---|---|----------|----------|
|    |    | 96       | 99       |
|    |    | 84       | 5.22 : 1 |
|    |    | 92       | 99       |
|    |   | >99      | >99      |
|  |  | 84       | 1 : 3.4  |
|  |  | >99      | >99      |
|  |  | >99      | >99      |

In 2017, the Wang group<sup>243</sup> reported the synthesis of phosphorus-doped nanomesh graphene (PG) through a thermal annealing approach (Fig. 34). MgO was used as a template and triphenylphosphine (TPP) served as both carbon and phosphorus source. The as-prepared PG with lamellar hexagonal structure and large specific surface area was applied for aerobic oxidative coupling of amines (Scheme 31) which are key intermediates for the preparation of agricultural chemicals, pharmaceuticals, and fine chemicals. The reactions were performed under neat and mild conditions using O<sub>2</sub> as the oxidant. The DFT calculation revealed that phosphorus doping into the

graphene matrix exhibited better catalytic performance compared with nitrogen-doped graphene and graphene, because of the longest elongation of O–O bonds and lowest adsorption energy of benzylamine. Additionally, the PG could be easily and effectively reused for six successive cycles.

In 2016, Szostak and his research team<sup>244</sup> introduced P-doped porous carbon materials by a very facile, rapid, and scalable method (Fig. 35). In this study, phytic acid, an abundant biomass molecule, was selected as starting material. These materials successfully catalyzed aerobic oxidation of both primary and secondary benzyl alcohols to the relevant



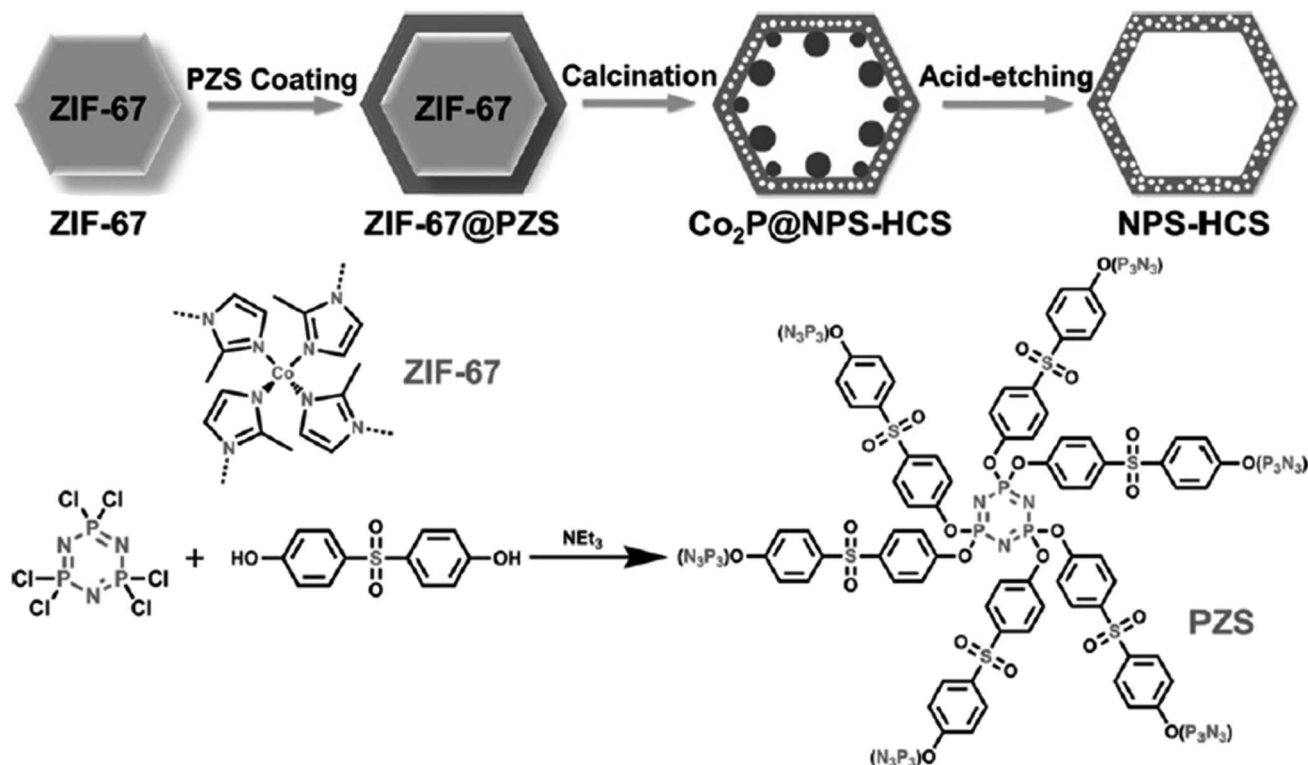


Fig. 40 Preparation of NPS-HCS. Reprinted with permission from ref. 250. Copyright 2016 John Wiley and Sons.

aldehydes or ketones (Scheme 32). Compared to the N-doped carbon materials, the P-doped carbon materials with higher work functions and lower activation energy showed superior efficiency in catalytic aerobic oxidation. Also, the selectivity trend for electron-deficient and electron-rich substrates was different from other heteroatom doped carbon catalysts.

An unexpected and unique catalytic mechanism was displayed, which was different from both N-doped graphene and GO afforded using high-temperature nitrification. The outstanding catalytic approach endowed the P-doped materials with not only high catalytic activity but also reusability.

In another study in 2018, Liu and co-workers<sup>245</sup> reported that boron-doped mesoporous carbon (B-C) can be used as a high-performance heterogeneous catalyst for the oxidative coupling of amines and the relevant imines were furnished in good to high yields and selectivity (Scheme 33). This heteroatom-doped carbon was synthesized by mixing earth-abundant biomass cellulose and  $\text{H}_3\text{BO}_3$ , followed by annealing in an inert atmosphere at elevated temperature (Fig. 36). Characterization data, including X-ray absorption near edge structure and X-ray photoelectron spectroscopy, displayed that B heteroatoms mainly existed in the form of  $\text{CBO}_2$  and acted as catalytic active centers.

Also, the proposed catalytic mechanism according to DFT calculation demonstrated that the synergistic effect of borane and oxygen in  $\text{CBO}_2$  accelerated the adsorption and dehydrogenation of benzylamine.

In 2018, the application of boron-doped graphene samples (BGs) as catalysts for the gas-phase oxidation of benzyl alcohol to benzaldehyde was reported by Li and co-workers.<sup>246</sup> These

materials with adjustable B amount of 0–2.90 at% were prepared by tuning the mass ratio of GO/boric acid. XPS analysis demonstrated that the graphitic  $\text{sp}^2$  boron species ( $\text{BC}_3$ ) could considerably increase the content of active sites ( $\text{C}=\text{O}$ ), as a result enhancing the catalytic activities. The benzyl alcohol conversion using BGs improved 2.35 times and the benzaldehyde selectivity reached 99.2%, compared to the un-doped graphene (G).

Sun and co-workers<sup>87</sup> presented a simple one-pot method for the introduction of nitrogen and sulfur heteroatoms into graphene sheets. Ammonium nitrate and diphenyl disulfide served as N and S sources. The S and N co-doped graphene (SNG) sample was utilized as a metal-free catalyst for catalytic oxidation of phenol by activation of peroxymonosulfate (PMS).

SNG exhibited a much higher apparent reaction rate constant than those of GO, rGO, S-rGO, and N-rGO. Kinetic studies demonstrated that reaction temperature, initial phenol concentration, PMS dosage, and catalyst loading significantly influenced the phenol removal efficiency.

According to both theoretical and experimental investigations, the synergistic effect of nitrogen and sulfur co-doping improved the activation of PMS in comparison with the pure and S- (or N-) sole-doped graphene.

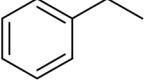
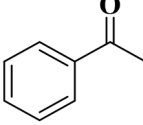
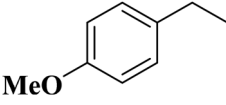
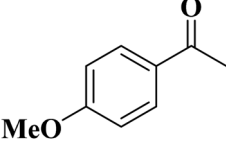
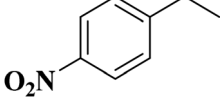
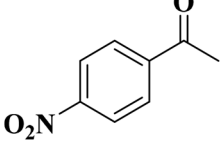
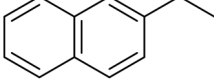
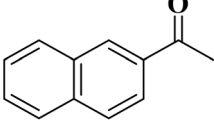
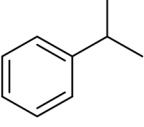
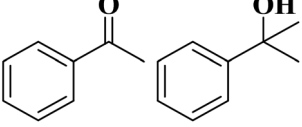
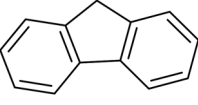
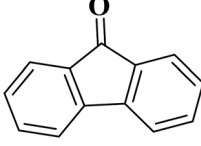
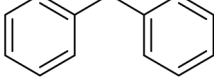
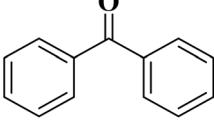
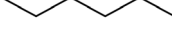
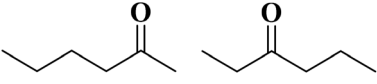
Also, classical quenching tests and EPR spectra indicated that both sulfate and hydroxyl radicals were formed and played key roles in phenol catalytic oxidation.

Besides, the theoretical calculations displayed that incorporation of S into N-doped graphene could remarkably change the electrostatic potential of graphene and surface charge distribution. Based on experimental observations, S acted as an



Table 11 Oxidation of aromatic alkanes in the presence of NPS-HCS

$$\text{R}^1\text{---}\text{R}^2 \xrightarrow[\text{H}_2\text{O}, 80\text{ }^\circ\text{C}]{\text{Catalyst, TBHP}} \text{R}^1\text{---}\text{C}(=\text{O})\text{---}\text{R}^2 + \text{R}^1\text{---}\text{C}(\text{OH})\text{---}\text{R}^2$$

| Substrate   | Product   | Con. (%) | Sel. (%)  |
|---|---|----------|-----------|
|    |    | >99      | 99        |
|    |    | >99      | 99        |
|    |    | 95       | 99        |
|    |   | >99      | 99        |
|  |  | 90       | 1.0 : 3.3 |
|  |  | >99      | 99        |
|  |  | >99      | 99        |
|  |  | 57       | 1.0 : 1.3 |

efficient co-dopant to further increase the catalytic performance of N-doped graphene in phenol oxidative decomposition with radicals, compared to B, P, and I.

Bordoloi *et al.*<sup>247</sup> prepared nitrogen and boron co-doped hierarchical porous carbon ( $\text{B}_x\text{CN}$ ) by means of a nanocasting route by utilizing ethylene diamine and  $\text{CCl}_4$  as the precursor of nitrogen and carbon, dimethylaminoborane as a new boron precursor in the presence of SBA-15 as the hard template (Fig. 37).

The newly synthesized material possessed high pore volume, versatile pore diameter, and large specific surface area. The surface area and pore diameter of  $\text{B}_x\text{CN}$  could be adjusted by tuning the concentration of the B source. XPS and solid-state MAS NMR results suggested the generation of N-B-C species in the catalyst structure. Moreover, DFT calculation showed the prevailing presence of monosubstituted isomer of b1 type in  $\text{B}_x\text{CN}$ .





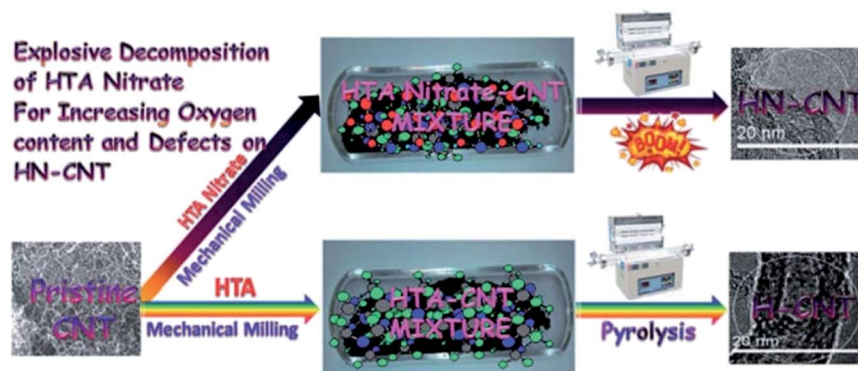


Fig. 41 Preparation of HN-CNT and H-CNT. Reprinted with permission from ref. 252. Copyright 2015 Royal Society of Chemistry.

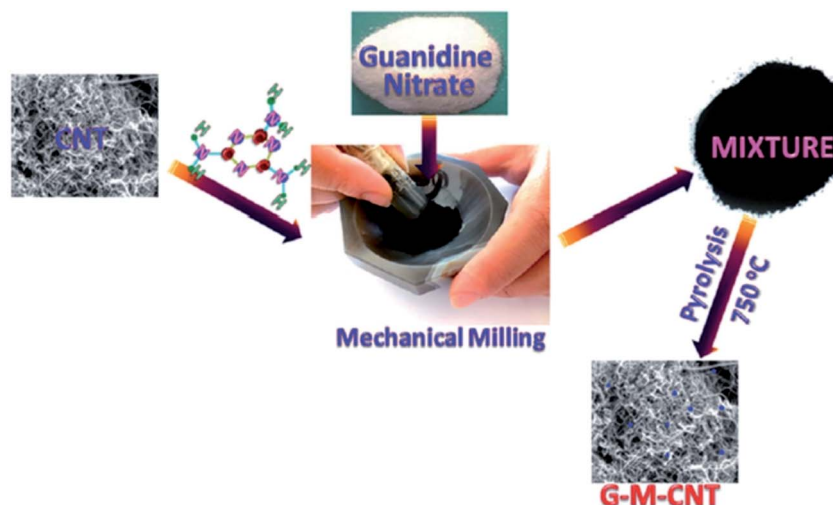


Fig. 42 Preparation of N-doped carbon nanotubes. Reprinted with permission from ref. 254. Copyright 2015 John Wiley and Sons.

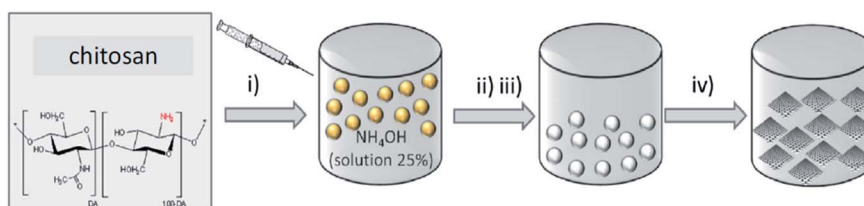


Fig. 43 Preparation of (N)G. Reprinted with permission from ref. 255. Copyright 2019 Elsevier.

$B_xCN$  was highly effective, selective, and stable for oxidative dehydrogenation of propane at low temperature, providing propylene in 84.6% yield without the attendance of any metal.

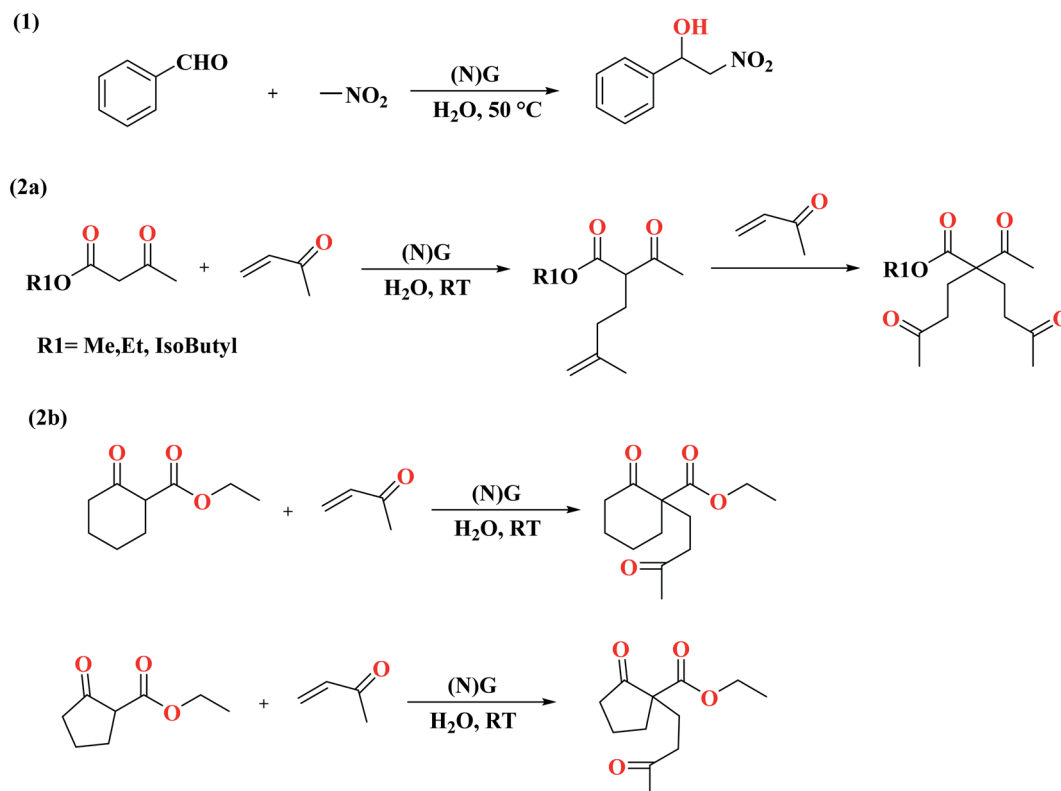
Lowering the HOMO energy and enhance in its absolute electronegativity are the main reasons for the improvement of the oxidation capability of the  $B_xCN$  material.

In a recent study, Luo *et al.*<sup>248</sup> reported a functionalization strategy to incorporate the oxygen atoms into the framework of N-doped carbon nanotubes (fabricated *via* a chemical vapor deposition technique) through the  $H_2O$ -assisted ozone ( $O_3/H_2O$ ) treatment with NCNT (Fig. 38). These groups showed the

specific catalytic property. The as-prepared oNCNT-3 catalyst (treated at vapor generator temperature at 40 °C for 2 h) was found to be effective and selective for oxidative coupling of benzylamine to imine at ambient pressure under solvent-free conditions (Scheme 34). The nitrogen atom adjacent to the  $C=O$  group modified the reactivity of carbonyl towards the activation of C-H as well as activated  $O_2$  molecule for bifunctionality. The benzylamine productivity was highest compared to other carbon-based catalysts which were reported.

An efficient and simple route to manufacture multi-heteroatoms (nitrogen, phosphorus, and sulfur) doped





Scheme 35 Henry (1) and Michael (2a and 2b) reaction.

ultrathin carbon nanosheets was offered by Cao and co-workers<sup>249</sup> in 2016 (Fig. 39). The synthesis procedure involved three steps and started with the synthesis of g-C<sub>3</sub>N<sub>4</sub> nanosheets with the thermal decomposition of urea. g-C<sub>3</sub>N<sub>4</sub> nanosheets functioned as porogen, extra N doping source, and morphology templates. Next, the g-C<sub>3</sub>N<sub>4</sub>@PZS nanosheets were formed by coating highly cross-linked poly(cyclotriphosphazene-co-4,4'-sulfonyldiphen-ol) (PZS) as C, N, P, S sources on g-C<sub>3</sub>N<sub>4</sub> nanosheets. Finally, the calcination of the g-C<sub>3</sub>N<sub>4</sub>@PZS nanosheets under flowing argon atmosphere at desired temperature led to the decomposition of g-C<sub>3</sub>N<sub>4</sub>

nanosheets, carbonization of PZS layer, and formation of NPS-CNS. During this process, N, P, and S heteroatoms in the PZS were homogenously incorporated into the carbon nanosheets. The catalytic ability of the resulting material was assessed in selective oxidation of aromatic alkanes in aqueous media (Table 10). Also, NPS-CNS was applied as an electrochemical catalyst for oxygen reduction reaction in alkaline solution.

In a separate study, the same group reported<sup>250</sup> the synthesis of nitrogen, phosphorus, and sulfur co-doped hollow carbon shells (NPS-HCS) (Fig. 40) and utilized the prepared material as

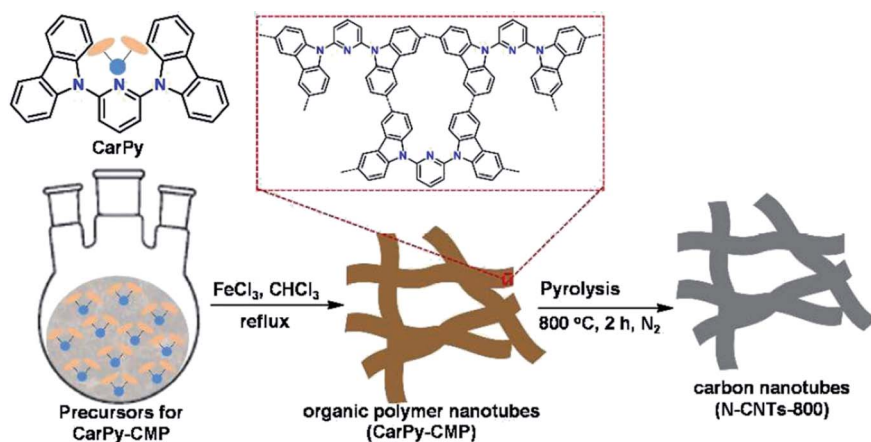
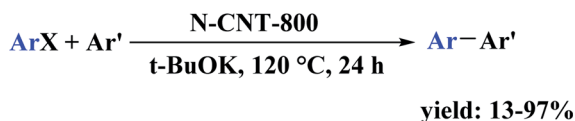


Fig. 44 Preparation of N-CNTs-t. Reprinted with permission from ref. 103. Copyright 2017 Royal Society of Chemistry.

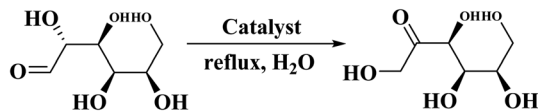




X = I, Br

Ar = Ph, 2-MeC<sub>6</sub>H<sub>4</sub>, 3-MeC<sub>6</sub>H<sub>4</sub>, 4-MeC<sub>6</sub>H<sub>4</sub>, 4-OMeC<sub>6</sub>H<sub>4</sub>, 4-tBuC<sub>6</sub>H<sub>4</sub>, 2-FC<sub>6</sub>H<sub>4</sub>, 3-FC<sub>6</sub>H<sub>4</sub>, 4-FC<sub>6</sub>H<sub>4</sub>, 4-CF<sub>3</sub>C<sub>6</sub>H<sub>4</sub>, 2-thienylAr' = Ph, 2-MeC<sub>6</sub>H<sub>4</sub>, 3-MeC<sub>6</sub>H<sub>4</sub>, 4-MeC<sub>6</sub>H<sub>4</sub>

Scheme 36 C–H arylation in the presence of N-CNTs-800.



Scheme 37 Isomerization of glucose catalyzed by MCN-2-DH.

a non-metallic carbocatalyst in the selective oxidation of aromatic alkanes in water (Table 11). In this study, the PZS polymer as a shell was first coated onto a ZIF-67 core. Subsequently, the resultant ZIF-67@PZS composite was pyrolyzed under flowing argon to generate the Co<sub>2</sub>P@NPS-HCS composite. Ultimately, after acid etching to remove Co<sub>2</sub>P nanoparticles, N, P, and S co-doped hollow carbon shells were prepared. The presence of ZIF-67 was essential for the preparation of NPS-HCS and led to the following beneficial results: (1) ZIF-67 acted as a structural template for PZS coating and therefore helped to maintain the structural integrity of the hollow carbon shells during the carbonization process; (2) the MOF helped to form a mesoporous structure, enhancing the surface area of catalyst through the release of gases after the

ZIF-67 decomposition; (3) the MOF increased the total content of nitrogen atoms in the NPS-HCS; (4) the ZIF-67 improved the wettability of the catalyst in H<sub>2</sub>O; (5) the Co species in the MOF promoted the graphitization of the C, which was crucial for excellent selectivity. This result was further confirmed by an additional test which indicated that if the cores of the catalysts comprise mixed metal MOFs (ZnCo-ZIFs) or only Zn (like ZIF-8), the resultant carbons could not obtain the catalytic efficiency similar to NPS-HCS because of limited graphitization.<sup>251</sup>

**2.3.4 Dehydrogenation reactions.** Zhao and co-workers<sup>252</sup> presented an inexpensive and facile strategy for fabricating a new N-doped carbon nanotube (HN-CNT) through the explosive decomposition of hexamethylenetetramine (HTA) nitrate (Fig. 41). The catalytic activity of HN-CNT in the direct dehydrogenation of ethylbenzene for preparation of styrene was higher than that of the parent CNT and H-CNT (synthesized by the pyrolysis of HTA). The characterization techniques displayed that the HN-CNT catalyst had improved surface ketonic C=O groups, 1.3% of surface nitrogen content, and enhanced structural defects compared to the prepared H-CNT. Also, the combination of the nitrogen adsorption-desorption

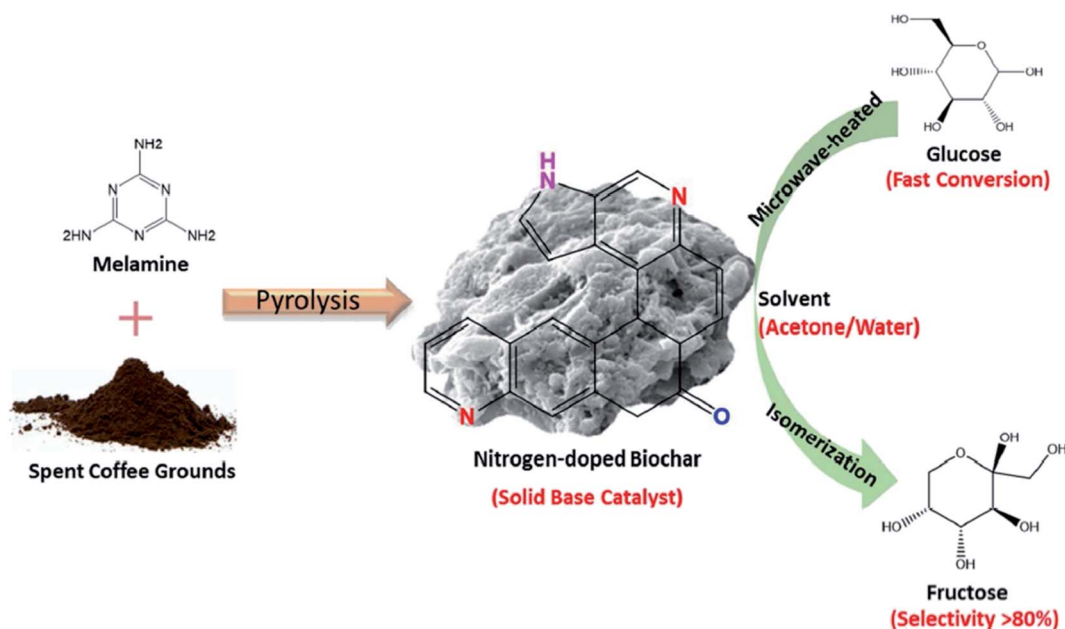


Fig. 45 Preparation of N-doped biochar and catalytic application in isomerization of glucose. Reprinted with permission from ref. 257. Copyright 2018 American Chemical Society.



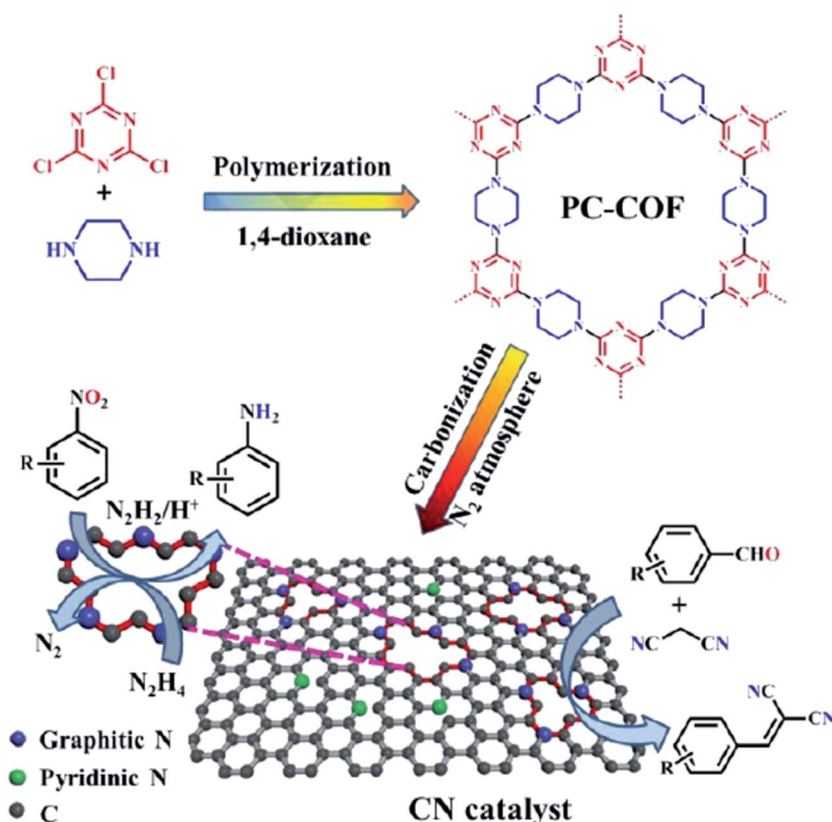
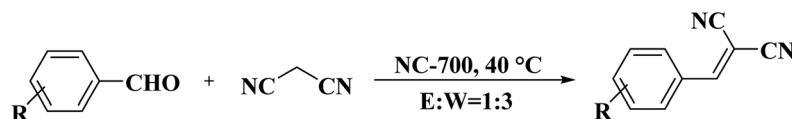


Fig. 46 Preparation of NC. Reprinted with permission from ref. 30. Copyright 2019 Elsevier.



R = H, 4-Cl, 4-Br, 4-F, 2-OH, 4-OH, 4-NO<sub>2</sub>, 4-OH-3-OMe, 3-Me, 3,4-(Me)<sub>2</sub>, 2-furyl, 5-hydroxymethyl-2-furyl

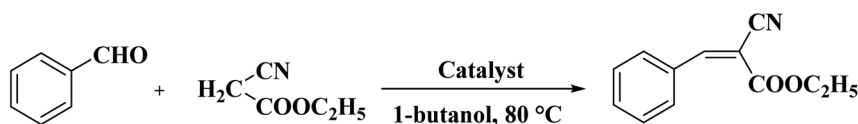
Scheme 38 Knoevenagel condensation of aromatic aldehydes with NC-700.

measurement results and the reaction results suggested that the direct dehydrogenation reaction was mainly performed on the HN-CNT external surface.

Tsubaki and colleagues<sup>253</sup> used nitrogen-doped graphenes as efficient catalysts in the dehydrogenation of ethanol and acetaldehyde was achieved as the sole product in all cases. These materials with various N contents were prepared through a one-pot hydrothermal method by using graphene oxide and urea as precursor and N source, respectively. XPS results revealed that three nitrogen atom types including graphitic, pyrrolic, and

pyridinic were doped on the carbon sheet and their contents were different. Besides, the authors found that both reaction temperatures and N-doped contents significantly influenced the catalytic performance of nitrogen-doped graphenes.

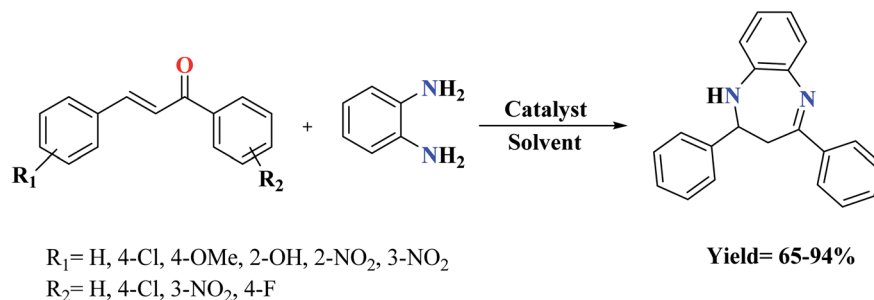
Zhao and co-workers<sup>254</sup> employed scalable and facile physical dry milling and pyrolysis methods to manufacture nitrogen-doped carbon nanotubes (CNTs) (Fig. 42). For the preparation of these samples, first, CNT was ground with melamine in the attendance of guanidine nitrate with various dosages, and next, pyrolyzed in diverse temperatures under flowing nitrogen.



Scheme 39 Knoevenagel condensation catalyzed by N-doped carbon catalysts.







Scheme 40 Synthesis of 1,5-benzodiazepine derivatives in the presence of S-doped graphene.

Dehydrogenation of ethylbenzene was performed for the evaluation of the catalytic activity of the synthesized N-doped CNTs. The authors stressed that the addition of guanidine nitrate possessed a significant influence on the catalytic performance, surface properties, and structure. The optimized N-doped CNTs demonstrated higher activity toward the formation rates of styrene than those of the commercially available K-Fe catalyst, the established nanodiamond, and parent CNTs. The superiority in the catalytic performance of N-doped CNTs was attributed to the smaller graphitic carbon crystallites, larger pore volume, and surface area, the basic properties originated from N-doping, and the defect- and C=O group-rich surface nature.

**2.3.5 Coupling reactions.** In 2019, the Garcia group<sup>255</sup> synthesized defective N-doped graphene [(N)G] *via* chitosan pyrolysis at 900 °C (Fig. 43). Chitosan contained nearly 3.7% of N atoms which were distributed as graphitic, pyrrolic and, pyridinic N species. The performance of [(N)G] as a basic catalyst was tested in two classical CAC bond-forming reactions including the Henry and the Michael additions (Scheme 35). DFT calculations revealed that nitrogen atoms were more resistant at the periphery of the graphene sheets and H adsorption on these sites can describe their catalytic activity. Based on these calculations the most active centers were pyridinic nitrogen species at the zig-zag edges of the sheets. Additionally, N atoms changed the reactivity of the carbon atoms. H<sub>2</sub>O was selected as an appropriate solvent to obtain excellent transformations in both reactions owing to the facile protonation of the N<sub>py</sub>. These protonated pyridinic nitrogen centers activate the neighbor carbon sites, with a suitable efficiency for the  $\alpha$ -C-H bond breaking.

Another strategy for the preparation of hierarchically porous N-doped carbon nanotubes was reported by Liu and co-

workers.<sup>103</sup> The resulting materials were prepared using morphology-preserved carbonization of carbazole- and pyridine bifunctionalized conjugated microporous polymers in various temperatures (400, 600, and 800 °C) under flowing nitrogen and without adding any template (Fig. 44). The N-CNTs-800 functioned as a superior catalyst for C-H arylation of benzene with good durability and simple recyclability for five cycles. This catalyst was also applicable for aryl iodides containing electron-releasing and electron-attracting groups, providing the products in good to high yields (Scheme 36). Besides, N-CNTs-800 displayed high catalytic activity for the hydrogenation of nitrobenzene to aniline. Furthermore, the selective oxidation of aromatic alkanes in aqueous media was successfully carried out over N-CNTs-800. The origin of these superior catalytic activities can be related to high BET surface area, the unique nanotubular structures, and the N doping.

**2.3.6 Isomerization reactions.** In 2019, Cui and co-workers<sup>256</sup> fabricated a number of mesoporous N-doped carbon materials by means of the carbonization of *p*-phenylenediamine disulfate. Also, they investigated the influences of desulfonation with sodium hydroxide and reduction treatments and found that the H<sub>2</sub>SO<sub>4</sub>/pPDA molar ratio illustrated a critical effect on the N content and the porous structure. The obtained materials were explored in the catalytic isomerization of glucose to fructose and among them MCN-2-DH revealed superb activity in aqueous media, affording fructose in good yield and selectivity (Scheme 37). Desulfonation with sodium hydroxide could increase the basicity of the samples because of the removal of sulfonic groups, whereas reduction could modify the nitrogen atoms and enhance the strength of the basic sites, and thus improving the catalytic performances in the reaction.



Fig. 47 Preparation of porous B,N-Cs. Reprinted with permission from ref. 260. Copyright 2020 John Wiley and Sons.

In 2019, Tsang and co-workers<sup>257</sup> developed a solid base N-doped biochar catalyst through two-step pyrolysis of spent coffee grounds and melamine as C and N sources, which was found to catalyze the isomerization of glucose to fructose (Fig. 45). This catalyst displayed higher selectivity compared with homogeneous base catalysts including amines and aqueous hydroxides and comparable catalytic efficiency. XPS results revealed the predominant formation of pyridinic N species on the surface of the biochar, which were mainly responsible for the strong basic properties in the catalyst. The authors also assessed the influence of co-solvent on base-catalyzed conversion and found that application of acetone enhances the overall basic properties using stabilizing protonated H<sub>2</sub>O clusters by hydrogen bonding, thereby leading faster glucose conversion and superior fructose selectivity in comparison to H<sub>2</sub>O.

**2.3.7 Knoevenagel condensation reactions.** Dong and his research team<sup>30</sup> synthesized N-doped carbon materials *via* self-templated pyrolysis of a triazinyl-containing two-dimensional covalent organic framework (2D COF), which was prepared by reaction of inexpensive and easily available piperazine and cyanuric chloride (Fig. 46). The catalytic performance of NC-700 catalyst with high lattice defects and abundant N atoms was remarkable in both Knoevenagel condensation of aromatic aldehydes (Scheme 38) and reduction of nitroarenes in aqueous media. Experimental and characterization results demonstrated that graphitic N species and their related defects were the main factors affecting catalyst activities.

In 2015, Arai and co-workers<sup>258</sup> employed N-doped carbon materials for the Knoevenagel condensation of ethyl cyanoacetate and benzaldehyde (Scheme 39). These catalysts were

prepared through the calcination of commercial polyacrylonitrile (PAN) and then ammoxidation for doping nitrogen (ammoxidation of the calcined PAN). The calcined PAN showed very low catalytic activity for the reaction, but it was significantly increased by the ammoxidation (but the ammoxidation remarkably increased its catalytic activity) and the improvement depended on the calcination temperature as well as ammoxidation temperature. XPS tests displayed the presence of pyridine-type and pyrrole/pyridone-type nitrogen atoms and the content of the pyridine N atoms were important factors to determine the catalytic performance. The N-carbon catalysts synthesized from PAN were much more effective compared to reported solid-based catalysts such as metal oxide-based catalysts, N-doped carbon nanotubes, and N carbon derived from activated carbon.

**2.3.8 Synthesis of 1,5-benzodiazepines.** In 2019, Tavakol *et al.*<sup>259</sup> introduced S-doped graphene as a new, simple and effective carbocatalyst for the preparation of seven-membered heterocyclic 1,5-benzodiazepines of various chalcones with 1,2-phenylenediamine (Scheme 40). This catalyst was obtained using acetylene as a C source and sulfur gas flow as a S source at 800 °C in chemical vapor deposition on copper foil. The benefits of this protocol were mild reaction conditions, high yield, and easy workup. More importantly, the catalyst was very stable and its efficiency was preserved up to ten cycles.

**2.3.9 Cycloaddition reaction.** In 2019, Lu and co-workers<sup>260</sup> synthesized a series of boron and nitrogen co-doped porous carbons (B,N-Cs) by combining with ball milling and pyrolysis (Fig. 47). Firstly, the mixture of boric acid (H<sub>3</sub>BO<sub>3</sub>) as the boron source, and glutamic acid (Glu), as the N-containing carbon precursor, with a molar ratio of 1 : 1 was ball-milled. Then, the

Table 12 Cycloaddition of CO<sub>2</sub> with epoxides catalyzed by GB-1-6-900/*n*-NBu<sub>4</sub>Br

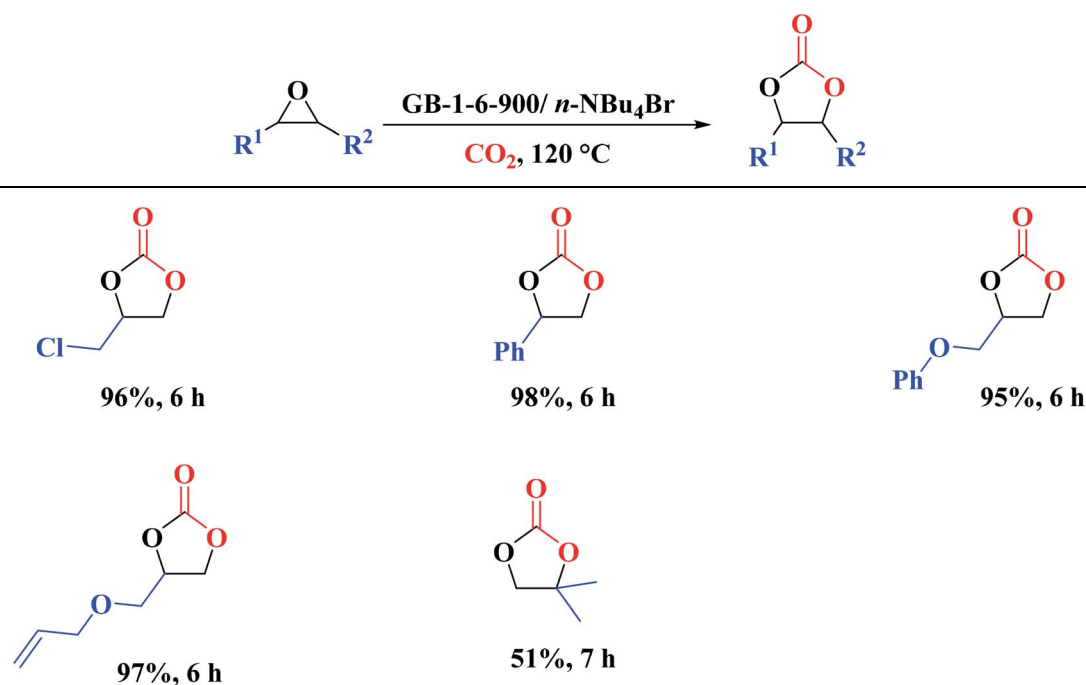


Table 13 The employed metal-free heteroatom-doped carbon catalysts in the various reactions

| Catalyst                      | Dopant | Application                                 | Yield or conversion%    | Ref. |
|-------------------------------|--------|---|-------------------------|------|
| NC-950                        | N      | Reduction of nitro compounds                | $C = 87.5\text{--}100$  | 187  |
| NG <sub>U/K-900</sub>         | N      | <i>N</i> -Formylation of amines             | $Y = 69$ to $>99$       | 188  |
| NCNTs-800                     | N      | Reduction of nitroarenes                    | $C = 70.3\text{--}100$  | 189  |
| N-CNTs                        | N      | Hydrogenation of nitrobenzene               | $C = 60$                | 190  |
| m-NCNTs                       | N      | Reduction of nitroarenes                    | $C = 63.7\text{--}100$  | 16   |
| NHG                           | N      | Hydrogenation of nitrobenzenes              | $Y = 93.6\text{--}99.1$ | 191  |
| NC-2                          | N      | Hydrogenation of nitrobenzene               | —                       | 192  |
| 3D-NGF                        | N      | Reduction of <i>p</i> -nitrophenol          | —                       | 193  |
| N-RGO mesh                    | N      | Reduction of 4-nitrophenol                  | $C = 99.5$              | 194  |
| NC-800                        | N      | Reduction of 4-nitrophenol                  | $C = 100$               | 195  |
| SG                            | S      | Hydrogenation of <i>p</i> -nitrophenol      | $C = 100$               | 196  |
| P-CNT                         | P      | Reduction of nitrobenzenes                  | $C = 90$ to $>99$       | 197  |
| PV-900                        | P      | Reduction of nitroarene compounds           | $C = 72.1\text{--}99.2$ | 198  |
| B-OLC-2                       | B      | Hydrogenation of nitroarenes                | $C > 99$                | 199  |
| B-CNTs-2                      |        |   |                         |      |
| S,N-CNT                       | S,N    | Hydrogenation of 4-aminophenol              | $C = 100$               | 200  |
| PDNSC-800                     | S,N    | Hydrogenation of nitrobenzenes              | $C = 92.7\text{--}99.9$ | 201  |
| BNG-800                       | B,N    | Hydrogenation of nitroarenes                | $Y = 85\text{--}99$     | 202  |
| B-NPC-1200                    | B,N    | Reduction of <i>p</i> -nitrophenol          | $C = 94$                | 203  |
| NPG                           | P,N    | Hydrogenation of nitroarenes                | $Y = 83.9\text{--}98.5$ | 204  |
| NPC                           | P,N    | Reduction of <i>p</i> -nitrophenol          | —                       | 186  |
| ONPC                          | O,N    | Hydrogenation of nitroarenes                | $C = 5.5\text{--}100$   | 205  |
| NC                            | N      | Hydrochlorination of acetylene              | $Y = 81$                | 167  |
| N@CBC-FE                      | N      | Hydrochlorination of acetylene              | $C = 75$                | 206  |
| NC-800                        | N      | Hydrochlorination of acetylene              | $C = 98$                | 207  |
| Z <sub>4</sub> M <sub>1</sub> | N      | Hydrochlorination of acetylene              | $C = 60$                | 208  |
| ZIF-8/SAC                     | N      | Hydrochlorination of acetylene              | $C = 81$                | 209  |
| NC                            | N      | Hydrochlorination of acetylene              | $C = 92$                | 210  |
| S/B-SAC                       | S      | Hydrochlorination of acetylene              | $C = 50$                | 211  |
| B,N-G                         | B,N    | Hydrochlorination of acetylene              | $C = 95$                | 212  |
| NP-C600                       | P,N    | Hydrochlorination of acetylene              | $C > 99.2\%$            | 213  |
| S,N-carbon                    | S,N    | Hydrochlorination of acetylene              | $C = 82.44$             | 214  |
| NSC                           | S,N    | Hydrochlorination of acetylene              | $C = 90$                | 215  |
| N-CNTs                        | N      | Epoxidation of styrene                      | $C = 85$                | 216  |
| NBND                          | N      | Oxidation of phenols                        | $C = 93.5\text{--}99.5$ | 217  |
| NBND                          | N      | Oxidation of alcohols                       | $C = 32.4\text{--}94.2$ | 217  |
| NG                            | N      | Oxidation of <i>p</i> -hydroxylbenzoic acid | —                       | 218  |
| NG                            | N      | Epoxidation of styrene                      | $C = 7.9$               | 219  |
| N-rGO                         | N      | Oxidation of phenol                         | —                       | 220  |
| M-G-1.5-800                   | N      | Oxidation of alkanes                        | $Y = 9.8$ to $>99$      | 221  |
| 67-CN-600                     | N      | Oxidative coupling of amines to imines      | $Y = 78$ to $>99$       | 222  |
| 67-CN-600                     | N      | Oxidation of cyclohexane                    | $C = 48$                | 222  |
| 67-CN-600                     | N      | Oxidation of toluene                        | $C = 6$                 | 222  |
| NH <sub>2</sub> -rGO          | N      | Oxidation of glucose to succinic acid       | $C = 100$               | 223  |
| NCNF                          | N      | Oxidation of arylalkanes                    | $C = 78\text{--}99$     | 224  |
| NC-800                        | N      | Oxidation of amines                         | $Y = 20\text{--}99.9$   | 225  |
| N-AC                          | N      | Oxidation of alcohols                       | $C = 21\text{--}24$     | 226  |
| meso-N/C-900                  | N      | Synthesis of nitriles                       | $Y = 0\text{--}93$      | 228  |
| N-doped carbon foam           | N      | Oxidation of ethylbenzene and pyridines     | $C = 24$ to $>99$       | 229  |
| NPC-700                       | N      | Aerobic oxidation of HMF                    | $C = 95.3$              | 230  |
| ALPC                          | N      | Oxidation of aromatic alkanes               | $C = 15\text{--}93$     | 231  |
| PCN <sub>x</sub>              | N      | Oxidation of HMF                            | $Y = 83$                | 232  |
| NC-950                        | N      | Oxidation of HMF                            | $Y = 95.1$              | 233  |
| NG                            | N      | Oxidation of phenol                         | —                       | 89   |
| NG                            | N      | Oxidation of HMF                            | $Y > 99$                | 234  |
| N-CNTs                        | N      | Oxidation of glycerol                       | $C = 36.5$              | 235  |
| NC-700                        | N      | Oxidation of 5-HMF                          | $Y = 83$                | 236  |
| NC-800-5                      | N      | Oxidation of D-xylose                       | $Y = 57.4$              | 237  |
| SEC                           | N      | Oxidative coupling of amines                | $Y = 21\text{--}98$     | 238  |
| (S)G                          | S      | Aerobic oxidation of styrene                | $C = 13$                | 92   |
| ACS-800                       | S      | Oxidation of 4-chlorophenol                 | —                       | 239  |
| SG                            | S      | Oxidation of benzylic alcohol               | $C = 20.86$             | 240  |
| MCel-PC4(800)                 | P      | Oxidation of benzyl alcohol                 | $Y = 99.7$              | 241  |



Table 13 (Contd.)

| Catalyst          | Dopant | Application                          | Yield or conversion%        | Ref. |
|-------------------|--------|--------------------------------------|-----------------------------|------|
| PC-700            | P      | Oxidation of benzyl alcohols         | $C < 1-99.8$                | 242  |
| PG                | P      | Aerobic oxidative coupling of amines | $C < 10-98$                 | 243  |
| PGc               | P      | Aerobic oxidation of benzyl alcohols | $C < 2-98.9$                | 244  |
| B-C               | B      | Oxidative coupling of amines         | $Y = 68-89$                 | 245  |
| BGs               | B      | Oxidation of benzyl alcohol          | $C = 21.5$                  | 246  |
| SNG               | S,N    | Oxidation of phenol                  | —                           | 87   |
| B <sub>3</sub> CN | B,N    | Oxidative dehydrogenation of propane | $Y = 84.6$                  | 247  |
| oNCNT-3           | O,N    | Oxidative coupling of benzylamine    | $Y = 66$                    | 248  |
| NPS-CNS-300-1000  | N,P,S  | Oxidation of aromatic alkanes        | $C = 84$ to $>99$           | 249  |
| NPS-HCS           | N,P,S  | Oxidation of aromatic alkanes        | $C = 57$ to $>99$           | 250  |
| HN-CNT            | N      | Dehydrogenation of ethylbenzene      | —                           | 252  |
| NG                | N      | Dehydrogenation of ethanol           | $C = 9.11$                  | 253  |
| N-CNTs            | N      | Dehydrogenation of ethylbenzene      | —                           | 254  |
| (N)G              | N      | Henry & Michael addition             | $Y = 80.2$ & $C = 41.2-100$ | 255  |
| N-CNTs-800        | N      | C-H arylation                        | $Y = 13-97$                 | 103  |
| MCN-2-DH          | N      | Isomerization of glucose             | $Y = 31.6$                  | 256  |
| N-doped biochar   |        | Isomerization of glucose             | $C = 22$                    | 257  |
| NC-700            | N      | Knoevenagel condensation             | $C = 98.6$ to $>99$         | 30   |
| NC                | N      | Knoevenagel condensation             | $Y = 99$                    | 258  |
| S-doped graphene  | S      | Synthesis of 1,5-benzodiazepines     | $Y = 65-94$                 | 259  |
| B,N-Cs            | N,B    | Cycloaddition reaction               | $Y = 51-98$                 | 260  |

B,N-C materials with high contents of boron and nitrogen up to 7 atom% and 10 atom%, respectively were obtained by pyrolysis of Glu/H<sub>3</sub>BO<sub>3</sub> composites in various temperatures. By tuning the molar ratio of H<sub>3</sub>BO<sub>3</sub> to Glu, the surface chemical states of B and N could be simply modulated. Also, with increasing H<sub>3</sub>BO<sub>3</sub> amount, the pore size of samples could be adjusted ranging from micropores to mesopores. The catalytic activity of as-designed B,N-Cs materials was greater than those of the physically mixed catalyst of NC-900 and B<sub>4</sub>C and the pure N doped carbon catalyst (NC-900) in the cycloaddition of CO<sub>2</sub> with epoxides (Table 12). The enhanced catalytic performance was related to the positive cooperative effect between N and B sites.

XPS data revealed that BN<sub>3</sub> in these catalysts served as a critical factor to facilitate the ring-opening process of epoxides.

### 3. Conclusions and future perspectives

Metals and metal oxides have been broadly applied as catalysts in different organic reactions. Heteroatom-doped carbon materials have outstanding advantages such as earth abundance, low-cost, high specific surface areas, pore volumes, large amounts of surface defects, strong tolerance to acidic/alkaline media, and structure tenability at the molecular and morphological levels and hence can be considered as ideal alternatives to the metal catalysts. Unlike metal alloys that often suffer from separation problems, good operational durability can be obtained for most of the heteroatom-doped carbons because of the covalent chemical bonds between the carbon and heteroatom.

In addition, due to their wide accessibility, environmental friendliness, and no heavy metal pollution, carbon catalysts are good candidates for green and sustainable chemistry.

In this review, we summarized recent advances in the development of metal-free heteroatom-doped carbon materials by focusing on their preparation and catalytic applications in organic transformations (Table 13).

By utilizing suitable post-treatment or direct synthesis strategies, heteroatoms (mainly N, B, P, and S) can incorporate into the framework of carbon materials to substitute for carbon atoms. The choice of synthetic conditions, including temperature, source of heteroatoms, and catalyst can modulate the arrangement and distribution of heteroatoms, which further alters the chemical and electronic properties of carbons. These improved chemical and electronic properties lead to a superb performance of heteroatom-doped carbons in the various organic transformations compared to un-doped carbon materials.

The future challenges and perspectives are as follows:

(1) New and suitable starting materials and synthetic strategies are demanded to design and fabricate these carbocatalysts with a large number of active sites and high density of heteroatoms which in turn can provide the materials with increased catalytic performance.

(2) From industrial and commercial perspectives, it is also necessary to develop simple and highly efficient methods for the large-scale production of new carbon materials with a well-defined structure at low cost.

(3) Though single heteroatom-doped carbon catalysts have been received much attention, further studies on the design and synthesis of dual-, tri-, and multi-heteroatom-doped carbons and investigate their application in various organic reactions would be of great interest.

(4) Despite the improvements achieved so far, it is still very difficult to control the content of heteroatom, distributional





uniformity, bonding formats, and some other features. This is especially valid for co-doping cases. All of these features directly or indirectly determine the properties of the doped carbons in catalytic reactions.

(5) The exact location of heteroatoms, the nature of their active sites in carbon materials, and their doping mechanism are still not clear. A combination of experimental studies, state-of-the-art characterizations, and powerful computational calculations are indeed highly required for the better understanding of the structure, mechanism, and kinetics of the catalytic center.

(6) Although N-doped carbon materials have been examined widely as catalysts in various organic transformations, it is evident from this review that there are other dopants such as S, P, and B beyond the N, with suitable physicochemical properties for the introduction into the carbon matrix. In addition, the use of heteroatoms such as selenium, tellurium, etc., can be also studied in the next investigations.

## Conflicts of interest

There are no conflicts to declare.

## Acknowledgements

We are thankful to Alzahra University research Council. We are also grateful to Iran National Science Foundation (INSF) for the financial support provided by the post-doctoral project (99006750).

## References

- H.-U. Blaser, A. Indolese, A. Schnyder, H. Steiner and M. Studer, *J. Mol. Catal. Chem.*, 2001, **173**, 3–18.
- Y. Gong, M. Li, H. Li and Y. Wang, *Green Chem.*, 2015, **17**, 715–736.
- J. Hagen, *Industrial catalysis: a practical approach*, John Wiley & Sons, 2015.
- J. A. Dumesic, G. W. Huber and M. Boudart, *Handbook of Heterogeneous Catalysis*, 2008.
- Y. Rangraz, F. Nemati and A. Elhampour, *Appl. Surf. Sci.*, 2020, **507**, 145164.
- B. Vellaichamy and P. Periakaruppan, *New J. Chem.*, 2017, **41**, 7123–7132.
- M. Li, F. Xu, H. Li and Y. Wang, *Catal. Sci. Technol.*, 2016, **6**, 3670–3693.
- M. Antonietti, N. Lopez-Salas and A. Primo, *Adv. Mater.*, 2019, **31**, 1805719.
- J. Oliver-Meseguer, J. R. Cabrero-Antonino, I. Domínguez, A. Leyva-Pérez and A. Corma, *Science*, 2012, **338**, 1452–1455.
- L. Liu and A. Corma, *Chem. Rev.*, 2018, **118**, 4981–5079.
- A. Corma, A. Leyva-Pérez and M. J. Sabater, *Chem. Rev.*, 2011, **111**, 1657–1712.
- S. K. Kaiser, R. Lin, S. Mitchell, E. Fako, F. Krumeich, R. Hauert, O. V. Safonova, V. A. Kondratenko, E. V. Kondratenko and S. M. Collins, *Chem. Sci.*, 2019, **10**, 359–369.
- J. Zhong, Y. Xu and Z. Liu, *Green Chem.*, 2018, **20**, 2412–2427.
- H. Xu and G. Luo, *J. Ind. Eng. Chem.*, 2018, **65**, 13–25.
- X.-L. Xu, J. Zhao, C.-S. Lu, T.-T. Zhang, X.-X. Di, S.-C. Gu and X.-N. Li, *Chin. Chem. Lett.*, 2016, **27**, 822–826.
- J. Shan, X. Sun, S. Zheng, T. Wang, X. Zhang and G. Li, *Carbon*, 2019, **146**, 60–69.
- K. Wang, P. Jiang, M. Yang, P. Ma, J. Qin, X. Huang, L. Ma and R. Li, *Green Chem.*, 2019, **21**, 2448–2461.
- M. R. Benziger, S. N. Talapaneni, S. Joseph, K. Ramadass, G. Singh, J. Scaranto, U. Ravon, K. Al-Bahily and A. Vinu, *Chem. Soc. Rev.*, 2018, **47**, 2680–2721.
- H. Huang and X. Wang, *J. Mater. Chem. A*, 2014, **2**, 6266–6291.
- D. Haag and H. H. Kung, *Top. Catal.*, 2014, **57**, 762–773.
- C. J. Shearer, A. Cherevan and D. Eder, *Adv. Mater.*, 2014, **26**, 2295–2318.
- X.-K. Kong, C.-L. Chen and Q.-W. Chen, *Chem. Soc. Rev.*, 2014, **43**, 2841–2857.
- P. Veerakumar, P. Thanasekaran, T. Subburaj and K.-C. Lin, *Journal of Carbon Research*, 2018, **4**, 54.
- A. K. Geim and K. S. Novoselov, in *Nanoscience and technology: a collection of reviews from nature journals*, World Scientific, 2010, pp. 11–19.
- C. E. N. E. R. Rao, A. E. K. Sood, K. E. S. Subrahmanyam and A. Govindaraj, *Angew. Chem., Int. Ed.*, 2009, **48**, 7752–7777.
- Y. Zhu, S. Murali, W. Cai, X. Li, J. W. Suk, J. R. Potts and R. S. Ruoff, *Adv. Mater.*, 2010, **22**, 3906–3924.
- Y.-J. Wang, D. P. Wilkinson and J. Zhang, *Chem. Rev.*, 2011, **111**, 7625–7651.
- Y. Gao, D. Ma, C. Wang, J. Guan and X. Bao, *Chem. Commun.*, 2011, **47**, 2432–2434.
- A. Primo, F. Neatu, M. Florea, V. Parvulescu and H. Garcia, *Nat. Commun.*, 2014, **5**, 1–9.
- X. Hu, Y. Long, M. Fan, M. Yuan, H. Zhao, J. Ma and Z. Dong, *Appl. Catal., B*, 2019, **244**, 25–35.
- R. Gao, L. Pan, J. Lu, J. Xu, X. Zhang, L. Wang and J. J. Zou, *ChemCatChem*, 2017, **9**, 4287–4294.
- J. Song, Z.-F. Huang, L. Pan, K. Li, X. Zhang, L. Wang and J.-J. Zou, *Appl. Catal., B*, 2018, **227**, 386–408.
- K. Gong, F. Du, Z. Xia, M. Durstock and L. Dai, *Science*, 2009, **323**, 760–764.
- S. Ni, Z. Li and J. Yang, *Nanoscale*, 2012, **4**, 1184–1189.
- L. Yang, S. Jiang, Y. Zhao, L. Zhu, S. Chen, X. Wang, Q. Wu, J. Ma, Y. Ma and Z. Hu, *Angew. Chem., Int. Ed.*, 2011, **50**, 7132–7135.
- D. Wei, Y. Liu, Y. Wang, H. Zhang, L. Huang and G. Yu, *Nano Lett.*, 2009, **9**, 1752–1758.
- Z. Li, H. Yu, T. Bian, Y. Zhao, C. Zhou, L. Shang, Y. Liu, L.-Z. Wu, C.-H. Tung and T. Zhang, *J. Mater. Chem. C*, 2015, **3**, 1922–1928.
- D. Xiong, X. Li, L. Fan and Z. Bai, *Catalysts*, 2018, **8**, 301.
- S. G. Peera, H.-J. Kwon, T. G. Lee and A. M. Hussain, *Ionics*, 2020, **26**, 1563–1589.
- J. Quílez-Bermejo, E. Morallón and D. Cazorla-Amorós, *Carbon*, 2020, **165**, 434–454.



- 41 D.-S. Yang, D. Bhattacharjya, S. Inamdar, J. Park and J.-S. Yu, *J. Am. Chem. Soc.*, 2012, **134**, 16127–16130.
- 42 B. Li and D. Su, *J. Phys. Chem. C*, 2013, **117**, 17485–17492.
- 43 K. Chizari, A. Deneuve, O. Ersen, I. Florea, Y. Liu, D. Edouard, I. Janowska, D. Begin and C. Pham-Huu, *ChemSusChem*, 2012, **5**, 102–108.
- 44 M. Latorre-Sánchez, A. Primo and H. García, *Angew. Chem., Int. Ed.*, 2013, **52**, 11813–11816.
- 45 E. J. Biddinger and U. S. Ozkan, *J. Phys. Chem. C*, 2010, **114**, 15306–15314.
- 46 C. Tang, H. F. Wang, X. Chen, B. Q. Li, T. Z. Hou, B. Zhang, Q. Zhang, M. M. Titirici and F. Wei, *Adv. Mater.*, 2016, **28**, 6845–6851.
- 47 X. Wang, G. Sun, P. Routh, D.-H. Kim, W. Huang and P. Chen, *Chem. Soc. Rev.*, 2014, **43**, 7067–7098.
- 48 K. N. Wood, R. O'Hayre and S. Pylypenko, *Energy Environ. Sci.*, 2014, **7**, 1212–1249.
- 49 E. K. Rideal and W. M. Wright, *J. Chem. Soc.*, 1926, **129**, 1813–1821.
- 50 S. K. Kaiser, Z. Chen, D. Faust Akl, S. Mitchell and J. Pérez-Ramírez, *Chem. Rev.*, 2020, **120**, 11703–11809.
- 51 S. Dang, *ChemSusChem*, 2010, **3**, 169–180.
- 52 L. Liu, Y. P. Zhu, M. Su and Z. Y. Yuan, *ChemCatChem*, 2015, **7**, 2765–2787.
- 53 R. Mirsafaei, M. M. Heravi, S. Ahmadi, M. H. Moslemin and T. Hosseinnnejad, *J. Mol. Catal. Chem.*, 2015, **402**, 100–108.
- 54 M. M. Heravi, S. Sadjadi, H. A. Oskooie, R. H. Shoar and F. F. Bamoharram, *Catal. Commun.*, 2008, **9**, 470–474.
- 55 M. M. Heravi, E. Hashemi, Y. S. Beheshtiha, K. Kamjou, M. Toolabi and N. Hosseintash, *J. Mol. Catal. Chem.*, 2014, **392**, 173–180.
- 56 M. M. Heravi, V. Zadsirjan, K. Bakhtiari, H. A. Oskooie and F. F. Bamoharram, *Catal. Commun.*, 2007, **8**, 315–318.
- 57 M. M. Heravi, K. Bakhtiari, A. Fatehi and F. F. Bamoharram, *Catal. Commun.*, 2008, **9**, 289–292.
- 58 S. Sadjadi, M. M. Heravi and M. Malmir, *Carbohydr. Polym.*, 2018, **186**, 25–34.
- 59 S. Sadjadi, M. Malmir and M. Heravi, *RSC Adv.*, 2017, **7**, 36807–36818.
- 60 S. Sadjadi, T. Hosseinnnejad, M. Malmir and M. M. Heravi, *New J. Chem.*, 2017, **41**, 13935–13951.
- 61 R. Mirsafaei, M. M. Heravi, T. Hosseinnnejad and S. Ahmadi, *Appl. Organomet. Chem.*, 2016, **30**, 823–830.
- 62 F. G. Kahangi, M. Mehrdad, M. M. Heravi and S. Sadjadi, *Sci. Rep.*, 2020, **10**, 1–11.
- 63 S. Sadjadi, M. Akbari, F. G. Kahangi and M. M. Heravi, *Appl. Clay Sci.*, 2020, **192**, 105640.
- 64 M. M. Heravi, S. Asadi, S. M. Hoseini Chopani and E. Jaderi, *Appl. Organomet. Chem.*, 2020, **34**, e5805.
- 65 S. Hosseinzadeh-Baghan, M. Mirzaei, H. Eshtiagh-Hosseini, V. Zadsirjan, M. M. Heravi and J. T. Mague, *Appl. Organomet. Chem.*, 2020, **34**, e5793.
- 66 R. Zoghi, M. M. Heravi, N. Montazeri, M. M. Zeydi and T. Hosseinnnejad, *Appl. Organomet. Chem.*, 2020, **34**, e5435.
- 67 S. Sadjadi, M. Akbari and M. M. Heravi, *ACS Omega*, 2019, **4**, 19442–19451.
- 68 S. Sadjadi, G. Lazzara, M. Malmir and M. M. Heravi, *J. Catal.*, 2018, **366**, 245–257.
- 69 M. M. Heravi, B. Heidari, V. Zadsirjan and L. Mohammadi, *RSC Adv.*, 2020, **10**, 24893–24940.
- 70 N. Lotfian, M. M. Heravi, M. Mirzaei and B. Heidari, *Appl. Organomet. Chem.*, 2019, **33**, e4808.
- 71 S. Sadjadi and M. M. Heravi, *Curr. Org. Chem.*, 2016, **20**, 1404–1444.
- 72 M. M. Heravi, B. Heidari, M. Ghavidel and T. Ahmadi, *Curr. Org. Chem.*, 2017, **21**, 2249–2313.
- 73 S. Sadjadi and M. M. Heravi, *RSC Adv.*, 2017, **7**, 30815–30838.
- 74 M. M. Heravi and T. Alishiri, *Heterocycles*, 2012, **85**, 545–586.
- 75 M. M. Heravi and S. Sadjadi, *J. Iran. Chem. Soc.*, 2009, **6**, 1–54.
- 76 L. Sun, L. Wang, C. Tian, T. Tan, Y. Xie, K. Shi, M. Li and H. Fu, *RSC Adv.*, 2012, **2**, 4498–4506.
- 77 Y. Wang, Y. Shao, D. W. Matson, J. Li and Y. Lin, *ACS Nano*, 2010, **4**, 1790–1798.
- 78 E. Yoo, J. Kim, E. Hosono, H.-s. Zhou, T. Kudo and I. Honma, *Nano Lett.*, 2008, **8**, 2277–2282.
- 79 D. R. Kauffman and A. Star, *Analyst*, 2010, **135**, 2790–2797.
- 80 S. Wang, L. Zhang, Z. Xia, A. Roy, D. W. Chang, J.-B. Baek and L. Dai, *Angew. Chem., Int. Ed.*, 2012, **51**, 4209–4212.
- 81 D. S. Su, J. Zhang, B. Frank, A. Thomas, X. Wang, J. Paraknowitsch and R. Schlögl, *ChemSusChem*, 2010, **3**, 169–180.
- 82 D. R. Dreyer, H.-P. Jia and C. W. Bielawski, *Angew. Chem., Int. Ed.*, 2010, **49**, 6686.
- 83 H. Sun, Y. Wang, S. Liu, L. Ge, L. Wang, Z. Zhu and S. Wang, *Chem. Commun.*, 2013, **49**, 9914–9916.
- 84 C. Biswas and Y. H. Lee, *Adv. Funct. Mater.*, 2011, **21**, 3806–3826.
- 85 D. Haag and H. H. Kung, *Top. Catal.*, 2014, **57**, 762–773.
- 86 C. Huang, C. Li and G. Shi, *Energy Environ. Sci.*, 2012, **5**, 8848–8868.
- 87 X. Duan, K. O'Donnell, H. Sun, Y. Wang and S. Wang, *Small*, 2015, **11**, 3036–3044.
- 88 D. Geng, S. Yang, Y. Zhang, J. Yang, J. Liu, R. Li, T.-K. Sham, X. Sun, S. Ye and S. Knights, *Appl. Surf. Sci.*, 2011, **257**, 9193–9198.
- 89 C. Wang, J. Kang, H. Sun, H. M. Ang, M. O. Tadé and S. Wang, *Carbon*, 2016, **102**, 279–287.
- 90 C. Su, M. Acik, K. Takai, J. Lu, S.-j. Hao, Y. Zheng, P. Wu, Q. Bao, T. Enoki, Y. J. Chabal and K. Ping Loh, *Nat. Commun.*, 2012, **3**, 1298.
- 91 Y. Gao, P. Tang, H. Zhou, W. Zhang, H. Yang, N. Yan, G. Hu, D. Mei, J. Wang and D. Ma, *Angew. Chem., Int. Ed.*, 2016, **55**, 3124–3128.
- 92 A. Dhakshinamoorthy, M. Latorre-Sanchez, A. M. Asiri, A. Primo and H. Garcia, *Catal. Commun.*, 2015, **65**, 10–13.
- 93 Y. Zhai, Z. Zhu and S. Dong, *ChemCatChem*, 2015, **7**, 2806–2815.
- 94 M. F. L. De Volder, S. H. Tawfick, R. H. Baughman and A. J. Hart, *Science*, 2013, **339**, 535–539.



- 95 V. Campisciano, M. Gruttadauria and F. Giacalone, *ChemCatChem*, 2019, **11**, 90–133.
- 96 S. Reich, C. Thomsen and J. Maultzsch, *Carbon nanotubes: basic concepts and physical properties*, John Wiley & Sons, 2008.
- 97 D. M. Guldi and N. Martín, *Carbon nanotubes and related structures*, VCH-Wiley, Weinheim, Germany, 2010.
- 98 A. C. Dillon, *Chem. Rev.*, 2010, **110**, 6856–6872.
- 99 L. Wang, H. Liu, R. M. Konik, J. A. Misewich and S. S. Wong, *Chem. Soc. Rev.*, 2013, **42**, 8134–8156.
- 100 S. A. Miners, G. A. Rance and A. N. Khlobystov, *Chem. Soc. Rev.*, 2016, **45**, 4727–4746.
- 101 D. Tasis, N. Tagmatarchis, A. Bianco and M. Prato, *Chem. Rev.*, 2006, **106**, 1105–1136.
- 102 Y. Zhang, J. Zhang and D. S. Su, *ChemSusChem*, 2014, **7**, 1240–1250.
- 103 Z. Yang, Z. Liu, H. Zhang, B. Yu, Y. Zhao, H. Wang, G. Ji, Y. Chen, X. Liu and Z. Liu, *Chem. Commun.*, 2017, **53**, 929–932.
- 104 S. K. Movahed, Z. Piraman and M. Dabiri, *J. Photochem. Photobiol., A*, 2018, **351**, 208–224.
- 105 H. Li, *Prog. Chem.*, 2016, **28**, 1462.
- 106 Y. Zheng, J. Liu, J. Liang, M. Jaroniec and S. Z. Qiao, *Energy Environ. Sci.*, 2012, **5**, 6717–6731.
- 107 S. M. Saufi and A. F. Ismail, *Carbon*, 2004, **42**, 241–259.
- 108 C. West, C. Elfakir and M. Lafosse, *J. Chromatogr., A*, 2010, **1217**, 3201–3216.
- 109 J. L. Figueiredo, *J. Mater. Chem. A*, 2013, **1**, 9351–9364.
- 110 K. Zhang, Z. Hu and J. Chen, *J. Eng. Chem.*, 2013, **22**, 214–225.
- 111 S. De, A. M. Balu, J. C. van der Waal and R. Luque, *ChemCatChem*, 2015, **7**, 1608–1629.
- 112 Y. Xia, Z. Yang and R. Mokaya, *Nanoscale*, 2010, **2**, 639–659.
- 113 B. Sakintuna and Y. Yürüm, *Ind. Eng. Chem. Res.*, 2005, **44**, 2893–2902.
- 114 J. H. Khan, F. Marpaung, C. Young, J. Lin, M. T. Islam, S. M. Alsheri, T. Ahamad, N. Alhokbany, K. Ariga, L. K. Shrestha, Y. Yamauchi, K. C. W. Wu, M. S. A. Hossain and J. Kim, *Microporous Mesoporous Mater.*, 2019, **274**, 251–256.
- 115 T. Kesavan, T. Partheeban, M. Vivekanantha, M. Kundu, G. Maduraiveeran and M. Sasidharan, *Microporous Mesoporous Mater.*, 2019, **274**, 236–244.
- 116 B. Li, H. Xiong and Y. Xiao, *Int. J. Electrochem. Sci.*, 2020, **15**, 1363–1377.
- 117 J. Lee, J. Kim and T. Hyeon, *Adv. Mater.*, 2006, **18**, 2073–2094.
- 118 R. C. Bansal, J.-B. Donnet and F. Stoeckli, *Active carbon*, 1988.
- 119 T. R. Gaffney, *Curr. Opin. Solid State Mater. Sci.*, 1996, **1**, 69–75.
- 120 X. Q. Zhang and A. H. Lu, *Materials for Carbon Capture*, 2020, pp. 29–95.
- 121 R. Ryoo, S. H. Joo and S. Jun, *J. Phys. Chem. B*, 1999, **103**, 7743–7746.
- 122 P. Zhang, H. Zhu and S. Dai, *ChemCatChem*, 2015, **7**, 2788–2805.
- 123 T. Asefa, *Acc. Chem. Res.*, 2016, **49**, 1873–1883.
- 124 M. Enterría and J. Figueiredo, *Carbon*, 2016, **108**, 79–102.
- 125 Y. Cao, S. Mao, M. Li, Y. Chen and Y. Wang, *ACS Catal.*, 2017, **7**, 8090–8112.
- 126 D. Salinas-Torres, M. Navlani-García, K. Mori, Y. Kuwahara and H. Yamashita, *Appl. Catal. Gen.*, 2019, **571**, 25–41.
- 127 T. Zhang and T. Asefa, *Adv. Mater.*, 2019, **31**, 1804394.
- 128 B. Wang, T. P. Ang and A. Borgna, *Microporous Mesoporous Mater.*, 2012, **158**, 99–107.
- 129 D. S. Su, S. Perathoner and G. Centi, *Chem. Rev.*, 2013, **113**, 5782–5816.
- 130 P. Zhang, J. Zhang and S. Dai, *Chem.–Eur. J.*, 2017, **23**, 1986–1998.
- 131 W. Zhang, F. Wang, X. Li, Y. Liu and J. Ma, *RSC Adv.*, 2016, **6**, 27313–27319.
- 132 L. Wang and X. Hu, *Chem. Asian J.*, 2018, **13**, 1518–1529.
- 133 Z. Luo, S. Lim, Z. Tian, J. Shang, L. Lai, B. MacDonald, C. Fu, Z. Shen, T. Yu and J. Lin, *J. Mater. Chem.*, 2011, **21**, 8038–8044.
- 134 X. Wang, X. Li, L. Zhang, Y. Yoon, P. K. Weber, H. Wang, J. Guo and H. Dai, *Science*, 2009, **324**, 768–771.
- 135 D. H. Lee, W. J. Lee and S. O. Kim, *Nano Lett.*, 2009, **9**, 1427–1432.
- 136 H. Gao, Z. Liu, L. Song, W. Guo, W. Gao, L. Ci, A. Rao, W. Quan, R. Vajtai and P. M. Ajayan, *Nanotechnology*, 2012, **23**, 275605.
- 137 J. Xu, G. Dong, C. Jin, M. Huang and L. Guan, *ChemSusChem*, 2013, **6**, 493–499.
- 138 E. Cruz-Silva, D. A. Cullen, L. Gu, J. M. Romo-Herrera, E. Muñoz-Sandoval, F. López-Urías, B. G. Sumpter, V. Meunier, J.-C. Charlier and D. J. Smith, *ACS Nano*, 2008, **2**, 441–448.
- 139 S. Some, J. Kim, K. Lee, A. Kulkarni, Y. Yoon, S. Lee, T. Kim and H. Lee, *Adv. Mater.*, 2012, **24**, 5481–5486.
- 140 L. Panchakarla, K. Subrahmanyam, S. Saha, A. Govindaraj, H. Krishnamurthy, U. Waghmare and C. Rao, *Adv. Mater.*, 2009, **21**, 4726–4730.
- 141 Z. Wang, C. Yu, D. Ba and J. Liang, *Vacuum*, 2007, **81**, 579–582.
- 142 S. K. Kaiser, K. S. Song, S. Mitchell, A. Coskun and J. Pérez-Ramírez, *ChemCatChem*, 2019, **12**, 1922–1925.
- 143 Y. Xue, B. Wu, L. Jiang, Y. Guo, L. Huang, J. Chen, J. Tan, D. Geng, B. Luo and W. Hu, *J. Am. Chem. Soc.*, 2012, **134**, 11060–11063.
- 144 Y. Luo, Z. Yang, W. Guo, H. Chen, T. Wang, Y. Liu, Y. Lyu, H. Luo and S. Dai, *J. Mater. Chem. A*, 2020, **8**, 4740–4746.
- 145 L. Zhao, P.-W. Xiao and B.-H. Han, *Porous Carbon Materials from Sustainable Precursors*, *Green Chem.*, 2015, **32**, 191–224.
- 146 G. Wu, A. Santandreu, W. Kellogg, S. Gupta, O. Ogoke, H. Zhang, H.-L. Wang and L. Dai, *Nano Energy*, 2016, **29**, 83–110.
- 147 J. Zhang, Z. Xia and L. Dai, *Sci. Adv.*, 2015, **1**, e1500564.
- 148 R. Ma, Y. Ma, Y. Dong and J.-M. Lee, *Nano Adv.*, 2016, **1**, 50–61.
- 149 Y. Deng, Y. Xie, K. Zou and X. Ji, *J. Mater. Chem. A*, 2016, **4**, 1144–1173.



- 150 G. Wu, C. M. Johnston, N. H. Mack, K. Artyushkova, M. Ferrandon, M. Nelson, J. S. Lezama-Pacheco, S. D. Conradson, K. L. More and D. J. Myers, *J. Mater. Chem.*, 2011, **21**, 11392–11405.
- 151 K. Chizari, A. Vena, L. Laurentius and U. Sundararaj, *Carbon*, 2014, **68**, 369–379.
- 152 S. Wang, C. Han, J. Wang, J. Deng, M. Zhu, J. Yao, H. Li and Y. Wang, *Chem. Mater.*, 2014, **26**, 6872–6877.
- 153 Z. Xia, L. An, P. Chen and D. Xia, *Adv. Energy Mater.*, 2016, **6**, 1600458.
- 154 T. Schiros, D. Nordlund, L. Pálková, D. Prezzi, L. Zhao, K. S. Kim, U. Wurstbauer, C. Gutiérrez, D. Delongchamp and C. Jaye, *Nano Lett.*, 2012, **12**, 4025–4031.
- 155 L. Dong, X. Chen, J. Ma, Q. Shao, A. Li, W. Yan and J. Zhang, *Russ. J. Electrochem.*, 2019, **55**, 1098–1109.
- 156 J. Quilez-Bermejo, E. Morallón and D. Cazorla-Amorós, *Carbon*, 2020, **165**, 434–454.
- 157 L. Xu, G. Pan, X. Liang, G. Luo, C. Zou and G. Chen, *J. Energy Chem.*, 2014, **23**, 498–506.
- 158 L. Lai, J. R. Potts, D. Zhan, L. Wang, C. K. Poh, C. Tang, H. Gong, Z. Shen, J. Lin and R. S. Ruoff, *Energy Environ. Sci.*, 2012, **5**, 7936–7942.
- 159 Z. Huang, Z. Liao, W. Yang, H. Zhou, C. Fu, Y. Gong, L. Chen and Y. Kuang, *Electrochim. Acta*, 2017, **245**, 957–966.
- 160 D. A. Bulushev, M. Zacharska, A. S. Lisitsyn, O. Y. Podyacheva, F. S. Hage, Q. M. Ramasse, U. Bangert and L. G. Bulusheva, *ACS Catal.*, 2016, **6**, 3442–3451.
- 161 Y.-H. Li, T.-H. Hung and C.-W. Chen, *Carbon*, 2009, **47**, 850–855.
- 162 R. Arrigo, M. E. Schuster, Z. Xie, Y. Yi, G. Wowsnick, L. L. Sun, K. E. Hermann, M. Friedrich, P. Kast and M. Hävecker, *ACS Catal.*, 2015, **5**, 2740–2753.
- 163 M. Zacharska, L. G. Bulusheva, A. S. Lisitsyn, S. Beloshapkin, Y. Guo, A. L. Chuvilin, E. V. Shlyakhova, O. Y. Podyacheva, J. J. Leahy and A. V. Okotrub, *ChemSusChem*, 2017, **10**, 720–730.
- 164 D. Guo, R. Shibuya, C. Akiba, S. Saji, T. Kondo and J. Nakamura, *Science*, 2016, **351**, 361–365.
- 165 Y. Zhao, J. Wan, H. Yao, L. Zhang, K. Lin, L. Wang, N. Yang, D. Liu, L. Song and J. Zhu, *Nat. Chem.*, 2018, **10**, 924–931.
- 166 J. Long, X. Xie, J. Xu, Q. Gu, L. Chen and X. Wang, *ACS Catal.*, 2012, **2**, 622–631.
- 167 R. Lin, S. K. Kaiser, R. Hauert and J. Pérez-Ramírez, *ACS Catal.*, 2018, **8**, 1114–1121.
- 168 Z. Li, J. Li, J. Liu, Z. Zhao, C. Xia and F. Li, *ChemCatChem*, 2014, **6**, 1333–1339.
- 169 R. Nie, M. Miao, W. Du, J. Shi, Y. Liu and Z. Hou, *Appl. Catal., B*, 2016, **180**, 607–613.
- 170 Y. Yang, L. Gu, S. Guo, S. Shao, Z. Li, Y. Sun and S. Hao, *Front. Chem.*, 2019, **7**, 761.
- 171 X. Xu, Y. Li, Y. Gong, P. Zhang, H. Li and Y. Wang, *J. Am. Chem. Soc.*, 2012, **134**, 16987–16990.
- 172 Z. Li, J. Liu, C. Xia and F. Li, *ACS Catal.*, 2013, **3**(11), 2440–2448.
- 173 Y. Gao, G. Hu, J. Zhong, Z. Shi, Y. Zhu, D. S. Su, J. Wang, X. Bao and D. Ma, *Angew. Chem., Int. Ed.*, 2013, **52**, 2109–2113.
- 174 M. N. Groves, A. S. W. Chan, C. Malardier-Jugroot and M. Jugroot, *Chem. Phys. Lett.*, 2009, **481**, 214–219.
- 175 C. Petit, G. W. Peterson, J. Mahle and T. J. Bandosz, *Carbon*, 2010, **48**, 1779–1787.
- 176 Y. Li, J. Wang, X. Li, D. Geng, M. N. Banis, Y. Tang, D. Wang, R. Li, T.-K. Sham and X. Sun, *J. Mater. Chem.*, 2012, **22**, 20170–20174.
- 177 M. Seredych, K. Singh and T. J. Bandosz, *Electroanalysis*, 2014, **26**, 109–120.
- 178 Y. Yan, Y.-X. Yin, S. Xin, Y.-G. Guo and L.-J. Wan, *Chem. Commun.*, 2012, **48**, 10663–10665.
- 179 X. Zhao, Q. Zhang, C.-M. Chen, B. Zhang, S. Reiche, A. Wang, T. Zhang, R. Schlögl and D. Sheng Su, *Nano Energy*, 2012, **1**, 624–630.
- 180 F. Li, D. Yang and H. Xu, *Chem.-Eur. J.*, 2019, **25**, 1165–1176.
- 181 X. Kou, S. Jiang, S.-J. Park and L.-Y. Meng, *Dalton Trans.*, 2020, **49**, 6915–6938.
- 182 Q. Abbas, R. Raza, I. Shabbir and A. G. Olabi, *J. Sci.: Adv. Mater. Devices*, 2019, **4**, 341–352.
- 183 P. Serp and B. Machado, *Nanostructured carbon materials for catalysis*, Royal Society of Chemistry, 2015.
- 184 R. Li, J. Zhao, D. Han and X. Li, *Catal. Commun.*, 2017, **97**, 116–119.
- 185 J. P. Paraknowitsch and A. Thomas, *Energy Environ. Sci.*, 2013, **6**, 2839–2855.
- 186 X. Xie, J. Shi, Y. Pu, Z. Wang, L.-L. Zhang, J.-X. Wang and D. Wang, *J. Colloid Interface Sci.*, 2020, **571**, 100–108.
- 187 C. Liao, B. Liu, Q. Chi and Z. Zhang, *ACS Appl. Mater. Interfaces*, 2018, **10**, 44421–44429.
- 188 Q. Shen, X. Chen, Y. Tan, J. Chen, L. Chen and S. Tan, *ACS Appl. Mater. Interfaces*, 2019, **11**, 38838–38848.
- 189 G. Li, S. Zheng, L. Wang and X. Zhang, *ACS Omega*, 2020, **5**, 7519–7528.
- 190 W. Xiong, Z. Wang, S. He, F. Hao, Y. Yang, Y. Lv, W. Zhang, P. Liu and H. A. Luo, *Appl. Catal., B*, 2020, **260**, 118105.
- 191 Z. He, J. Liu, Q. Wang, M. Zhao, Z. Wen, J. Chen, D. Manoj, C. Xie, J. Xi, J. Yu, C. Tang, Z. Bai and S. Wang, *J. Catal.*, 2019, **377**, 199–208.
- 192 N. Liu, L. Ding, H. Li, M. Jia, W. Zhang, N. An and X. Yuan, *J. Colloid Interface Sci.*, 2017, **490**, 677–684.
- 193 J. Liu, X. Yan, L. Wang, L. Kong and P. Jian, *J. Colloid Interface Sci.*, 2017, **497**, 102–107.
- 194 Y. Dai, J. Zhou, C. Huang, Q. Gu, Y. Zeng, W. Xu, X. Meng, W. Fu and Y. Sun, *Part. Part. Syst. Char.*, 2018, **35**, 1700395.
- 195 Z. Wang and Q. Chen, *ChemistrySelect*, 2018, **3**, 1108–1112.
- 196 Z. Wang, R. Su, D. Wang, J. Shi, J.-X. Wang, Y. Pu and J.-F. Chen, *Ind. Eng. Chem. Res.*, 2017, **56**, 13610–13617.
- 197 X. Chen, Q. Shen, Z. Li, W. Wan, J. Chen and J. Zhang, *ACS Appl. Mater. Interfaces*, 2020, **12**, 654–666.
- 198 R. Gao, L. Pan, J. Lu, J. Xu, X. Zhang, L. Wang and J.-J. Zou, *ChemCatChem*, 2017, **9**, 4287–4294.
- 199 Y. Lin, S. Wu, W. Shi, B. Zhang, J. Wang, Y. A. Kim, M. Endo and D. S. Su, *Chem. Commun.*, 2015, **51**, 13086–13089.
- 200 F. Wang, S. Song, K. Li, J. Li, J. Pan, S. Yao, X. Ge, J. Feng, X. Wang and H. Zhang, *Adv. Mater.*, 2016, **28**, 10679–10683.





- 201 X. Hu, X. Sun, Q. Song, Y. Zhu, Y. Long and Z. Dong, *Green Chem.*, 2020, **22**, 742–752.
- 202 F. Yang, Y. Cao, Z. Chen, X. He, L. Hou and Y. Li, *New J. Chem.*, 2018, **42**, 2718–2725.
- 203 C. Van Nguyen, S. Lee, Y. G. Chung, W.-H. Chiang and K. C. W. Wu, *Appl. Catal., B*, 2019, **257**, 117888.
- 204 J. Xi, Q. Wang, J. Liu, L. Huan, Z. He, Y. Qiu, J. Zhang, C. Tang, J. Xiao and S. Wang, *J. Catal.*, 2018, **359**, 233–241.
- 205 Q. Wei, F. Qin, Q. Ma and W. Shen, *Carbon*, 2019, **141**, 542–552.
- 206 Y. Liu, H. Zhang, X. Li, L. Wang, Y. Dong, W. Li and J. Zhang, *Appl. Catal. Gen.*, 2021, **611**, 117902.
- 207 F. Lu, D. Xu, Y. Lu, B. Dai and M. Zhu, *Chin. J. Chem. Eng.*, 2021, **29**, 196–203.
- 208 X. Li, J. Zhang and W. Li, *J. Ind. Eng. Chem.*, 2016, **44**, 146–154.
- 209 X. Li, J. Zhang, Y. Han, M. Zhu, S. Shang and W. Li, *J. Mater. Sci.*, 2018, **53**, 4913–4926.
- 210 S. Chao, F. Zou, F. Wan, X. Dong, Y. Wang, Y. Wang, Q. Guan, G. Wang and W. Li, *Sci. Rep.*, 2017, **7**, 1–7.
- 211 X. Qi, W. Chen and J. Zhang, *RSC Adv.*, 2020, **10**, 34612–34620.
- 212 B. Dai, K. Chen, Y. Wang, L. Kang and M. Zhu, *ACS Catal.*, 2015, **5**, 2541–2547.
- 213 J. Zhao, B. Wang, Y. Yue, G. Sheng, H. Lai, S. Wang, L. Yu, Q. Zhang, F. Feng, Z.-T. Hu and X. Li, *J. Catal.*, 2019, **373**, 240–249.
- 214 J. Wang, F. Zhao, C. Zhang, L. Kang and M. Zhu, *Appl. Catal. Gen.*, 2018, **549**, 68–75.
- 215 X. Dong, S. Chao, F. Wan, Q. Guan, G. Wang and W. Li, *J. Catal.*, 2018, **359**, 161–170.
- 216 H. Fu, K. Huang, G. Yang, Y. Cao, H. Wang, F. Peng, Q. Wang and H. Yu, *ACS Catal.*, 2019, **10**, 129–137.
- 217 Y. Lin, Z. Liu, Y. Niu, B. Zhang, Q. Lu, S. Wu, G. Centi, S. Perathoner, S. Heumann, L. Yu and D. S. Su, *ACS Nano*, 2019, **13**, 13995–14004.
- 218 P. Liang, C. Zhang, X. Duan, H. Sun, S. Liu, M. O. Tade and S. Wang, *ACS Sustain. Chem. Eng.*, 2017, **5**, 2693–2701.
- 219 G. Wen, Q. Gu, Y. Liu, R. Schlögl, C. Wang, Z. Tian and D. S. Su, *Angew. Chem., Int. Ed.*, 2018, **57**, 16898–16902.
- 220 S. Indrawirawan, H. Sun, X. Duan and S. Wang, *J. Mater. Chem. A*, 2015, **3**, 3432–3440.
- 221 Z. Ma, H. Zhang, Z. Yang, G. Ji, B. Yu, X. Liu and Z. Liu, *Green Chem.*, 2016, **18**, 1976–1982.
- 222 X. Wang and Y. Li, *J. Mater. Chem. A*, 2016, **4**, 5247–5257.
- 223 C. Rizescu, I. Podolean, J. Alberro, V. I. Parvulescu, S. M. Coman, C. Bucur, M. Puche and H. Garcia, *Green Chem.*, 2017, **19**, 1999–2005.
- 224 R. Huang, C. Cao, J. Liu, D. Sun and W. Song, *Chem. Commun.*, 2019, **55**, 1935–1938.
- 225 K. Wang, P. Jiang, M. Yang, P. Ma, J. Qin, X. Huang, L. Ma and R. Li, *Green Chem.*, 2019, **21**, 2448–2461.
- 226 H. Watanabe, S. Asano, S.-i. Fujita, H. Yoshida and M. Arai, *ACS Catal.*, 2015, **5**, 2886–2894.
- 227 S.-I. Fujita, S. Asano and M. Arai, *J. Mol. Catal. Chem.*, 2016, **423**, 181–184.
- 228 S. Shang, W. Dai, L. Wang, Y. Lv and S. Gao, *Chem. Commun.*, 2017, **53**, 1048–1051.
- 229 G.-X. Qin, Y. Hao, S. Wang and Y.-B. Dong, *Appl. Catal. Gen.*, 2020, **591**, 117400.
- 230 N. Teng, J.-L. Li, B.-Q. Lu, Y.-Q. Wang, S.-Y. Jia, Y.-X. Wang and X.-L. Hou, *N. Carbon Mater.*, 2019, **34**, 593–599.
- 231 Y. Sun, J. Hao, X. Zhu, B. Zhang, H. Yin, S. Xu, C. Hou and K. Liu, *Carbon Lett.*, 2020, **30**, 133–141.
- 232 S. Verma, M. N. Nadagouda and R. S. Varma, *Sci. Rep.*, 2017, **7**, 1–6.
- 233 Y. Ren, Z. Yuan, K. Lv, J. Sun, Z. Zhang and Q. Chi, *Green Chem.*, 2018, **20**, 4946–4956.
- 234 G. Lv, H. Wang, Y. Yang, X. Li, T. Deng, C. Chen, Y. Zhu and X. Hou, *Catal. Sci. Technol.*, 2016, **6**, 2377–2386.
- 235 N. Gupta, O. Khavryuchenko, A. Villa and D. Su, *ChemSusChem*, 2017, **10**, 3030–3034.
- 236 K. T. V. Rao, Y. Hu, Z. Yuan, Y. Zhang and C. Xu, *Chem. Eng. J.*, 2021, **404**, 127063.
- 237 Z. Li, Y. Huang, X. Chi, D. Li, L. Zhong, X. Li, C. Liu and X. Peng, *Green Energy Environ.*, 2021, 1–19.
- 238 Y. Sun, C. Hou, X. Cao and K. Liu, *J. Mater. Sci.*, 2021, **56**, 6124–6134.
- 239 Y. Guo, Z. Zeng, Y. Li, Z. Huang and Y. Cui, *Catal. Today*, 2018, **307**, 12–19.
- 240 Z. Wang, J. Shi, D. Wang, Y. Pu, J.-X. Wang and J.-F. Chen, *Chem. React. Eng.*, 2019, **4**, 507–515.
- 241 Z. Long, L. Sun, W. Zhu, G. Chen, X. Wang and W. Sun, *Chem. Commun.*, 2018, **54**, 8991–8994.
- 242 X. Hu, M. Fan, Y. Zhu, Q. Zhu, Q. Song and Z. Dong, *Green Chem.*, 2019, **21**, 5274–5283.
- 243 F. Yang, X. Fan, C. Wang, W. Yang, L. Hou, X. Xu, A. Feng, S. Dong, K. Chen, Y. Wang and Y. Li, *Carbon*, 2017, **121**, 443–451.
- 244 M. A. Patel, F. Luo, M. R. Khoshi, E. Rabie, Q. Zhang, C. R. Flach, R. Mendelsohn, E. Garfunkel, M. Szostak and H. He, *ACS Nano*, 2016, **10**, 2305–2315.
- 245 Y. Zhai, M. Chu, C. Xie, F. Huang, C. Zhang, Y. Zhang, H. Liu, H. Wang and Y. Gao, *ACS Sustain. Chem. Eng.*, 2018, **6**, 17410–17418.
- 246 W. Cheng, X. Liu, N. Li, J. Han, S. Li and S. Yu, *RSC Adv.*, 2018, **8**, 11222–11229.
- 247 R. Goyal, B. Sarkar, A. Bag, F. Lefebvre, S. Sameer, C. Pendem and A. Bordoloi, *J. Mater. Chem. A*, 2016, **4**, 18559–18569.
- 248 H. Wei, Y. Ma, J. Luo, K.-H. Wu, W. Xie, G. Wen, C.-L. Chiang, W. Yan, S. Perathoner, G. Centi and Y. Liu, *Carbon*, 2020, **170**, 338–346.
- 249 Y.-N. Zhu, C.-Y. Cao, W.-J. Jiang, S.-L. Yang, J.-S. Hu, W.-G. Song and L.-J. Wan, *J. Mater. Chem. A*, 2016, **4**, 18470–18477.
- 250 S. Yang, L. Peng, P. Huang, X. Wang, Y. Sun, C. Cao and W. Song, *Angew. Chem.*, 2016, **128**, 4084–4088.
- 251 S. Yang, Y. Zhu, C. Cao, L. Peng, S. Li, D. Zhai and W. Song, *Nanoscale*, 2017, **9**, 13538–13545.
- 252 Z. Zhao, Y. Dai, G. Ge, X. Guo and G. Wang, *RSC Adv.*, 2015, **65**, 53095–53099.
- 253 S. Li, W. Wang, X. Liu, X. Zeng, W. Li, N. Tsubaki and S. Yu, *RSC Adv.*, 2016, **6**, 13450–13455.



- 254 Z. Zhao, Y. Dai, G. Ge and G. Wang, *ChemCatChem*, 2015, **7**, 1135–1144.
- 255 N. Candu, I. Man, A. Simion, B. Cojocaru, S. M. Coman, C. Bucur, A. Primo, H. Garcia and V. I. Parvulescu, *J. Catal.*, 2019, **376**, 238–247.
- 256 Y. Wang, J. Wang, Y. Zhang, F. Song, Y. Xie, M. Wang, H. Cui and W. Yi, *Catal. Lett.*, 2020, **150**, 493–504.
- 257 S. S. Chen, I. K. M. Yu, D.-W. Cho, H. Song, D. C. W. Tsang, J.-P. Tessonnier, Y. S. Ok and C. S. Poon, *ACS Sustain. Chem. Eng.*, 2018, **6**, 16113–16120.
- 258 S.-i. Fujita, A. Katagiri, H. Watanabe, S. Asano, H. Yoshida and M. Arai, *ChemCatChem*, 2015, **7**, 2965–2970.
- 259 M. T. Jafari-Chermahini, H. Tavakol and W. Salvenmoser, *ChemistrySelect*, 2020, **5**, 968–978.
- 260 L. Y. Zhao, X. L. Dong, J. Y. Chen and A. H. Lu, *Chem.–Eur. J.*, 2020, **26**, 2041–2050.

